Coupling of a biomass gasifier with a packed rock bed thermal storage

Marta Soler Costa

June, 2019

Table of contents

Summary

The present project role is to study and model the interaction between a sensible heat storage by means of rocks and an electrically heated biomass gasifier to find a possible synergy between these two technologies and study its feasibility. It starts from the data of the biomass gasifier that was developed by DTU KT over years of investigation and from the experimental characterization of the high temperature thermal energy storage (HT-TES) in rock beds at DTU Energy. A high-temperature thermal energy storage in rock bed is a possible solution to the energy storage issue when using renewable sources.

At the end of 2018, DTU Energy built an enhanced second prototype of a rock bed storage, with 3,2 m^3 of rocks and a vertical flow configuration, that can store heat at temperatures up to 650°C. Its experimental characterization has been an important part of the current work by doing several tests and analyzing its operation, mainly by studying the charge and discharge phases with different flow rates in order to find its best performance and roundtrip efficiency. The unit contains 5.394 kg of Swedish stones of the type diabase and a description of the testing facility is provided.

After an overview of the equations considered for the data post-processing and calculation of heat losses, the validation and results of the rock bed operation are presented. The final roundtrip efficiency value found for the rock bed analyzed is around 76%.

Once the feasibility of a rock storage was proven, its coupling with a biomass gasifier could provide a range of synergies going forward. The outlet air of the HT-TES, heated by the heat stored into the rocks, can be used to provide heat to the gasifier. The gasifier needs heat for the high-temperature conversion of solid fuel into a combustible product gas.

The coupling of a scaled rock bed with an electrically heated biomass gasifier has been modelled considering two configurations: a direct recirculation of the rock bed outlet air after the heat exchanger with the gasifier, and the use of a HRSG (Heat Recovery Steam Generator) to afterwards produce electricity. Air recirculation during the rock bed charge phase was always assumed.

These coupling configurations were evaluated per different electricity hourly prices of several years due to the number of charge-discharge phases and its duration change depending on the price point set as a border to distinct between time to buy or sell the electricity.

The results showed that HT-TES in rock beds has a role to play in future sustainable energy systems and they are also applicable at larger scales and potentially useful for any country of the world. The coupling between a theoretical scaled rock bed with an electrically heated biomass gasifier turned out to be economically profitable in most of the cases.

1 Introduction

1.1 Motivation

The Earth's climate has changed throughout history. Just in the last 650.000 years there have been seven cycles of glacial advance and retreat, with the abrupt end of the last ice age about 7.000 years ago marking the beginning of the modern climate era, and of human civilization. Most of these climate changes are attributed to very small variations in Earth's orbit that change the amount of solar energy our planet receives [1].

The current warming trend is of particular significance because most of it is extremely likely (greater than 95 percent probability) to be the result of human activity since the mid-20th century and proceeding at a rate that is unprecedented over decades to millennia. This fact is an evidence of the rapid climate change. His most visible results are: global temperature rise, warming oceans, shrinking ice sheets, glacial retreat, decreased snow cover, sea level rise, declining Artic sea ice, extreme natural events and ocean acidification [1].

For all of this, organizations like the European Commission have set some climate strategies and targets for reducing its greenhouse gas emissions progressively up to 2050. For the year 2020 the targets for the European Union are to cut 20% of greenhouse gas emissions (from 1990 levels), to have a 20% of EU energy from renewables and to have an improvement of 20% in energy efficiency. The long-term strategy is the transformation towards a low-carbon economy by the year 2050 [2].

In the Denmark context, the polices on climate change mitigation have established the long-term goal of making Denmark fossil free by 2050, meaning that the entire energy demand – electricity, heating, industry and transportation – is to be met by renewable energy generation by 2050. Already in 2030, the Danish government is aiming at 50% of the Danish gross energy consumption is to be supplied by renewable energy generation [3].

One of the main challenges for the green transition is how to store the energy produced from renewable sources which fluctuate, such as solar and wind power. This makes it critically important to be able to convert and store the energy as needed and at low cost.

Although Danish waters have strong winds with some of the best conditions for wind energy, it is a problem that this energy can't be stored for days when there is more production than demand.

Energy storage can contribute to better use of renewable energy in the electricity system since it can store energy produced when the conditions for renewable energy are good but demand may be low. This more variable power generation pattern has significantly increased the need for flexibility in the electricity grid. Storage could help balance electricity supply and demand over several different time periods, from fast storage in seconds or minutes to longer storage over days.

The technology presented for storage is eco-friendly and the materials utilized are abundant, natural and cheap. Besides, it can be combined with existing power plants, district heating, compressed air technologies or processes that require high temperature. This system is also applicable at bigger scale and useful for any country of the world.

1.2 Objectives

The present work is part of the project “HT-TES – High Temperature Thermal Energy Storage” which is a collaboration between the Danish utility SEAS-NVE (project manager), DTU Energy, Aarhus University, Rockwool, Dansk Energi and Energinet.dk. The Danish consultant engineers Niras contributed to the construction of the device. HT-TES is partially funded by the Danish Energy Technology Development and Demonstration Program (EUDP) and ended in April 2019.

The main goal of this thesis is to study and model the interaction between a sensible heat storage unit that uses rocks as the storage material, with a biomass gasifier and verify the feasibility and economic improvement of this coupling. To achieve it, first it is necessary to experimentally characterize the operation behavior of the rock bed storage unit built in the university research campus of Risø DTU National Laboratory for Sustainable Energy campus and verify its usefulness for storing energy. After obtaining the experimental results for the characterization of the rock bed, the theoretical coupling of the storage unit with a biomass gasifier will be studied to check the effectivity and possible synergies between the two technologies.

To achieve the main goal, a series of specific objectives have been set:

- Carry out several tests with the rock bed experimental setup during all the period of study.
- Study and calculate the energy behavior of the experimental setup during the charge and discharge phases. Find out its roundtrip efficiency.
- Investigate and study the operation of biomass gasifiers and decide the characteristics of the gasifier in which the thesis will be focused.
- Study a possible synergy between a sensible heat storage and a biomass gasifier. It will be necessary to scale the rock bed as well.

The aim of this framework is to define a good method of operation between both technologies that allows to obtain economic savings taking advantage of electricity prices fluctuations.

1.3 Project scope

This section presents the delimitations of the present thesis, that is, what it includes and excludes the work presented together with a description of the main decisions and approaches that have been taken.

Mainly the thesis is divided into two parts: first, the experimental characterization of the rock bed built in Risø DTU campus and then, its theoretical coupling with a biomass gasifier.

The experimental rock bed setup construction was finished in January 2019 and all tests carried out and analyzed were run from February until May 2019. Hypothesis about its operation were assumed after some verifications:

- Same flow rate in each inlet pipe.
- Axisymmetric air distribution for the 360 degrees of the rock bed.

- Exact locations and correct measured values of thermocouples.
- Heat resistance of all the materials and elements used up to 600°C.
- Equal thermal properties of the materials during all tests run.

The behavior of the rock bed in storage mode has not been studied, and the flow rates to run the different tests were limited by the heaters for the charge and by the fans power for the discharge. The type and size of the used rocks were chosen after previous tests and analysis realized in the campus, so they were the same for all tests. The storage material was decided to be Swedish diabase crushed rocks, with dimensions in the range 8-11 mm [4].

To study the interaction between a rock bed storage unit and a gasifier it has been chosen the electrically heated biomass gasifier for being the simplest version of producing synthetic natural gas (SNG).

The data of the biomass gasifier was developed by DTU KT (Chemical Engineering) and provided by DTU MEK (Mechanical Engineering) who investigated the operation of different biomass gasifiers for over 10 years [5].

The operation efficiency of the scaled rock bed has been considered to be a 10% higher than the one found in the rock bed analyzed because heat losses would represent a smaller part in a bigger thermal storage unit [6]. The study of materials resistance, behavior and thermal properties of the rocks at such high temperatures is not part of this project, as well as the economic analysis of the components.

The thesis is further delimited to focusing on western Denmark market regarding electricity prices to compare the economic viability of the coupling.

This study has been realized as a previous study of a future PhD project about the integration of a thermal energy storage with a biomass gasifier to the Danish energy grid.

Dissemination of results from the project is another important part of the project from the standpoint of DTU. Details about dissemination that was part of this thesis are given in Appendix A.

1.4 Energy storage

Energy storage is the capture of energy produced at one time for use it when needed. This is an option to save the production of more energy and without necessarily reverting to fossil energy sources. Thereby it contributes to the development and decarbonisation of the whole energy system.

Energy storage plays an important role in enabling to develop a low-carbon electricity system. Energy storage can supply more flexibility and balancing to the grid, providing a back-up to intermittent renewable energy. Locally, it can improve the management of distribution networks, reducing costs and improving efficiency. In this way, it can ease the market introduction of renewables, accelerate the decarbonisation of the electricity grid, improve the security and efficiency of electricity transmission and distribution (reduce unplanned loop flows, grid

congestion, voltage and frequency variations), stabilize market prices for electricity, while also ensuring a higher security of energy supply [7].

Currently, in the EU, there is limited storage energy system (around 5% of total installed capacity) almost exclusively from pumped hydro-storage, mainly in mountainous areas (Alps, Pyrenees, Scottish Highlands, Ardennes, Carpathians) [2].

At any moment in time, the consumption of electricity has to be perfectly matched with the generation of electricity. This balance is necessary in all electricity grids to maintain a stable and safe electricity supply. Energy storage can help deal with fluctuations in demand and generation by allowing excess electricity to be saved for periods of higher electricity demand.

By using more energy storage, a country can decrease its energy imports, improve the efficiency of the energy system, and keep prices low by better integrating variable renewable energy sources [2].

In a sustainable energy system, any energy production should not be lost but be stored and then used during the periods with bad conditions for renewables energies or recovered when there is more demand than production. Electricity can also be converted to heat or gas and stored for a subsequent use in heating, mobility or industry.

1.4.1 Current technologies

Nowadays, a variety of technologies exist to store electricity, including batteries, compressed air and chemical storage, but by far the most common technology to date is pumped hydro storage. The growing need for flexibility in the energy system would benefit from new storage solutions and innovation. Pumped hydro plants have already been implanted in most feasible places and they can't be increased much more due to geographical limitations.

Some emerging storage technologies are gradually becoming competitive. Over the last century, the energy storage has evolved and adapted to changing energy requirements and advanced in technology. There are three main types of energy storage technologies:

Chemical storage

Mainly batteries, they transform chemical energy into electricity. This electrochemical process does not involve the transfer of heat, so Carnot limitations are avoided and processes can be very efficient (typically greater than 85%). There are two different types of batteries: solid state batteries (rechargeable); a range of electrochemical storage solutions, including capacitors and advanced chemistry batteries (Nickel, Lithium-Ion and Sodium-Sulphur), and flow batteries; where the energy is stored directly in the electrolyte-solution for longer cycle life, and quick response times [4].

Nowadays batteries are mainly used for small amount of energy storage applications like in consumer electronics and cars due to their excessive cost. They have limited capacity and longevity due to the gradual weakening of the battery**.**

Mechanical storage

It converts electric energy into kinetic energy and then back again when electrical demand peaks [8]:

- Pumped hydroelectric storage (PHS): technology based on storing potential energy by operating a turbine or a generator in reversed mode to pump water from the lower reservoir to the higher one taking advantage of low-energy cost. Later, when demand grows, water is released in order to generate back electricity to the grid passing through the turbine. It is a mature technology and it has and will play a critical role for storage and leveling the fluctuating output of renewable energies. The PHS plants can achieve a round-trip efficiency greater than 75%, and a discharge period longer than 20 hours. Traditional hydropower requires high standards and is less suitable for Denmark.

- Compressed air energy storage (CAES): uses surplus energy to compress air and store it underground or in a tank. The air compressor is powered using electricity from renewable energy or during off-peak periods of the electricity network. When demand exceeds supply a gas turbine is fired up rapidly thanks to the compressed air in advance. CAES increases the efficiency and the start-up time of the generator. Without heat recovery of this technology, the efficiency is very low.

- Flywheel: a device consisting of a motor/generator attached to a large rotating mass. When there is an excess of energy it is stored as rotational energy by increasing the spinning velocity and extracted by working as a generator. A flywheel is able to capture energy from intermittent energy sources over time, and deliver a continuous supply of uninterrupted power to the grid.

Thermal storage

Thermal energy storage (TES) technologies reserve energy produced in the form of heat or cold. TES includes different technologies according to the application. For heating services such as low temperature storage in water tanks, or high temperature molten salts for thermal storage in Concentrated Solar Power (CSP). The technology is based on the store of energy as heat taking advantage of low-cost materials. It can be used afterwards directly for heat supply or to be converted into electricity by a thermodynamic cycle depending on the range of temperatures [9].

This method has a great capacity and is an environmentally friendly way of storing energy. It can provide electricity and district heating and it is easy to connect to an existing cogeneration plant. Low temperature thermal storage of district heating is widespread, but high-temperature thermal storage is still under development.

2 High Temperature Thermal Energy Storage (HT-TES)

This project is focused on the thermal energy storage in the form of heat at high temperature. HT-TES is a crucial technology ensuring continuous generation of power from renewable energies and plays a major role in the industrial field. HT-TES units storage heat at a so high temperature that it can be recovered either in form of heat or electricity by means of a steam cycle [10].

Thermal energy storage (TES) systems have the potential of increasing the effective use of thermal energy equipment and of facilitating large-scale switching. They are normally useful for correcting the mismatch between the supply and demand of energy.

There are mainly two types of TES systems, sensible storage systems and latent storage systems. As the temperature of a substance increases, its energy content also increases. The energy released (or absorbed) by a material as its temperature is reduced (or increased) is called sensible heat [11].

Choosing the optimal storage material remains a great challenge. From the literature, it is understood that the natural rock is a good suitable material for HT-TES in concentrating heat.

2.1 Packed rock bed thermal storage unit

A packed rock bed is a simple technique to store heat allowing high overall thermal efficiency. It is being investigated in the research campus of Risø from the Danmarks Tekniske Universitet (DTU).

In systems where air is heated, the low density of air makes impractical to store the collected energy by storing the heated air itself. It is therefore necessary to transfer the heat from the air to a denser medium for storage. As a material for this denser medium, the rock bed has the following advantages [12]:

- It exposes a large surface area for the heat transfer.
- It is relatively cheap and readily available in most locales.
- It is inert and stable over a very wide temperature range.

The technology of a rock bed thermal storage unit is a cheap way to build an energy store since the stones can remain for hundreds of years. For example, thermal energy storage in rock beds is the most common type of energy storage for those solar-thermal conversion systems which circulate air. In this work, air is also considered the heat transfer fluid (HTF).

In the rock bed three states are considered: charge, storage and discharge. They all can last from hours to days. Charging the bed is achieved by flowing hot air that enters through the top of bed (downward) and transfers heat to the rocks (storage material). To recover the stored energy from the bed (discharge phase), a low temperature air circulates in the opposite direction (from the bottom) and it is heated by the rocks. Charging from the top allows maintaining of thermal stratification in the bed, and the discharge from the bottom helps the fluid to recover the maximum

heat. The recovered fluid is at a higher temperature and can be used to produce electricity in a power cycle or district heating.

This technology of storage offers several advantages such as efficiency, reliability, environmentally friendliness and low investment cost.

In the supply chain of electricity and heating, storage can take place at many points. HT-TES is a flexible device that can affect many of the positions of the chain. The purpose of this work is to study the behavior of a rock bed storage unit which can store the surplus of energy (in the form of heat) produced by all different sources and release it when needed to the grid as showed in the next scheme.

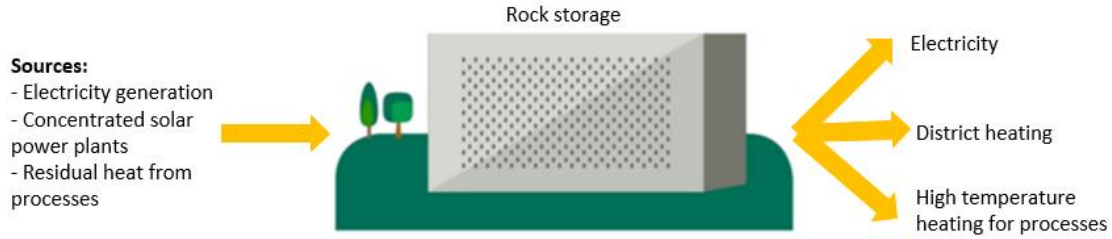

Figure 1. Location of the rock bed in the current energy grid.

A rock bed thermal storage system is a promising energy storage technology in terms of cost, scale and the possibility to work over a wide temperature range.

2.2 Related work

Thermal storage with rocks is frequently used for drying. Several studies of rock heat storage using solar collectors for drying have been carried out, for example the use of rock bed at the bottom of collectors in Jain (2007) [13] and Aboul-Enein et al. (2000) [14] or that separated from collectors in Tambunan et al. (2010) [15].

Thermal storage research on high temperature of rock bed is commonly used to drive turbines in concentrated solar power systems [[16] Zenangeh et al., 2012; [17] Allen et al., 2014; [18] Allen et al., 2016; [19] Cascetta et al., 2014]. The fluids used in these studies include oil, molten salt, and air. Therefore, the use of rocks as the heat storage material is considered to be a potential for biomass combustion which is also generated at high temperature [20].

Nowadays, most of the rock beds are studied to be suitable for solar thermal power plants at temperatures of approximately 500-600°C, but little has been published in this field [21].

The first investigations in rock-bed thermal energy storage dates back to 1929. Schumann [22] proposed an analytical solution for the problem of thermal interaction of a flowing fluid through a porous medium for a step variation of the inlet air temperature. To understand all the models and analytical solutions that have been developed to solve that problem is necessary the knowledge of the physical properties of the interacting media and the heat transfer coefficient between fluids and solids presented in many investigators [23][24][25].

Based on Schumann's solution, Shitzer and Levy [26] presented an analytical solution to the transient thermal behavior of a vertical rock-bed thermal storage system obtained in terms of

infinite double series. By means of Duhamel's theorem, then, they calculated bed and fluid temperatures in response to arbitrary fluid inlet temperatures. Other modeling studies were based on the work originally done by Schumann and many models were developed for a temperature range of 60-200°C employing as a fluid oil, water or air. Fewer studies were analyzed for higher temperature ranges. Most of the models considered temperature-invariant fluid and solid properties, approximations that introduce uncertainties.

Hollands [12] discussed the modes of operation of the bed, the bed layout and volume, among other aspects. In this case, he ensured the most effective use of storage by using his layout where, during charge periods, the direction of air flow is opposite to that when the bed is being discharged. For similar reasons it is preferable that the rock bed be oriented so that the air flow is in vertical (upward and downward) direction, and not in the horizontal direction.

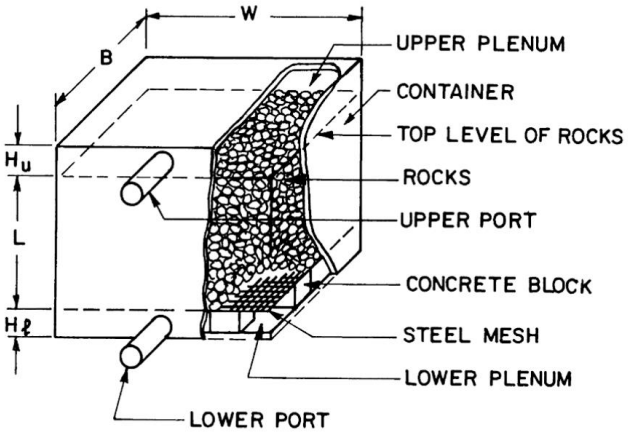

Figure 2 Sketch of a typical rock-bed storage unit [12].

Later, a thermal energy storage system, consisting of a packed bed of rocks as storing material and air as high-temperature heat transfer fluid was analyzed for concentrated solar power applications by Zanganeh [16]. It was designed, fabricated and tested a pilot-scale and simulated by means of a dynamic two-phase heat transfer model. The tank is immersed in the ground and has a truncated cone shape for exploiting the effect of lateral earth pressure at higher load bearing and for reducing the normal force on the walls during thermal expansion of the rocks by guiding them upwards. An additional advantage of the conical shape of the storage tank is the larger storing volume on top of the tank comparing it to a cylindrical shaped, where the temperature is highest, leading to a higher volume-to-surface ratio and hence smaller losses from the lateral walls. The relatively smaller volume at the bottom, where most of the energy is already extracted from the air, results in lesser necessary storing material.

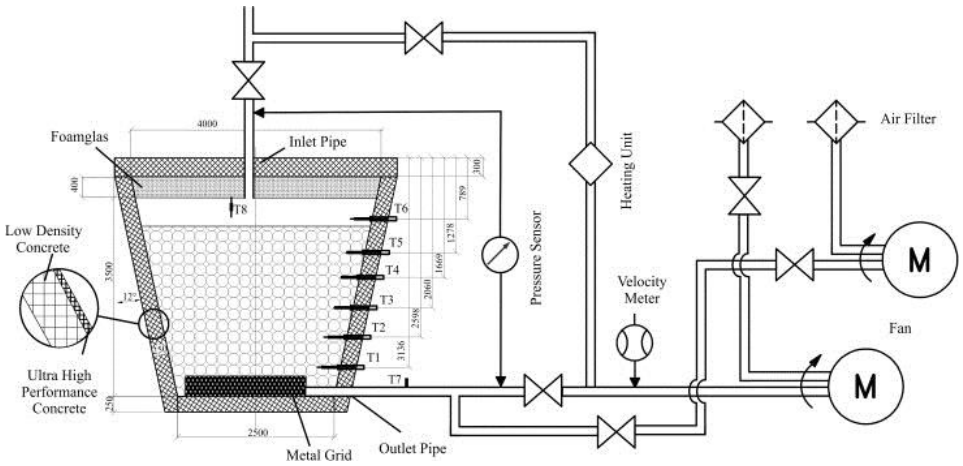

Figure 3 Schematic of the pilot-scale thermal storage configuration and experimental setup presented by Ref. [16].

During last year, in 2018, in the energy department of DTU a first prototype of HT-TES with rocks was studied. DTU first built a rectangular-shaped experimental setup, called the Shoebox. It is significantly larger than a regular shoe box with its 1 m² of cross-section and 1,5 m long, and isolated later [27].

Its results were optimistic, so it was decided to build a new improved version, the one that is being studied in this thesis. Among other things, the main significant difference between these two configurations is that in the new device the air is sent vertically into the stone storage instead of horizontally. Several rock bed configurations have been studied to define how buoyancy affects the performance of the storage. Due to those previous studies the experimental setup object of this project has an optimized shape to take advantage of the buoyancy effect.

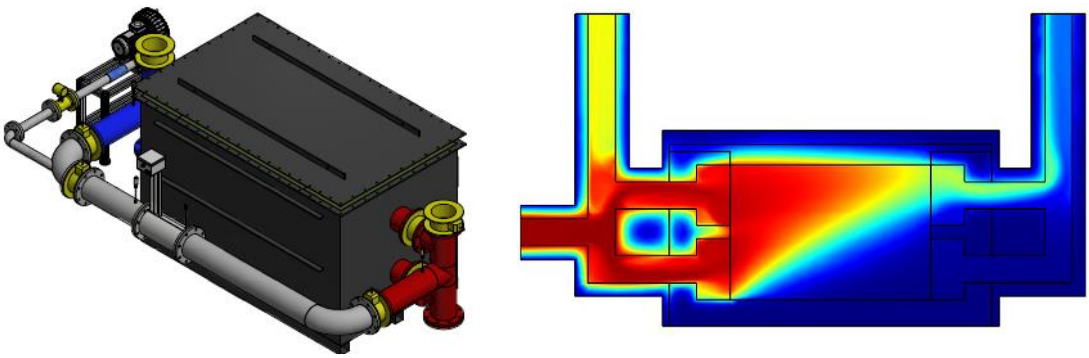

Figure 4 CAD image of the Shoebox and temperature distribution after 6 hours of pushing air at 600°C [5][27].

3 Materials and methods

In this section is described the apparatus that was built to run tests and study the behavior of a rock bed thermal energy storage unit. The configuration of this experimental setup was designed in order to improve the performance of the previous one studied in DTU, the Shoebox. The shape of the new device has been optimized to take advantage of the buoyancy effect. The size of the rocks has been also changed to smaller ones since they showed to have a better performance. Preceding the first apparatus designed it was investigated many different types of rocks and thermal insulation materials for its construction. Below it is explained the description of the whole testing facility.

3.1 Experimental setup description

The rock bed experimental setup used to test and monitor the temperature distribution, airflow, and efficiency of an HT-TES system was made with a capacity of approximately 3,2 m³ of rocks, which is equivalent in terms of thermal energy storage capacity to almost 1 MWh. A diagram of the basic operation of the rock bed and its description is reported below to understand how the system works.

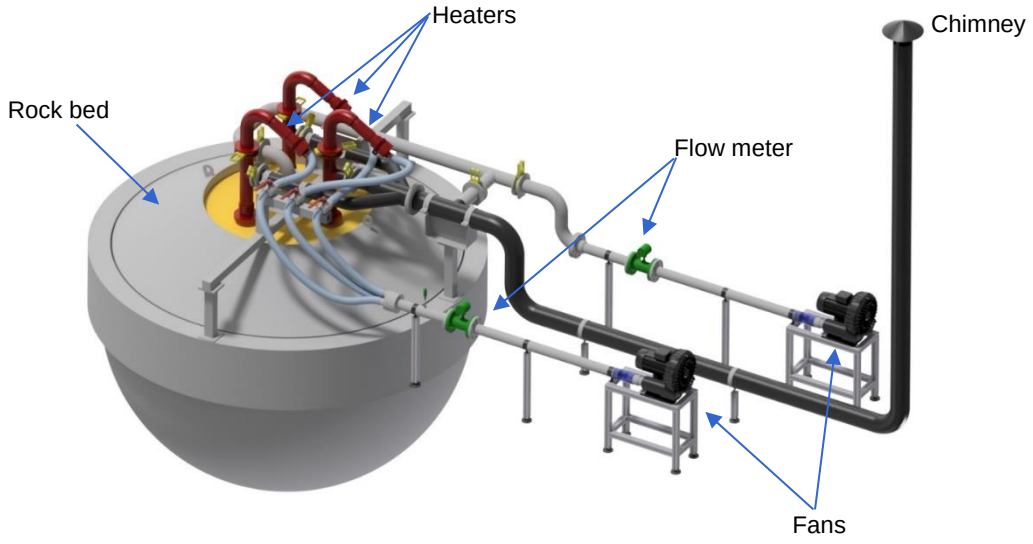

Figure 5 Rock bed experimental setup CAD image with main elements highlighted.

There are two principle modes of operation, charge and discharge phases. It can also remain in a storage mode, this is when the rock bed is charged and all the valves are closed, keeping the heat stored inside it.

For the charging phase, ambiance air is blown by the fan of charge. The inlet air is sent to the heaters and then it enters inside the rock bed, warming up the stones. The heaters set consists of three heaters that heat the air by means of electrical resistances, so that the air reaches 600°C (chosen value to perform all the tests) before entering the droplet. The power of the heaters is controlled by choosing the inlet volumetric flow rate. Every heater used has a maximum power of 15 kW, so the maximum charging capacity is 45 kW. The heated air enters the droplet from the upper part and the outlet pipe is located in the bottom part of the droplet, so the air has to circulate

through all the high of the setup and it leaves the droplet coming back out inside a central pipe located in the middle of the facility.

The discharge phase uses a different configuration. The inlet pipe is another one that also takes the air from the ambiance and blows it to the internal part of the droplet. In this case, the air enters from the central pipe and it goes from the bottom part to the heaters' pipes located on the top heating up by the hot rocks previously charged. This configuration of the discharging air let to recover the heat in the best way taking advantage of the buoyancy effect. Before reaching the heaters, the air is diverted and collected to the outlet pipe.

Below, an overall diagram of the experimental setup with all the components is reported:

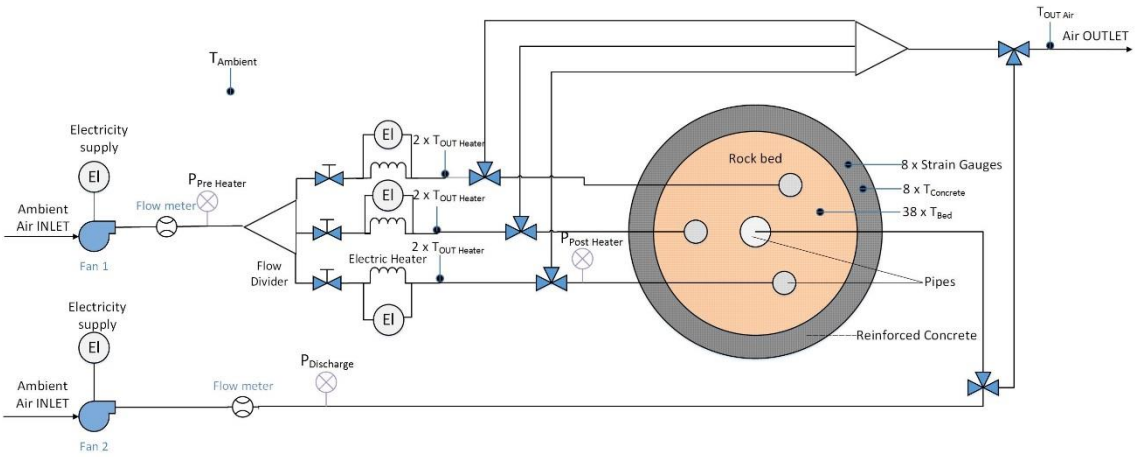

Figure 6 Scheme of the experimental setup. El: electricity supply, P: pressure gauges, T: thermocouples.

The facility has some valves that allow to obtain the different configurations of the droplet. The air-handling system (fans, heaters, valves and pipes) and the rest of the equipment were chosen to ensure the execution of numerous experiments. The rock bed itself is a semi-sphere of 1 m radius united to a cone-shaped cover, and it has been called Droplet due to its shape. The upper part of the setup is exposed to air whereas the lower one is buried and surrounded by soil.

The rocks are located inside a container made of steel, AISI 304. All the metal parts of the installation are made of the same material. This container and all the pipes of the setup are very well isolated with materials of a very low thermal conductivity, explained later.

Below there is a scheme and a CAD image of the set up to show the facility constructed and to exemplify the air flows during the charge and discharge phase respectively.

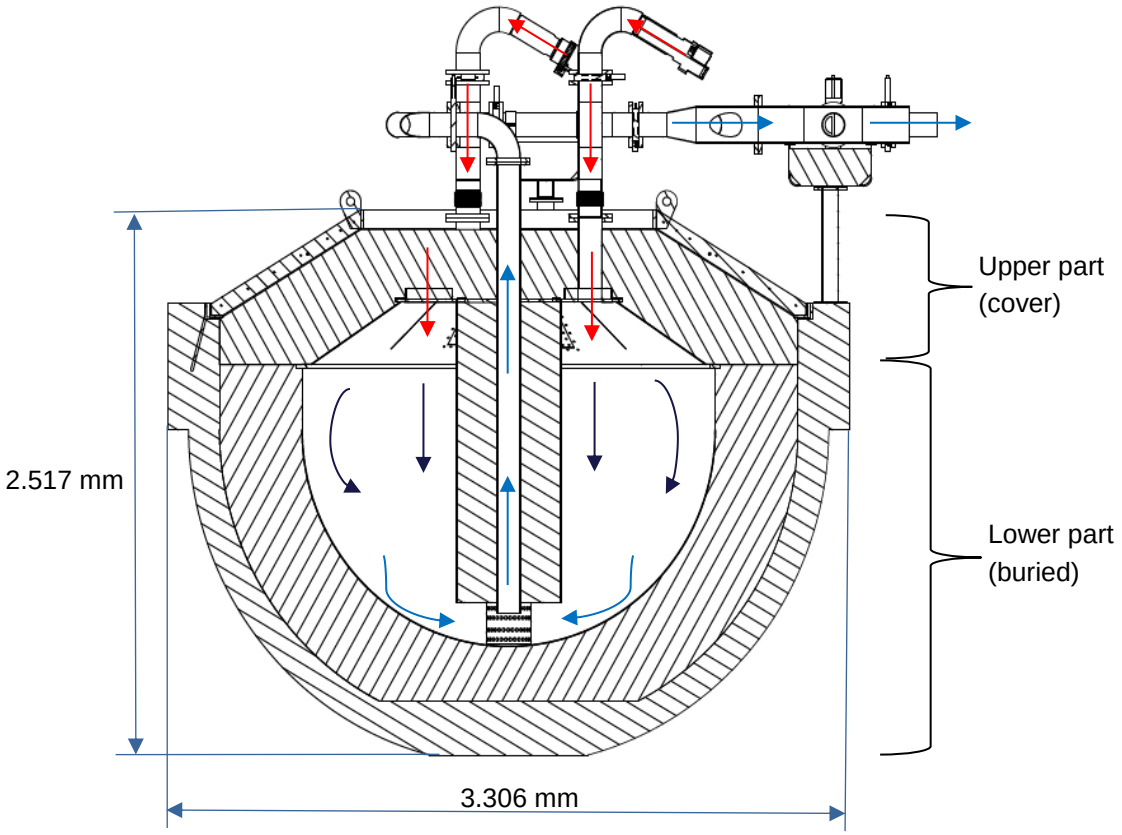

Figure 7 Scheme to exemplify the path followed by the air during the charge of the Droplet and its dimensions.

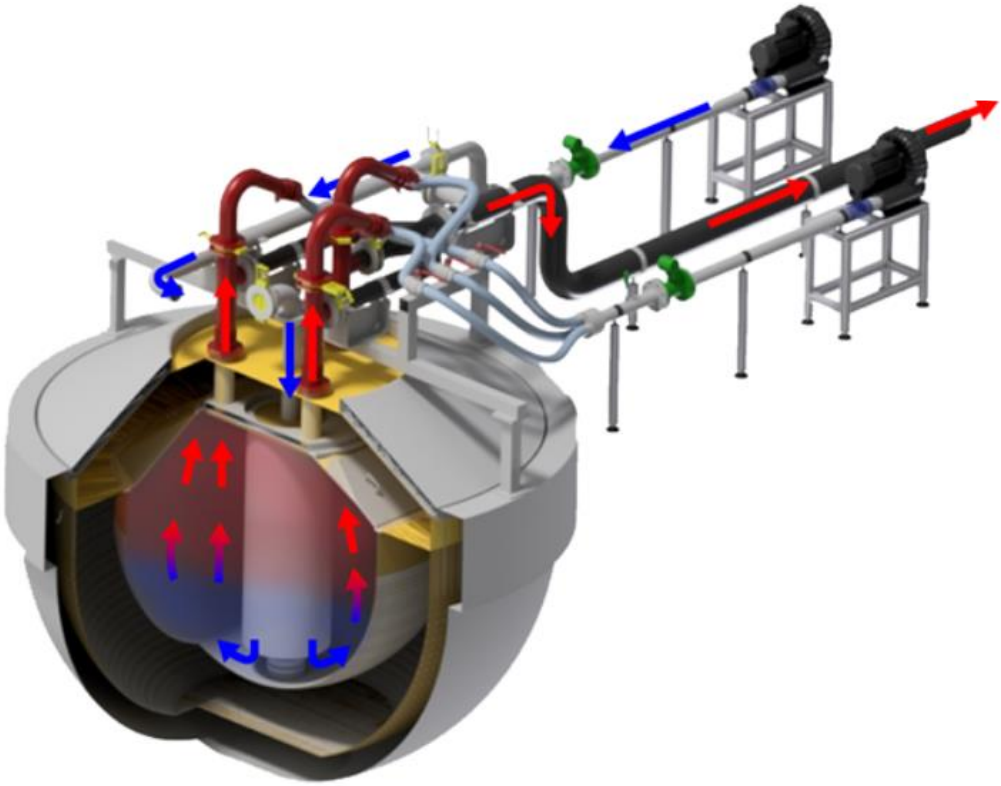

Figure 8 CAD image of the overall facility plus the air path during the discharge mode.

Thanks to this configuration of the rock bed, which extracts the recovering air from the top of the device, we take advantage of the buoyancy effect since hot air tends to distribute in the upper part due to its lower density with respect to the air at lower temperature.

To know more about its construction, consult the Heat Storage Installation Manual for Mock-up written by NIRAS on May 2018.

3.1.1 Thermal storage material

The solid storage material used is diabase from South Sweden which is considered a good candidate for storage due to its thermal, mechanical and chemical stability, high heat capacity, and good thermal conductivity. It was chosen also for its great availability. The Swedish diabase contains about 70-80% plagioclase, 20-30% pyroxene and minor (<1%) biotite and oxides. Its main properties are reported in *Table 1*. Then it is presented the specific heat of Swedish diabase depending on the temperature.

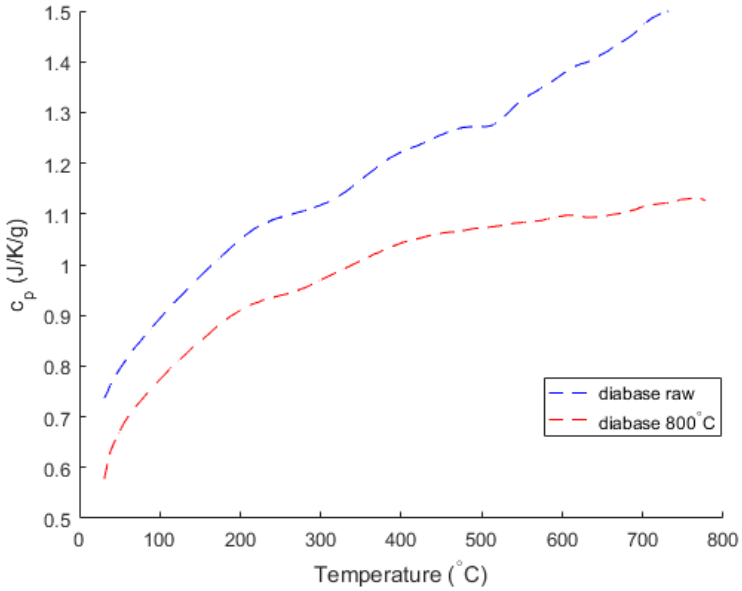

Figure 9 Specific heat capacity for Swedish Diabase. The blue curve was measured for the raw material and the red one was obtained for samples heated repeatedly in an oven for two weeks. Values provided by Aarhus University – Geology Department.

The thermal storage material needs to meet certain criteria including high thermal conductivity, high specific heat capacity, high density and thermal stability. This type of rock was selected over ten different rocks ranging that were studied by carrying out numerous thermal experiments. The candidates were selected by the specific heat capacity and also by their availability of rocks in suitable sizes and their prices. Swedish diabase rocks are found in many quarries, for example in Sweden and in Bornholm. More information about the process of the selection of the rocks is found in A. S. Pedersen's paper [4].

The use of irregular, asymmetric rock particles results in unpredictable pressure drop through the packed bed. Not only do the friction factors differ from one rock set to another, they are apparently dependent on the packing direction of the rock relative to the fluid flow direction [17].

It is not specifically clear the heat capacity of the rocks throughout all the experiments because it changes during the time, there is oxidation and chemical changes.

The Droplet uses rocks that are sieved between 8 and 11 mm. To fill the tank, they were used 5.394 kg of Swedish diabase, which provide the thermal energy storage capacity of the device.

Figure 10 Image of the Droplet filled with diabase rocks before the distribution manifold was installed.

3.1.2 Isolating materials

To avoid having a large amount of energy losses through the walls when the droplet is charging and storing the heat, the rock bed has been covered and protected with enough isolating materials to achieve a good performance of the experimental setup. The insulation is essential to retain the heat stored in the stones.

The tank, made of 316 stainless steel, that contains the rocks is surrounded by multiple layers of Skamol bricks Supra type in the lower part. The bricks were cut and shaped to fit the semi-spherical shape with a total thickness of 400 mm. The inner surface of insulation was applied with a 15-20 mm layer of wet cement-based mortar to ensure a good mechanical connection on the full contact surface with the lower steel. After the Skamol there is a layer of reinforced concrete (150 mm of thick) to ensure the position of the setup.

A cone-shaped shell of steel is the cover of the rock bed positioned on the flange of the lower shell. Over them there is a layer of Superwool of more and less 400 mm of thick (variable value due to the inclination). And on the top, there is a 75 mm layer of Rockwool.

All pipes are insulated with minimum 200 mm high temperature insulation, Superwool type, and with Rockwool type for lower temperature sections. And around the central support beam this insulation is reduced to fit.

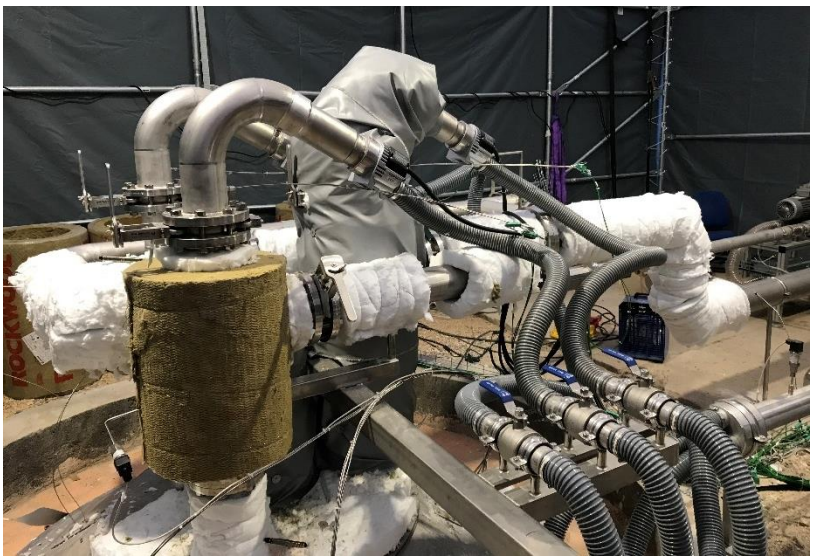

Figure 11 Picture taken during the construction of the Droplet. Insulation process is not complete and some bare sections are visible.

The values of the main thermophysical properties of rocks, as well as all the insulation materials are reported in *Table 1*.

Table 1 Thermophysical properties of the materials.

Material	Specific heat C_p (kJ/kg-K)	Density ρ (kg/m³)	Thermal conductivity k (W/m-K)
Swedish Diabase	*Figure 9*	3.002	3
Steel AISI 304	585	7.930	22,50 (600°C)
Skamol	800	700	0,155
Concrete	880	2.200	1,65 (800°C)
Superwool	1.050	128	0,08 (400°C)
Rock wool	1.050	150	0,035 (10°C)

More details about the properties of the materials are given in the technical sheets in the Appendix B.1.

For a visualization of the construction process, below an exploded view of the different layers of the rock bed together with the description of their material and thickness are shown.

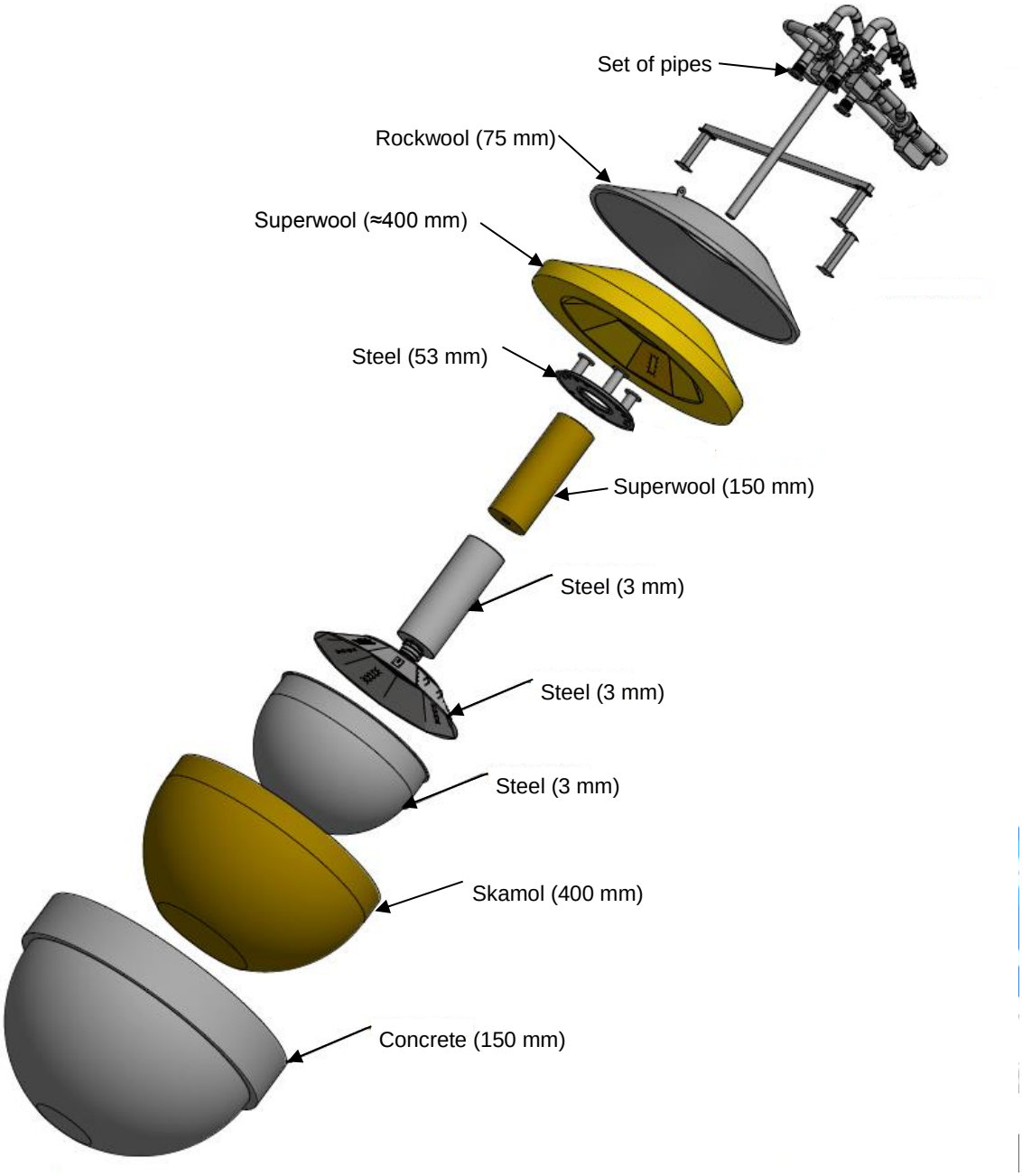

Figure 12 Exploded view of the rock bed construction.

The reinforced concrete has thermal compatibility between the steel and the concrete. In response to changing temperatures it is expected to not cause unacceptable stresses neither in expansion nor in compression states.

Figure 13 Pictures of the reinforced concrete construction. On the left, steel reinforcement structure, and on the right, reinforcement filled and covered by the concrete.

During all the tests carried out, the temperature in the reinforced concrete didn't exceed 60°C. This layer does not operate at high temperatures so there is no danger regarding the behavior of these materials. Therefore, their properties will not change during the different states of charge.

Below, it is added a photo of the final facility constructed. A tend was placed to protect the device from rain water.

Figure 14 A view of the top of the energy storage model at DTU Risø campus fully complete and ready for testing.

3.1.3 Auxiliary elements

Both fans are a Becker SV 300/1, single stage, air cooled, with a maximum air flow rate of 325 m³/h for 50Hz. The two flow meters are a Bell Turbine Flow Sensor GFT-A-100-S(X)-S-S-N, with a repeatability of ±0.2% and an accuracy of ±1.5% of reading. The flow rate can be manually regulated and checked via these flow meters. The heating elements are a Leister LE 10 000 HT, which has a maximum power consumption of 15 kW and can heat air up to 900°C. The reference value for the control of the provided heat is the one logged by a thermocouple located directly downstream the heater. More details are reported in the Appendix B.2.

The unit is connected to the rock bed by means of 100 mm diameter pipes, except the ones connected to the fans that have a DN 80 and the outlet pipe that goes to the chimney that is DN 150. All pipes exposed to high temperatures are made of AISI 316 stainless steel and covered with insulating material (Rockwool SeaRox SL 660, 100 mm of thickness).

Valves DN100 were used to govern the direction of the air flow and switch between charge and discharge configurations. They withstand a maximum temperature of 650°C.

All the other elements utilized for the construction of the experimental setup can reach a temperature value of 800°C although the behavior of some of them cannot be assured.

3.1.3.1 Data acquisition

The droplet has a set of different meters used by the data acquisition system in all tests:

- Thermocouples: to know the temperatures over a range of points of the setup like inside the rock bed, in the pipes or in the concrete. The temperature control device is a solid-state relay, RS SSP3A250BDT, controlled by a PID system with a response time of 8,33 ms, both turning on and off. Each heater is controlled separately, the reference value for the control is the one logged by a thermocouple put directly downstream the heater (label heater control). Hence, once set the temperature value for the test, the PID control the power supplied to the heater in order to obtain the present value of the temperature equal to the set value.

  Temperature logging was carried out by means of 38 thermocouples Type K (Nickel Chromium) complying with IEC 584, with an accuracy of ±1.5°C in the temperature range from -40 to 375°C and of ±2.5°C from 375 to 1000°C. A NI 9213 DAQ was used to record thermocouples data, with an accuracy <0.25°C if coupled with type K thermocouples. NI 9203 DAQ was adopted to log all data different from temperatures.

  There are 3 vertical sections defined inside the rock bed at 3 different angles, in a disposition of the top inlet pipe at 120° from each other. They are called east, northwest and southwest sections because of their location. An overall illustration of the thermocouples' location is given in *Figure 15*.

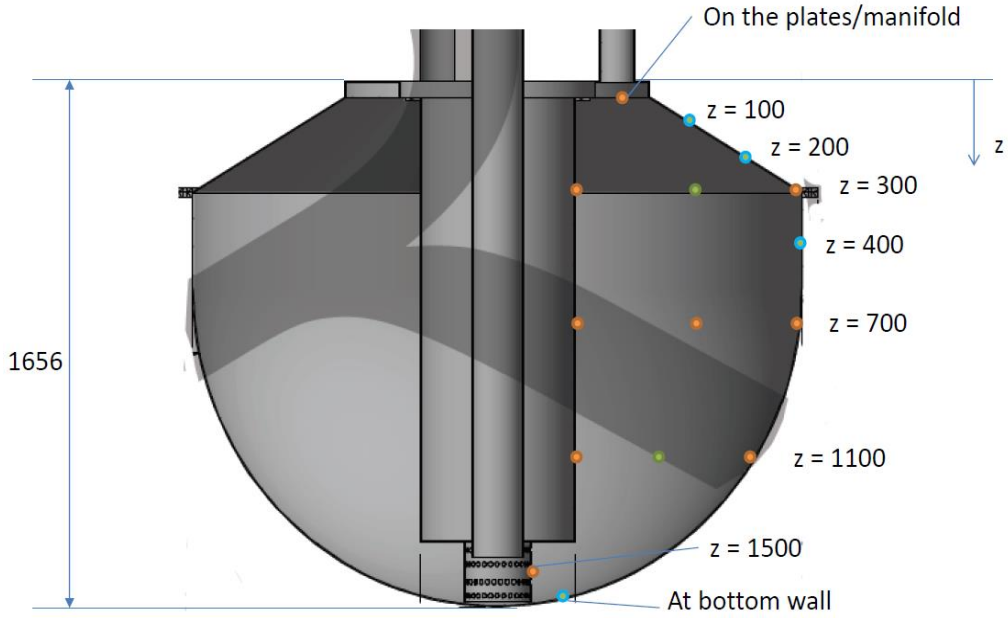

Figure 15 Thermocouples location inside the rock storage.

Inside the rock bed there is a total of 38 thermocouples installed. For each section, thermocouples at z equal 300, 700 and 1.100 mm are located at the inner wall of the rock bed, at the midpoint between the inner and the outer walls, and at the outer wall. They have also one thermocouple on the manifold and another one at z equal 1.500 mm. Only the east section has the thermocouples drawn in blue. And the southwest section also has one thermocouple at the bottom. All these temperature meters allow to get a full overview of how the heat is distributed in the stones.

The thermocouples located inside the rock bed have been named according to their location. Their name starts with a Z followed by the distance in millimeters from the set point. Then, for the nine thermocouples located in the middle, it is added an R and a number 1 for the internal radius, a 2 for the middle radius and a 3 for the external one. These names are followed by the letters E, NW or SW if they are in the east, northwest or southwest face respectively.

Besides, there are 6 more thermocouples to check and control the temperature of the inlet air right after the heaters, 3 in the outlet pipe located progressively farther from the rock bed and 1 to measure the ambient temperature.

On the concrete there are 8 thermocouples installed; three on the top, four in the middle and one in the bottom (see *Figure 16*). The concrete can deal without problem a temperature of 50°C, but we must take care if this is exceeded.

- Flow meters: one in the inlet pipe of charge and another one in the inlet of the discharge. Thanks to these flow meters we can regulate the power given the droplet.

- Power meter: to know the overall electrical consumption of the fans and heaters during every phase, charge or discharge. They are mainly to check the amount of energy that is put into the droplet in every test and to know the energy consumption of its recovery.

Power meter characteristics: KAMSTRUP 382Mx7, with rated voltage 230 V ± 10%, nominal frequency 50 Hz ± 2% and an average maximum permissible error of +0.1%.

- Pressure gauges: the experimental setup has 3 pressure gauges; one before the heaters, one after the heaters and the last one is located at the discharge pipe. They allow to calculate the pressure drop of the apparatus. Pressure measurements were performed adopting three DMP 343 pressure transmitters, with an accuracy according to IEC 60770 of 0.35%.

- Strain gauges: to measure the strain suffered on the concrete there are collocated 8 strain gauges glued to the reinforcement, although we only controlled the value of four of them. Their distribution is shown in the following image.

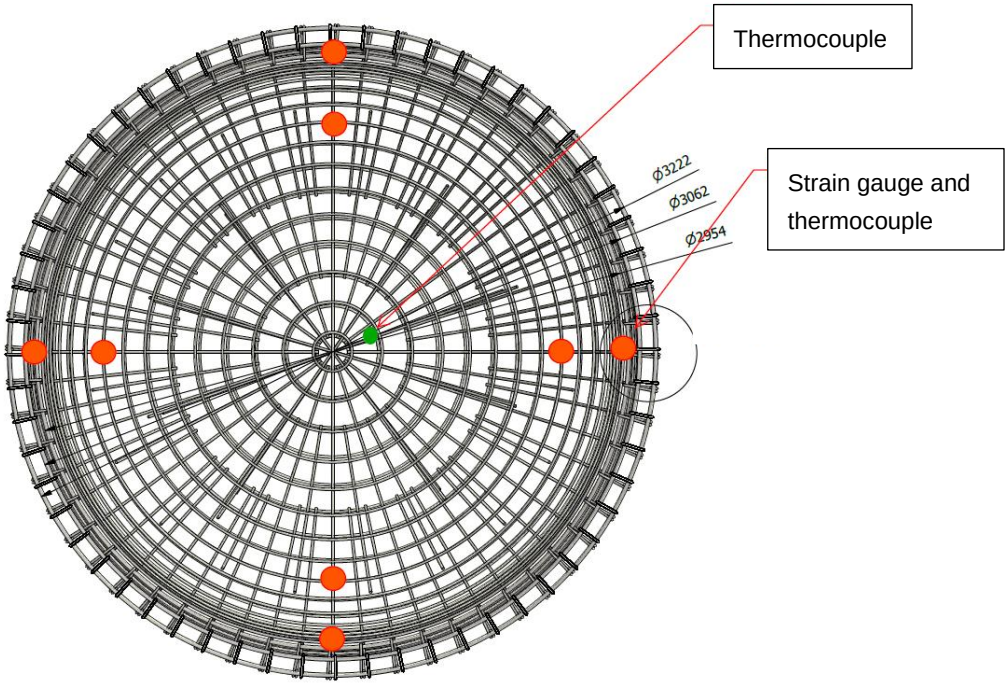

Figure 16 Strain gauges and thermocouples location in the reinforced concrete.

3.2 Experimental procedure

The characterization of the rock bed included charge and discharge phase analysis. In order to study and quantify the performance of the testing facility many criteria could be considered.

The main degree of freedom used to vary the operating conditions was the charge air flow rate, which resulted in different charge rates in terms of power (kW). Two configurations were set up: slow flow rate, 120 m³/h of volumetric flow rate of air what corresponds to 27 kW, and fast flow rate, air flow rate at 200 m³/h corresponding to 44 kW, close to the power limit of the heating unit. The power provided to the rock bed is calculated according to Equation 1:

$$P_{provided} = \frac{E_{provided}}{t_{test}} \qquad \text{(Eq.1)}$$

$E_{provided}$ is the amount of energy provided by fan and heater units, which is measured by the power meter, and t_{test} is the duration of the test.

This degree of freedom allowed the evaluation of the stored heat at different air velocities, therefore different inertia and heat exchange capacity. In order to obtain comparable results between tests, the 27 kW charge phases had a duration of 26 h, whereas the 44 kW ones lasted 16 h. These both types of charge result in a similar total energy input, providing around 700 kWh. The maximum theoretical heat capacity of the Droplet was assumed to be around 990 kWh, which results from Equation 2:

$$C_{th} = \frac{m_r c_{p,r} (T_{heater} - T_{amb})}{3.600} \quad \text{(Eq.2)}$$

Where C_{th} represents the thermal capacity in kWh of the Droplet; m_r is the mass of rocks that was put inside the rock bed, 5.394 kg; $c_{p,}$ is the specific heat capacity of the rocks at the operating temperature, with a value of 1,12 kJ/(kg·K); T_{heater} is the storage temperature, assumed uniform and constant at 600°C; T_{amb} is the inlet ambient air during discharge, considered 10°C for this purpose. The contribution of the air to the storage capacity is considered negligible.

The setup value of the heaters in all the tests was 600°C, and air temperature at the inlet of the rock bed was measured to be in the range 585-605°C, where this difference was due to higher or lower heat losses between the heater and the inlet of the rock bed given by different ambient temperature throughout the whole testing period.

The discharge rate was also modified between 120, 150, 200, 250 and 300 m³/h to study the different behavior of power extraction from the rock bed.

In order to study the distribution of the air inside the rock bed in the angular direction, inlet valves were manipulated to block the path of the air to one heater. The goal of this degree of freedom was to be able to charge the Droplet with only one or two heaters instead of three.

4 Rock bed calculations

The main aspect to take into account in order to study the performance of the Droplet is to calculate his thermal energy storage behavior together with the charge and discharge processes. The focus of this analysis is based on the temperature distribution inside the rock bed, what allows us to calculate the energy stored in the form of heat. The ideal storage scenario requires a vertical thermal gradient and a uniform diffusion of the heat.

An energy balance of the rock bed is presented below in order to understand its working principle during the charge phase. It is also attached a visual description of the main heat fluxes in *Figure 17*.

$$E_{stored} = E_{inlet} - E_{lost\ walls} - E_{outlet} \quad \text{(Eq.3)}$$

$$E_{provided\ heaters} = E_{inlet} + E_{inlet\ losses} \quad \text{(Eq.4)}$$

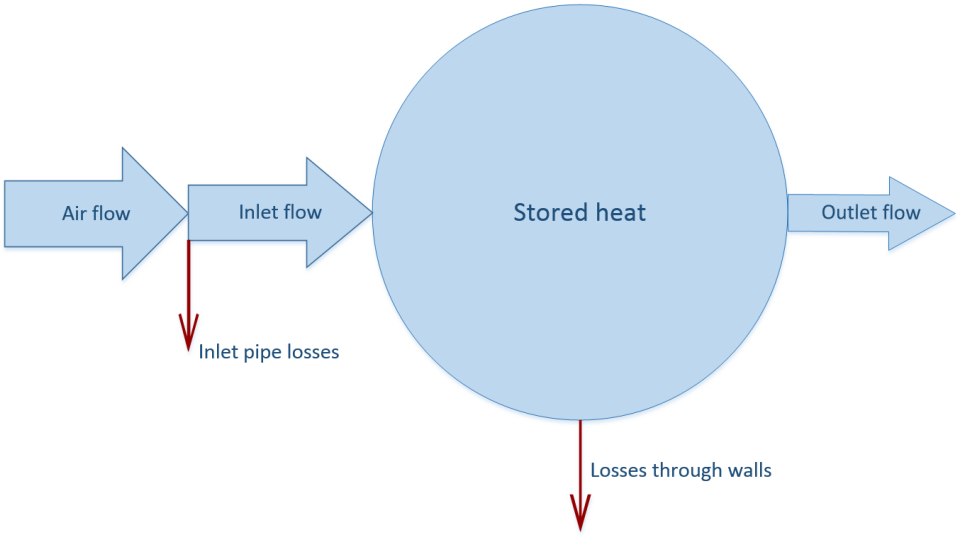

Figure 17 Scheme of the heat fluxes during the charge phase.

The energy provided by the heaters in the diagram is represented by "*air flow*" which is the air flow rate right at the outlet of the heaters. "*Inlet pipe losses*" is the term that accounts the heat dissipation along the inlet pipe that connects the heaters with the entrance of the rock bed, it includes a part of energy that gets stored in the isolation of this pipe and a constant value of energy dissipated to the ambient. "*Inlet flow*" is the difference between the energy of the air flow after the heaters and the inlet pipe losses, the temperature at the inlet of the rock bed is logged by a thermocouple. "*Stored heat*" is the energy stored inside the rock bed. "*Losses through walls*" represents all the heat losses that take place through the insulating walls. "*Outlet flow*" is the amount of energy lost to the ambient through the air outlet pipe, energy that was not stored inside the rock bed mostly due to a high state of charge.

Regarding the discharge phase, a description of its energy flows is provided in *Figure 18*. The main parameter to consider is the "*recovery flow*", which is the amount of heat recovered from inside

the rock bed and that comes out through the outlet pipe during the discharge phase. In this case, no outlet pipe losses are considered given that the thermocouple that measures the temperature of the recovery air flow is located right at the outlet of the rock bed. During the discharge phase "*losses through walls*" are still present. Depending on the air flow rate of discharge and of the discharge time there will remain more or less energy stored inside the rock bed, $E_{remaining}$.

$$E_{recovered} = E_{stored} - E_{lost\ walls} - E_{remainig} \quad \text{(Eq.5)}$$

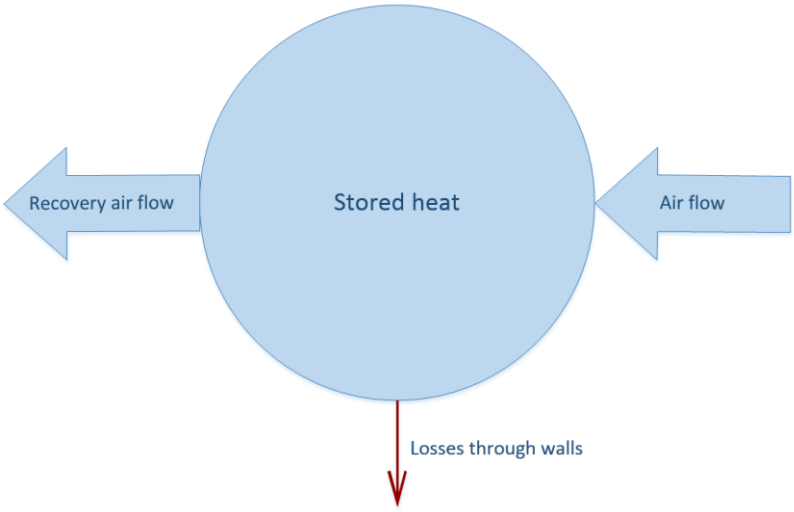

Figure 18 Energy balance for discharge phase.

4.1 Inlet and outlet flows

The energy associated with the air flow at the heaters, at the entrance of the rock bed, the outlet flow during the charge phase and the recovery air flow are calculated the same way:

$$P = \rho \dot{V}(h - h_{amb}) \quad \text{(Eq.6)}$$

$$E = \int_{t_0}^{\bar{t}} P\, dt \quad \text{(Eq.7)}$$

where the density ρ is taken at ambient conditions, given that the volumetric flow rate $\dot{V}$ is measured at normal conditions (Nm^3/h). h is the specific enthalpy of the air flow where the temperature of interest is logged (out of the heater for the provided energy, at the entrance of the rock bed for the inlet power, at the beginning of the outlet pipe for the outlet and recovery case). As the temperature logging occurs every second, the enthalpy can be considered as time-dependent and the overall energy contribution comes out of an integration over the timespan of interest. In addition to this, the value of h is calculated on the basis of the COMSOL material library, where all the thermo-physical properties of air are available. In particular a polynomial fitting of the specific heat capacity $c_{p,\mathrm{AIR}}$ is given as:

$$C_{p,AIR} = 1047{,}63657 - 0{,}372589265 \cdot T + 9{,}45304214 \cdot 10^{-4} \cdot T^2 - 6{,}02409443 \cdot 10^{-7} \cdot T^3 + 1{,}2858961 \cdot 10^{-10} \cdot T^4 \quad \text{(Eq.8)}$$

From here, the specific enthalpy, entropy and exergy are calculated:

$$h = \int_{T_{ref}}^{\bar{T}} C_{p,AIR}(T)\, dT \qquad \text{(Eq.9)}$$

$$s = \int C_{p,AIR}\, \frac{dT}{T} - \int R_{AIR}\, \frac{dp}{p} \qquad \text{(Eq.10)}$$

$$b = (h - h_{amb}) - T_{amb}(s - s_{amb}) \qquad \text{(Eq.11)}$$

where R_{AIR} is the ideal gas constant (8,314 kJ/(kg-K)) divided by the molecular mass of air (29 kg/kmol). The contribution of the pressure was neglected because the pressure drop across the rock bed is very small.

The exergy value is found by multiplying the specific term for the mass flow and integrating over time, as in:

$$B = \int_{t_0}^{\bar{t}} \rho \dot{V} b\, dt \qquad \text{(Eq.12)}$$

4.2 Energy and exergy stored

To calculate the values of stored energy and exergy inside the rock bed, the Droplet has several thermocouples located in three sections, described above. They were used to measure the temperature in different spots but describing a poor reconstruction of the temperature distribution of the bed (see *Figure 19*). For this reason, these experimental data were refined by interpolating between values and extrapolating them to the volume limits, providing 1.000 elements on each section (50 in vertical direction and 20 for the width of the cross-sectional area). The entire area at the top of the bed was assumed to be equal to the thermocouple measurement in the middle of the flow to improve interpolation results. For the regions of the bed outside the volume enclosed by the thermocouples, the temperature value of the closest thermocouple was considered uniform up to the external border. *Figure 20* shows the final result of temperature values.

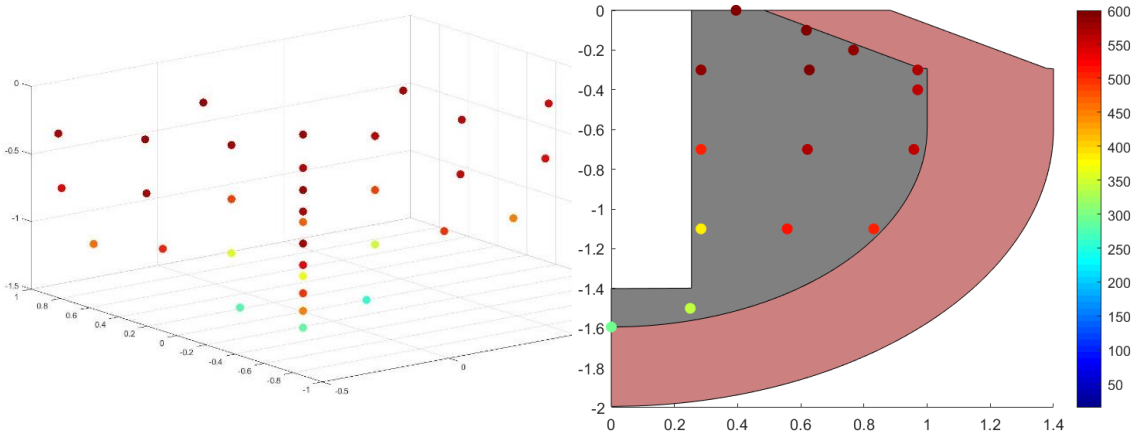

Figure 19 Thermocouple readings visualization.

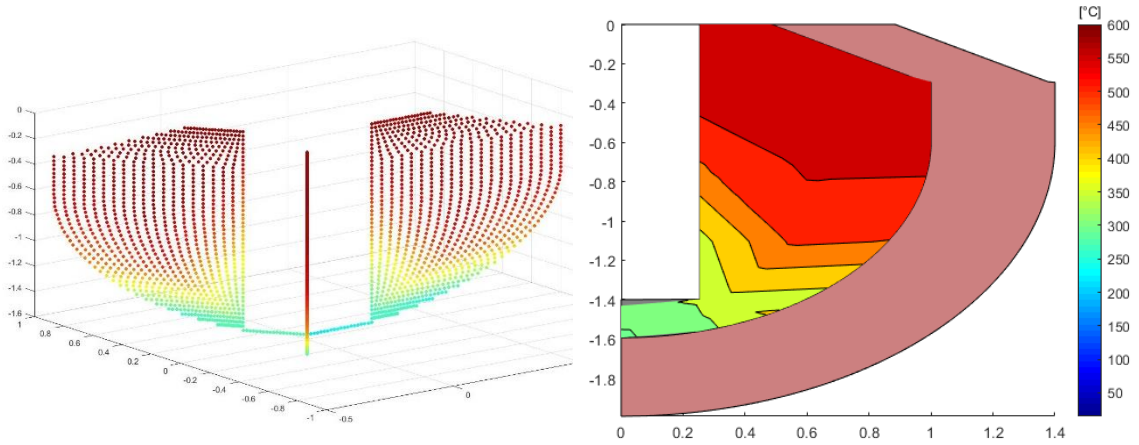

Figure 20 Thermocouple temperatures interpolated and extrapolated.

For every thermocouple it was considered a specific volume corresponding to its position. Each thermocouple section was considered to be the same through 120° respect the vertical axis in order to obtain the three-dimensional temperature distribution. So, for each one of these volumes the internal energy and exergy were calculated, and the sum of all the elements provided the overall stored in the rock bed.

The internal energy is calculated as follows:

$$u = \int_{T_{ref}}^{\bar{T}} C_{p,r}(T)\, dT \qquad \text{(Eq.13)}$$

where $C_{p,r}(T)$ is the specific heat capacity of the rocks (*Figure 9*) and T_{ref} is the reference temperature at which u is equal to zero. Then the specific entropy and exergy are given by:

$$s = \int C_{p,r}\, \frac{dT}{T} \qquad \text{(Eq.14)}$$

$$b = u - T_{amb} s \qquad \text{(Eq.15)}$$

In order to obtain the overall value of stored internal energy E_{stored} or stored exergy B_{stored}, each of these elements was multiplied by its mass, namely the density of the rocks ($\rho_r = 3.002\ kg/m^3$) multiplied by ($1 - \varepsilon$) where ε is the porosity ($0{,}45$) and by each volume of the elementary domains. Then, the contribution of all the elements was summed up.

$$E_{stored} = \int_V (1-\varepsilon)\rho_r \left(u(T_{amb}) - u\left(T_{storage}\right)\right) dV \qquad \text{(Eq.16)}$$

4.3 Heat lost along the input pipe

From where the heaters warm up the air until it enters to the rock bed there are some heat losses. A quantity of heat is stored in the isolation layers of the inlet pipe, and a small but constant flow of heat is lost through them to the environment during the entire charge period. The heat losses along the inlet pipe are calculated on the basis of an enthalpy difference between the two ends where the temperature is logged. The first end is right downstream the three heaters where the

temperature is obtained by one thermocouple in each inlet pipe. The second one is considered to be at *Z=0* of the rock bed, so right before the air enters the rock bed. In these cases, the average of the three temperatures measurements was considered to calculate the enthalpy in each end, h_{start} and h_{end} in the equations reported below.

$$P_{inlet\ losses} = \rho \dot{V} (h_{start} - h_{end}) \quad \text{(Eq.17)}$$

$$E_{inlet\ losses} = \int_{t_0}^{\bar{t}} P_{inlet\ losses}\, dt \quad \text{(Eq.18)}$$

4.4 Thermal resistance through droplet walls

Thermal resistance networks are commonly employed to analyze steady state heat transfer. They have a similar functionality to electrical resistance networks used in electrical engineering and allow for easy calculation of the total thermal resistance in a system whether it is composed of resistances in series, parallel or both.

In this case, the heat loss from the contents of the tank in contact with the surface of the setup is composed mainly by three different types of resistances. The first one considers the conductive resistance of the tank walls in series. And it is followed by the convective and radiative resistance to the surround environment in parallel. The present analysis is described by the thermal resistance network below.

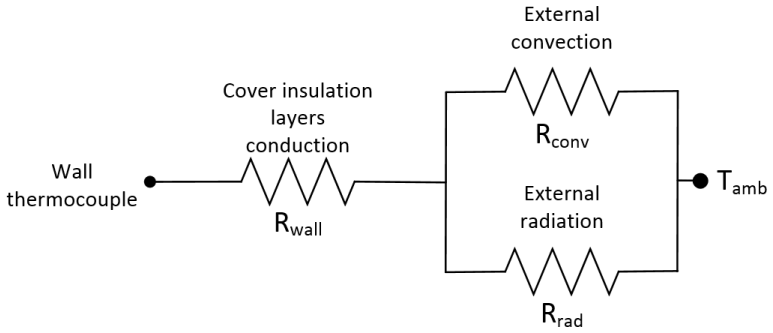

Figure 21 Electric analogy for the heat exchange through the surface walls.

As it can be seen in the figure above, the thermal path considered goes from the thermocouple closest to the wall of the droplet to its external environment. In this instance the total resistance may be calculated by adding the total resistance for the series segment and the total resistance for the parallel segment as described.

$$R_{total} = R_{wall} + \frac{R_{conv} R_{rad}}{R_{conv} + R_{rad}} \quad \text{(Eq.19)}$$

For the part of the walls that are buried in the ground there is only conduction of the heat to the exterior of the setup and it can be represented as follows.

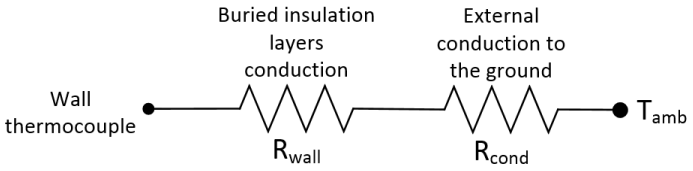

Figure 22 Electric analogy for the heat exchange through the buried walls.

4.4.1 Conductive resistance equations through insulation layers

Starting from the inside of the walls surrounding the rocks the conductive resistance is calculated for each insulation layer of the bed. For the upper part of the Droplet it is used the plane wall formula whereas for the rest it is used the spherical calculation method.

$$\text{Plane Wall: } R_{wall} = \frac{x}{kA} \; ; \quad \text{Spherical Wall: } R_{sph} = \frac{r_2 - r_1}{4\pi r_1 r_2 k} \qquad \text{(Eq.20)}$$

*It is assumed that perfect contact occurs between the surfaces of two components.

The inner thermal resistance is found adding the conductive resistance of all the insulation layers of the rock bed for each part.

$$R_{internal} = \sum_i R_{cond_i} \qquad \text{(Eq.21)}$$

The specific heat flux resulting from the wall thermocouple to the external surface of the Droplet is therefore:

$$q_{walls} = \frac{T_w - T_s}{R_{internal}} \qquad \text{(Eq.22)}$$

where the subscript "w" indicates the internal thermocouple close to the wall and "s" refers to the external surface of the droplet.

4.4.2 External radiative heat transfer

The walls of the cover of the droplet are exposed to the atmosphere. The radiative heat flux (Q_{rad}) is significant and it can be described by the equation:

$$Q_{rad} = A\varepsilon\sigma\,({T_s}^4 - {T_{amb}}^4) \qquad \text{(Eq.23)}$$

where A is the area of the external element, ε is the surface emissivity, σ is the Stefan-Boltzmann constant, T_s is the wall surface temperature and T_{amb} the temperature of the air of the room in which the testing facility is placed.

Equation 22 can be written as [28]:

$$Q_{rad} = 4A\varepsilon\sigma\,{T_m}^3(T_s - T_{amb}) \qquad \text{(Eq.24)}$$

where T_m is the average thermodynamic temperature of the surface and the surrounding surfaces. Particularly, the average between T_s and T_{amb}. Considering h_{rad} and dividing by A, the result for the specific heat flux by radiation is:

$$q_{rad} = h_{rad}(T_s - T_{amb}) \qquad \text{(Eq.25)}$$

4.4.3 External convective heat transfer

The convective heat transfer coefficient is defined as the following equation:

$$h_{conv} = \frac{q_{conv}}{(T_s - T_{amb})} \quad \text{(Eq.26)}$$

where q_{conv} is the convective heat flux, T_s is the surface temperature and T_{amb} is the air temperature. The convective heat transfer coefficient is strongly influenced by the geometry and the wind velocity outside the droplet. In this case, the contribution of the heat flux is mainly caused by the natural convection. The natural component is a function of the temperature difference between surface and air and it also considers the slope angle of the plane.

This expression suggests defining a dependent dimensionless parameter termed the Nusselt number. This parameter is equal to the dimensionless temperature gradient at the surface, and it provides a measure of the convection heat transfer occurring at the surface.

$$Nu_L = \frac{\mathrm{hL}}{k} \quad \text{(Eq.27)}$$

where L is the characteristic length for the given geometry and k the thermal conductivity of the fluid.

For the horizontal upper surface of the droplet the correlation for the Nusselt number used was [29]:

$$Nu_L = 0{,}54\mathrm{Ra}_L^{1/4} \quad \text{(Eq.28)}$$

Valid for $10^4 \leq Ra_L \leq 10^7$. Where Rayleigh number is defined as:

$$Ra_L = \frac{\mathrm{g}\beta(\mathrm{T}_s - \mathrm{T}_{amb})\mathrm{L}^3}{v\alpha} \quad \text{(Eq.29)}$$

In Rayleigh expression g is the gravitational constant, β is the volumetric thermal expansion coefficient equal to $1/T_{amb}$, ν is the kinetic viscosity (μ/ρ), and α is the thermal diffusivity ($k/\rho c_p$).

At the top inclined surfaces is used the equation for vertical plates and in computing the plate Rayleigh number g must be replaced by: $g \cdot cos\,\theta$. Assuming laminar flow ($10^4 \leq Ra_L \leq 10^9$):

$$Nu_L = 0{,}59\mathrm{Ra}_L^{1/4} \quad \text{(Eq.30)}$$

In this case, θ is 59° and Rayleigh number is:

$$Ra_L = \frac{\mathrm{g}\cos\theta\beta(\mathrm{T}_s - \mathrm{T}_{amb})\mathrm{L}^3}{v\alpha} \quad \text{(Eq.31)}$$

Joining the effects of the convection and radiation for the external heat transfer to the environment, the overall specific heat flux is found:

$$q = q_{conv} + q_{rad} = (\mathrm{h}_{conv} - h_{rad})(\mathrm{T}_s - \mathrm{T}_{amb}) \quad \text{(Eq.32)}$$

4.4.4 Conduction to the ground

As regards the rest of the droplet, the spherical part which is buried and surrounded by soil, there are two phenomena occurring: thermal energy is conducted from the surface of the droplet into the ground and the energy is stored by the temperature rise associated.

In this case has been considered a transient problem in which the solution is function only of time and the temperature varies in only one spatial dimension. It occurs when the object itself, in this case the soil, is semi-infinite. A semi-infinite body means that the material is bounded on one edge but extends to infinity in the other [30].

The transient response to an increase of the temperature at the surface of the body, can be characterized as a "thermal wave" that penetrates from the surface into the solid. The depth of the penetration (δ_t) grows as time increases and therefore the amount of material affected by the surface change also increases. According to G. Nellis and S. Klein [30], penetration depth can be described as:

$$\delta_t \cong 2\sqrt{\frac{k}{\rho c}\,t} \qquad \text{(Eq.33)}$$

where k is the conductivity of the soil, ρ the density and c the specific heat capacity. An energy balance can be done by including the conduction into the surface and the energy storage:

$$q_{cond} = \frac{dU}{dt} \qquad \text{(Eq.34)}$$

The thermal resistance to conduction into the thermally affected region through the material that lies within the thermal wave (R_g) is approximated as a spherical wall with the thickness of the thermal wave.

$$R_g \approx \frac{\delta_t}{4\pi r_s(r_s + \delta_t)k} \qquad \text{(Eq.35)}$$

where r_s is the radius of the external surface of the Droplet. The ground acts like a thermal resistance to heat transfer from the surface where R_g increases with time as the thermal wave grows, and therefore the distance over which the conduction occurs increases too. So, the rate of conduction heat transfer through the ground is:

$$q_{cond} = \frac{T_s - T_g}{R_g} \approx \frac{4\pi r_s(r_s + \delta_t)k(T_s - T_g)}{\delta_t} \qquad \text{(Eq.36)}$$

where the subscripts "s" and "g" refer to the surface of the rock bed and to the ground, respectively. There is also a vertical part of the wall buried, its thermal resistance and heat transfer is calculated as shown below:

$$R_g \approx \frac{\delta_t}{A_c k} \qquad \text{(Eq.37)}$$

$$q_{cond} = \frac{T_s - T_g}{R_g} \qquad \text{(Eq.38)}$$

where A_c is the cross-sectional area of the material.

4.5 Heat stored in the insulation layers

Doing an energy balance on the storage unit, it is pretty direct to understand that the amount of energy which is not stored inside the rock bed nor lost is accumulated in the layers of insulation material since they have a specific heat capacity. The contribution of the energy stored in the insulation explains partially the performance differences of the tests since it depends on their initial temperature.

The bed was discretized as explained for the heat losses through the walls. For each insulation layer, the inner and outer temperature was calculated starting from the heat lost through the walls and its thermal resistance. The average of the concrete's temperature was considered as the surface temperature. The energy stored in the insulation layers was then calculated as next equation shows:

$$E_{insulation} = \rho_{insulation}\, V_{insulation}\, c_{p,insulation} \frac{(\bar{T}_{insulation} - T_{initial})}{3.600} \qquad \text{(Eq.39)}$$

where $\bar{T}_{insulation}$ is the average temperature between the inner and the outer one for each layer, and the subscript "*insulation*" refers to each insulation layer. $T_{initial}$ is the temperature of the walls at the beginning of the charge.

It also has been calculated the time that takes the heat of inside the droplet to arrive at the outside part of the Droplet in the buried zone. The thermal diffusivity along the walls of the droplet follows the next equation:

$$\delta_t \cong 2\sqrt{\frac{k}{\rho c}\, t} \qquad \text{(Eq.40)}$$

where k is the conductivity, ρ the density and c the specific heat capacity of every material.

The next table shows the properties and the time result for each isolation material of the construction:

Table 2 Isolation materials properties.

Material	δ_t (m)	C_p (J/kg K)	ρ (kg/m³)	k (W/m K)	Time
Steel AISI 304	0,003	585	7.930	22,50	0,46 s
Skamol	0,400	800	700	0,155	40,14 h
Concrete	0,150	880	2.200	1,65	1,83 h

So, the effect of the heat stored inside the droplet takes around **42 hours** to arrive at the concrete's surface.

4.6 Figures of merit

To characterize the operation of the studied rock bed, the first and second principle of thermodynamics have been considered in the analysis [6]. From the study of various tests performed, it is clear that a considerable fraction of heat is stored in the insulation layers. Their relative importance in a small-scale system like the one described here is around 15% in terms of energy stored.

The parameters of interest are:

• Charge efficiency:

$$\eta_{CH} = \frac{E_{stored}}{E_{provided}} \quad \text{(Eq.41)}$$

where E_{stored} is the amount of heat stored inside the rock bed, whereas $E_{provided}$ is the energy provided to the system by the heaters and the fan, even if this second one has a negligible contribution. This parameter identifies the capability of the storage facility to store energy from an external energy income.

• Discharge efficiency:

$$\eta_{DIS} = \frac{E_{recovered}}{E_{stored} + E_{insulation}} \quad \text{(Eq.42)}$$

where $E_{recovered}$ is the amount of energy recovered by the air flow during the discharge phase. This parameter accounts for the ability of the experimental setup to recover the stored energy considering the energy stored in the insulation layers.

• Roundtrip thermal efficiency:

$$\eta_{RT} = \frac{E_{recovered}}{E_{provided}} \quad \text{(Eq.43)}$$

It represents the portion of energy which is available downstream the storage unit with respect to the provided one. Theoretically, it should be the result of the product between charge and discharge efficiencies, but due to the heat stored into the insulation layers, a correct estimation of the final values by means of this product is not possible.

Energies considered in the charge and roundtrip expressions are calculated with different approaches. The charge efficiency equation considers only the energy stored in the rocks and ignores heat stored in the insulation and other components. However, for a small setup as the one tested in this work, the heat stored outside the rock bed can be significant. The roundtrip efficiencies, instead, are defined as the heat recovered by the discharge air flow calculated as the integral over time of the air enthalpy difference between outlet and inlet. The roundtrip efficiency therefore accounts for the heat stored in the insulation, providing the overall efficiency of the storage unit. The difference between these two calculation methods can result in higher roundtrip efficiencies than charge efficiencies [27].

• State of charge:

$$SOC = \frac{E_{stored}}{U_{maxstorable}} \quad \text{(Eq.44)}$$

where $U_{\mathrm{max}storable}$ is the heat storage capacity (C_{th}) of the testing facility and it is equal to 990 kWh, as described previously. It identifies the level of utilization of the storage unit in terms of thermal capacity.

As regards the second principle of thermodynamics the figures of merit are:

• Second principle charge efficiency:

$$\eta_{II,CH} = \frac{B_{stored}}{B_{provided}} \quad \text{(Eq.45)}$$

where $B_{provided}$ is the exergy provided by the heaters and the fan. Its meaning is the same as the corresponding first principle parameter, but in terms of exergy.

• Second principle discharge efficiency:

$$\eta_{II,DIS} = \frac{B_{recovered}}{B_{stored} + B_{insulation}} \quad \text{(Eq.46)}$$

This parameter accounts for the exergy that can be made available in a real-life application, starting from the stored exergy.

• Second principle roundtrip efficiency:

$$\eta_{II,RT} = \frac{B_{recovered}}{B_{provided}} \quad \text{(Eq.47)}$$

This figure of merit represents the fraction of exergy, contained in the recovery air flow, that can be converted into reversible work with respect to the overall provided exergy during the previous charge phase. As in the first principle case, the roundtrip efficiency should be resulting from the product of charge and discharge efficiencies, but the non-negligible presence of heat stored into the insulation layers does not lead to accurate results.

Additional parameters of interest are the maximum temperature that rocks reach during the charge phase, as a measure of the concentration of heat in the hottest point of the bed, and the recovery air temperature for the discharge phase, which is a direct measure of the impact of this storage unit in a real application.

5 Rock bed experimental results

In this chapter the operation of the Droplet is studied experimentally. First, a sequence of considerations and validations from the experimental tests is presented, followed by the study of the charge and discharge phases to search the most efficient operation mode of the rock bed.

5.1 Considerations and validations

The firsts realized tests were useful to make some checks about the behavior of the new apparatus. Then, it is reported the verifications that have been carried out to be sure of the hypothesis and assumptions that can be done.

5.1.1 Inlet flow rate

One of the firsts considerations was to confirm that the flow rate that goes to each heater is the same, assuming an operation of the heaters identical. For this, in every test, it is checked the temperature at which the heaters send the air to the Droplet.

For each heater there are two thermocouples to check the temperature of the heated air, the monitor and the control one. The monitor thermocouples are used to check the temperature of the air after the heaters and the control ones compare the temperature of the air with that of control so that the heater can act to match these two temperatures.

Regarding the test started on the 25th of march to reach the limit of the heaters, it can be demonstrated that the flow rate that circulates through each inlet pipe is one third of the total flow rate, so each heater receives the same flow rate.

$$\frac{\dot{V}}{3} = \dot{v}_1 = \dot{v}_2 = \dot{v}_3 \qquad \text{(Eq.48)}$$

This test was run at 600°C and started at a flow rate of 275 m³/h. In this case, the heaters were not able to heat so much flow up to 600°C, they are not enough powerful and so, the inlet air temperature values reached were between 452°C and 485°C. It is noticed that there is a difference between the three heaters, but it is not big enough to contradict that the flow rate is the same in each pipe, less than 7% of error. According to this test the second heater receives a little more flow as it reaches lower temperature values.

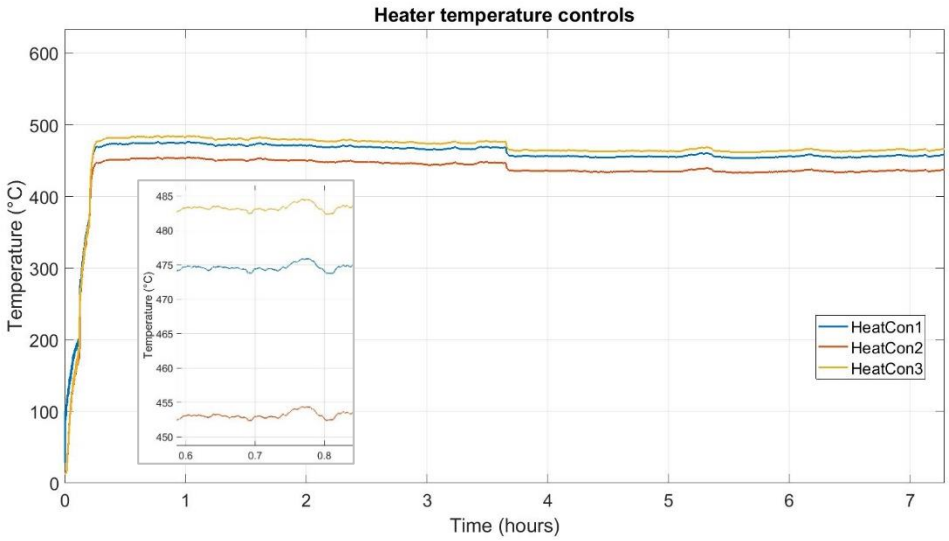

Figure 23 Heaters temperature control thermocouples at maximum flow rate and a temperature set value of 600°C.

For a test carried out at 195 m³/h, the temperature of the monitor and control of the heaters are the same for each pipe given the same input value of heater temperature. The following pictures shown the behavior of the temperature of the air after the heaters. For this test the input temperature of the heaters was 600°C.

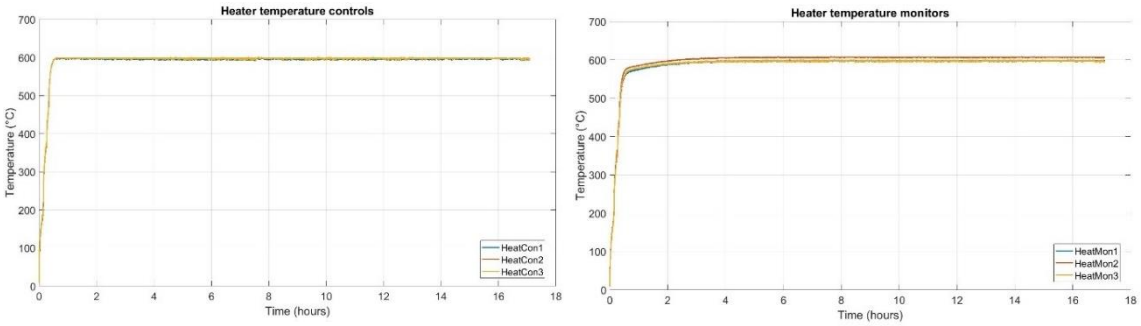

Figure 24 Heaters control and monitor thermocouples evolution of a test at 195 m³/h and 600°C for 16,5 hours.

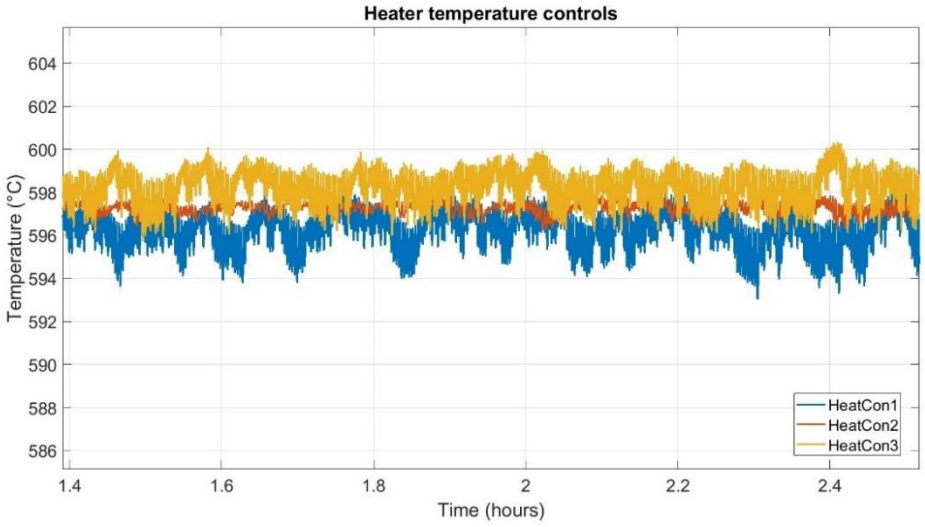

Figure 25 Zoom of the behavior of the heaters control thermocouples.

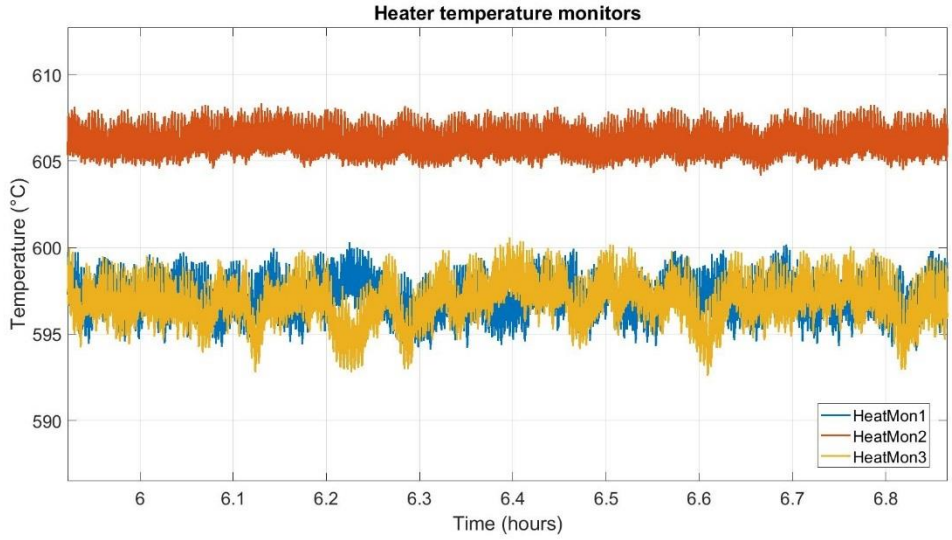

Figure 26 Zoom of the behavior of the heaters monitor thermocouples

The difference between the three temperatures is negligible since the maximum difference between them is lower than 9°C for the control temperatures and lower than 17°C for the monitor ones, without considering the divergences of the first half hour of rising the temperature. It means that the heating difference between the three heaters is about 1,5% for the control values and 2,8% for the monitor values.

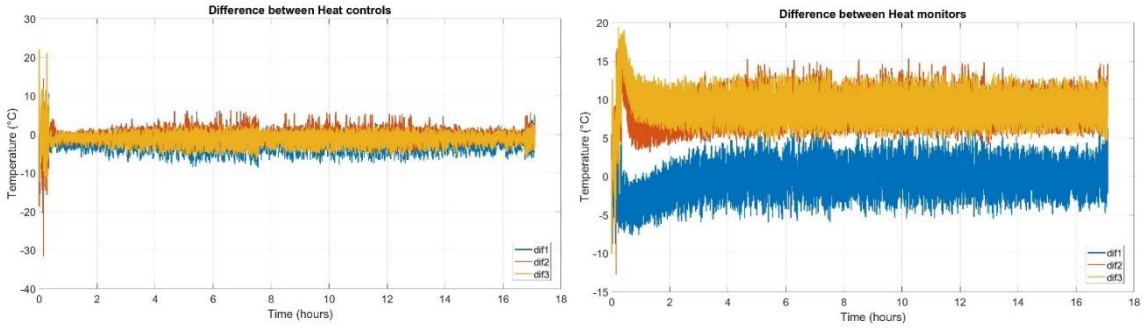

Figure 27 Difference between heaters temperatures, control and monitors measures.

Not in all the tests the result was so exact, there were some deviations, but nothing to think that the flow rate was not the same per pipe. For example, in the test performed on the 11th of march the behavior of the heaters 1 and 3 was the same in both cases, for the monitor and the control, whereas they differed from the behavior of the second heater. In the following pictures it can be appreciated that the heater number two had some turbulences.

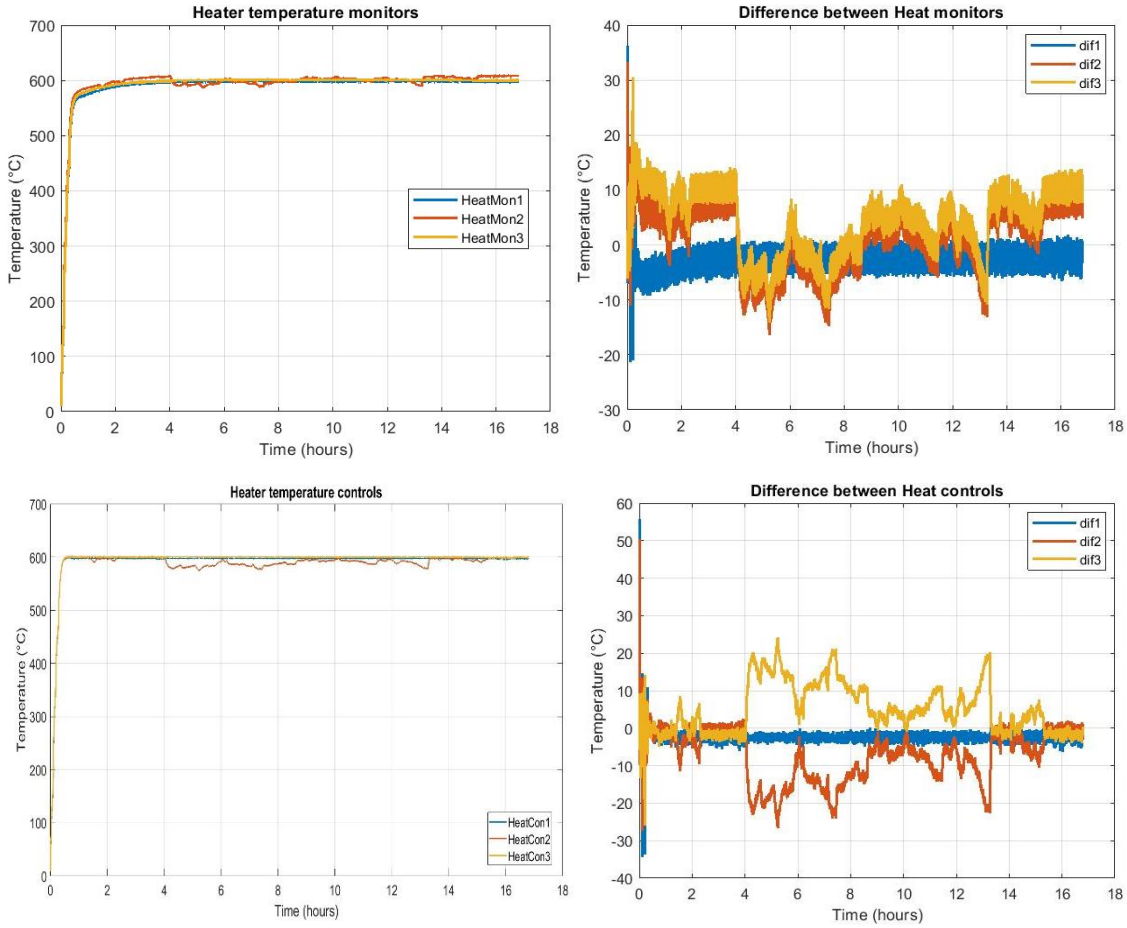

Figure 28 Heaters temperatures and differences for a test with small turbulences in heater 2.

The mean variance of the temperatures between the three heaters for the monitor values and the control ones along all the period is 15,72°C, without considering the first hour due to that during this period the temperature of the heaters is raised and is not the same for all. A fairly low value of variance.

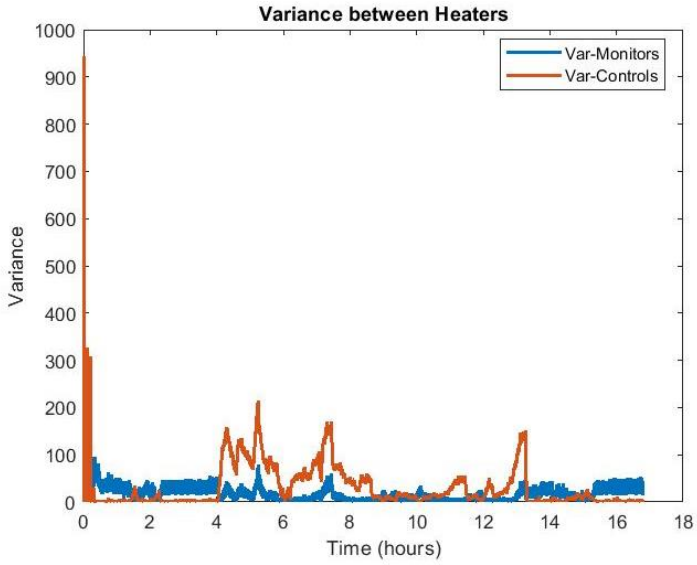

Figure 29 Variance between monitor and control heater thermocouples measures.

Next the mean and the difference between the monitor and control values is shown for each heater.

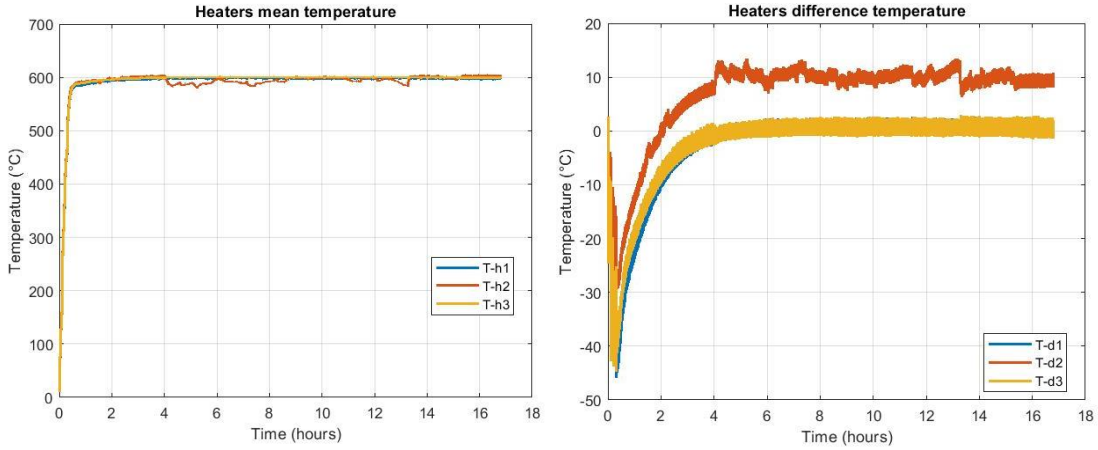

Figure 30 Mean values between each heater thermocouple and difference between them.

It can be seen that the behavior of the monitor thermocouple and the control one, are very similar for the three heaters, although heater number two has on average a difference of 10 degrees between them.

Therefore, it can be concluded that the flow rates that flow through each heater's pipe are balanced.

5.1.2 Thermocouple locations

All the thermocouples placed in the droplet were supposed to be in the same coordinates for each face. It has been noticed that there are three thermocouples in the rock bed that behave differently than those that are placed in the same position but on another side. This fact is not an inconvenience since at the end of the charge their temperature is practically the same. These thermocouples are the following ones: Z30R1-E, Z70R2-E and Z30R3-E, all of them in the east face. This fact can be appreciated in the next image:

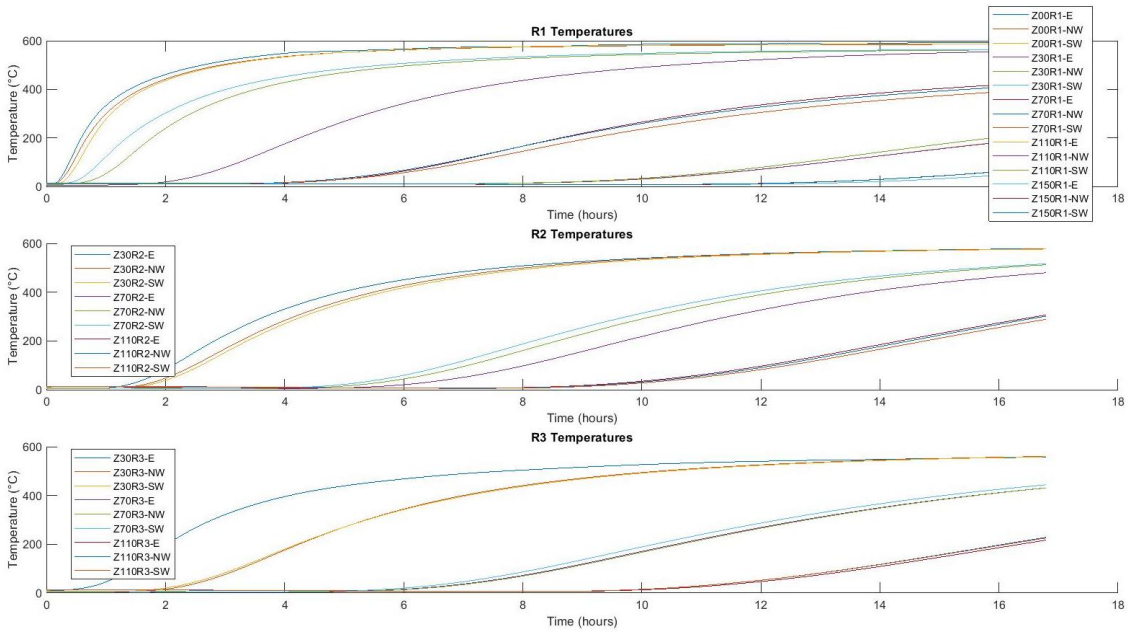

Figure 31 All thermocouple temperatures for a charge at 195 m³/h during 17 hours at 600°C.

In the first graph of the image above it can be appreciated that the temperature's evolution of the thermocouple Z30R1-E is slower than the one realized by the thermocouples located in the same position but in the other faces. The same fact happens but in a smaller factor for the Z70R2-E thermocouple. For the case of the Z30R3-E thermocouple, showed in the last graph, it evolves faster than the ones located in Z30R3 but in the other faces. But, at the end, they all reach the same temperature depending on their high.

Apart from these differences, it can be assumed that the rest of thermocouples behave the same way for every face.

5.1.3 Inlet flow distribution

At the same time, it is necessary to ensure that the heat is distributed correctly in the storage unit. The next consideration that was checked was the air flow distribution in the angular direction of the Droplet. There are three entrances of the heated air flow and then it is distributed into smaller holes thanks to a manifold. In addition, there are only three locations in the angular direction where thermocouples are mounted inside the Droplet and this is not enough to ensure the temperature in all the volume of the stone storage.

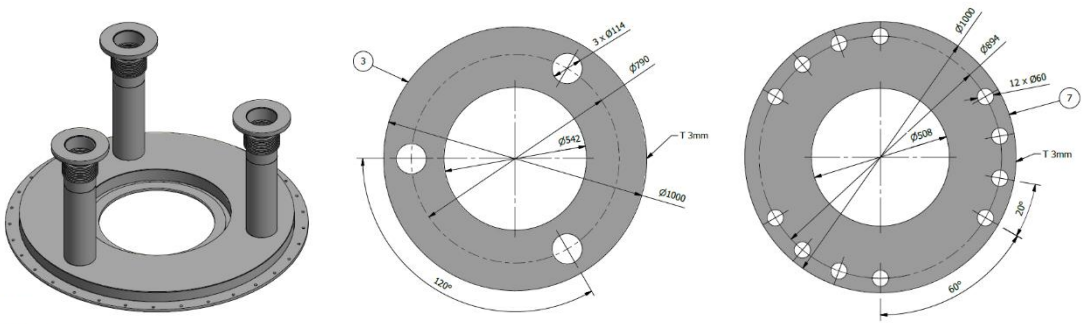

Figure 32 CAD images of the manifold. Isometric view and bottom view of the entrance and exit holes.

With this premise, a hypothesis is that the air distribution is not equal for all the 360 degrees after the manifold, and so, the air distribution is not the same inside the Droplet. For this reason, there were carried out two tests with one heater turned off, which is a worst-case scenario for inlet temperature distribution. When one heater is shut off, one third of the bed is not provided air flow directly and the air flow to the section with no heater must be provided by the neighboring heaters. If the temperature distribution in the angular direction is not significantly affected by shutting off one heater, then the flow distribution manifold is adequately designed.

Two experiments were run to compare results with two and three heaters: one where air flow to each heater is maintained constant and one where total energy used to charge the bed is constant. The results were compared regarding measured temperatures and total heat recovered.

The next images show the evolution of the temperature for each thermocouple located in a different zone. Each figure shows thermocouples located in the same vertical and radial locations. The only difference between thermocouple locations is the angular placing. Both results for all three heaters and only two heaters are plotted on each figure to give a visualization of the temperature distribution for each experiment.

5.1.3.1 One heater shut off with air flow to heaters held constant

In this study the flow rate was adapted to keep the same flow rate in the pipes to the heaters that were on. So, the total flow rate was two thirds of the one utilized in a normal operation. The heater switched off was the heater number 2 which is the one closest to the northwest thermocouples face.

Looking at the behavior of the inlet temperature, thermocouples located at *Z=0*, it is observed that the final temperature is almost equal for every face.

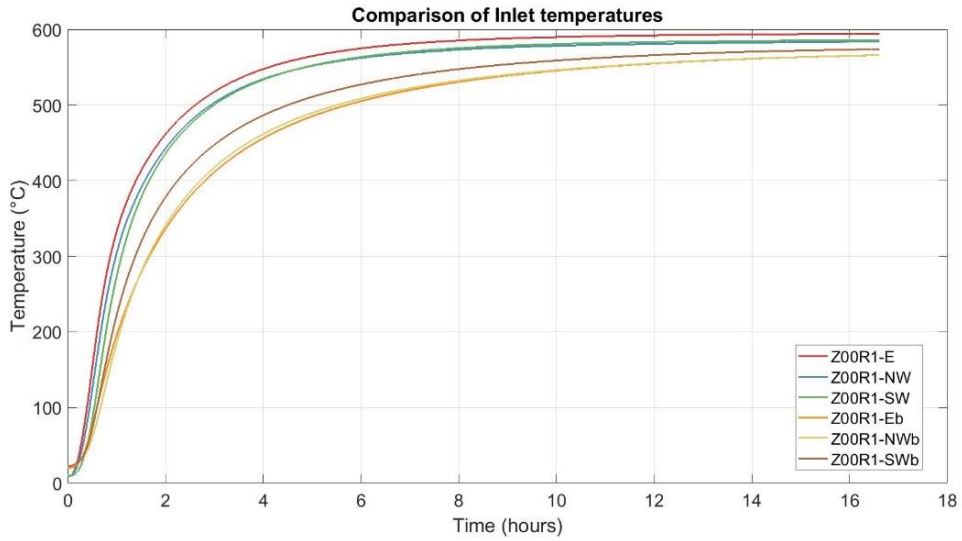

Figure 33 Comparison of the temperature in the top part of the droplet between a fast charge test and one heated with heater 2 off.

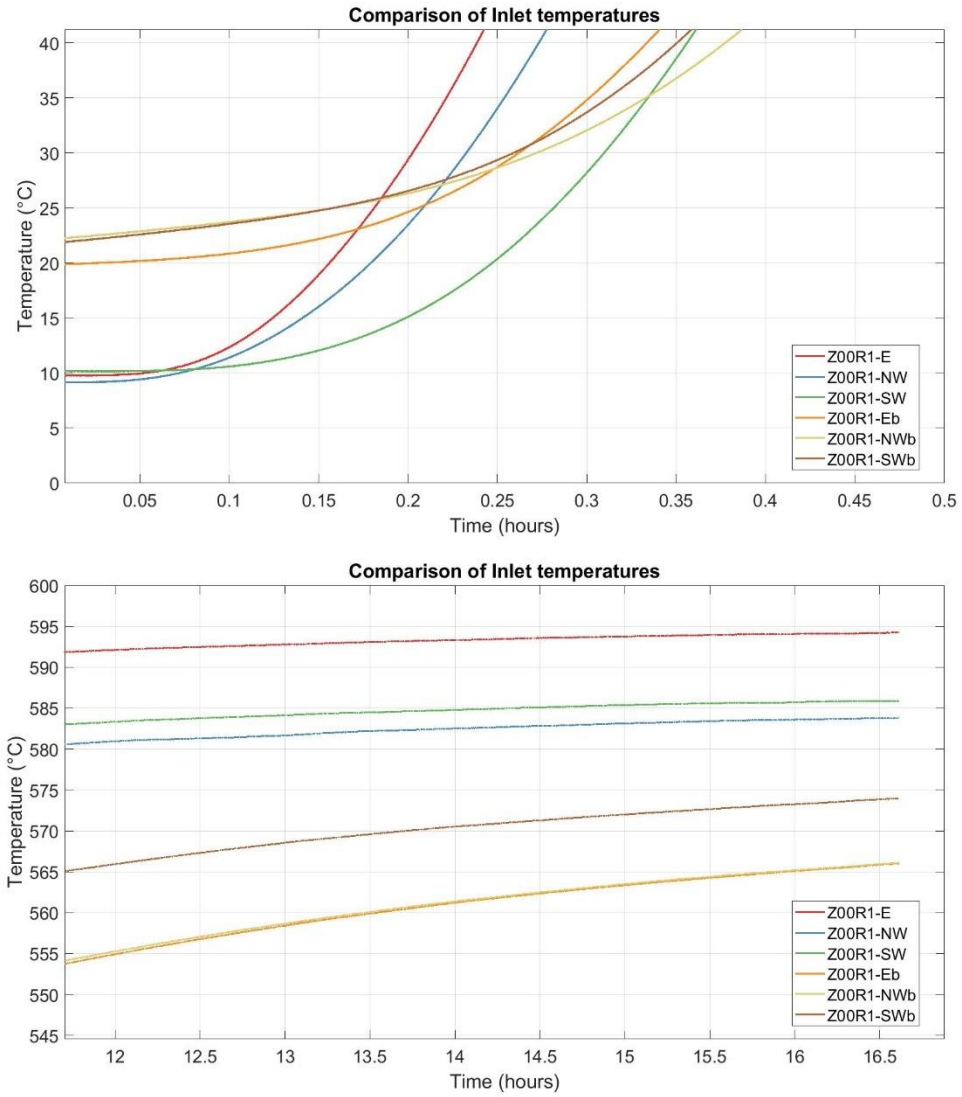

Figure 34 Zoom at the beginning and at the end of the charge.

The test carried out with one heater off, shows a slower increase in temperature, but at the end of the charge the three faces reach a temperature of almost 600°C without a difference of the face unheated. At the end of the test the maximum difference between all inlet temperatures is less than 5%. This shows that the inlet manifold does distribute air flow along the entire top surface of the rock bed.

Looking at the thermocouples located inside the rock bed for these two tests it can be concluded that there is no difference between the behavior of the faces provided with thermocouples and the ones in between. There is not a big difference of the evolution and final state between the behavior of the thermocouples located in the three faces comparing them with a normal test or a test carried out using only two heaters.

Unluckily, the starting point of these two tests isn't the same in every thermocouple, but it can be observed that the behavior and the relativity of each thermocouple, compared with the ones located at the same position but at another angular location, is the same either in a normal test or in a test realized with one heater off.

With all this, it has been accepted to consider the Droplet axisymmetric. So, for all the 120°, with respect to the vertical axis, it can be considered to have the same temperature's distribution in every location for each face.

Next, there is represented the evolution of the temperature during the charge phase for every thermocouple position. In every plot there is drawn the results in each thermocouple face and for both tests, normally heated and only with two heaters. The main reason of this graphs' comparison is to check that the performance of the face unheated directly is the same as if its corresponding heater was turned on. They prove to have the same conduct in both tests and in all faces for every thermocouple position.

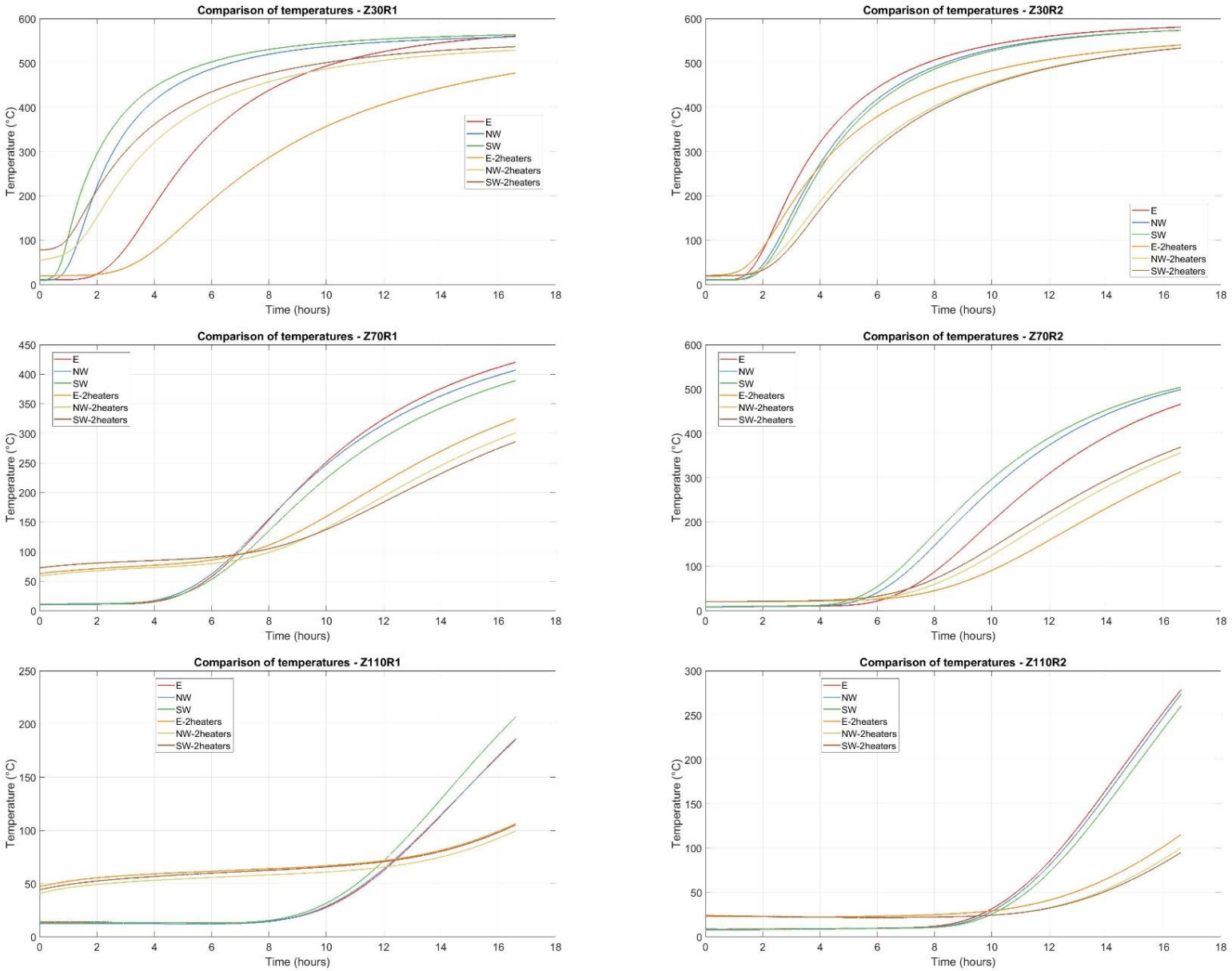

Figure 35 Comparison of the evolution of the temperatures for each thermocouple position between a normal test and one carried out with one heater off. (R1 and R2)

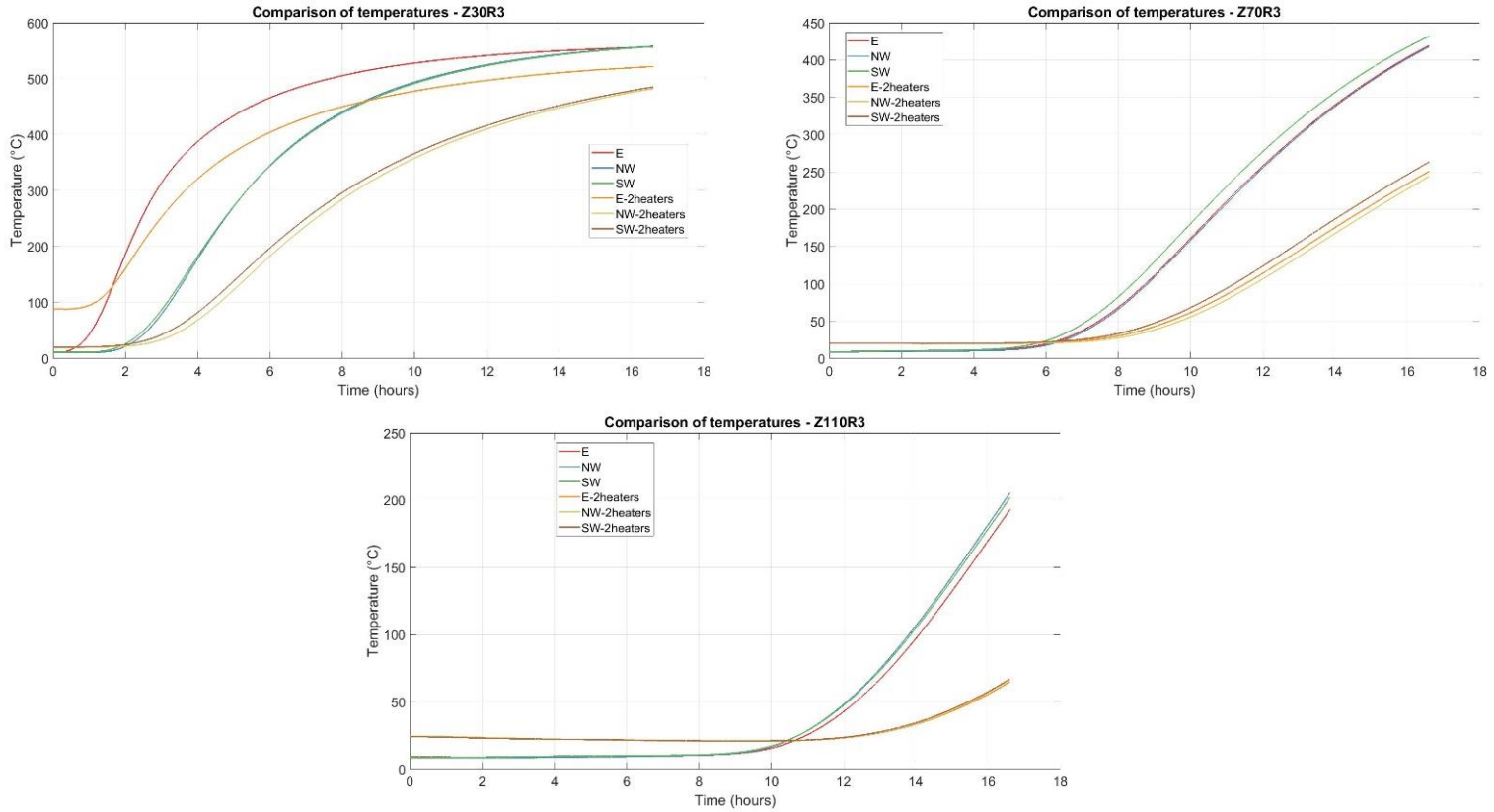

Figure 36 Comparison of the evolution of the temperatures for each thermocouple position between a normal test and one carried out with one heater off. (R3)

To look deeper in the differences between both tests, it has been plotted the temperature difference of NW face over SW face for each thermocouple position. The most important value of their differences is the one at the end of the charge, when they reach the maximum temperature.

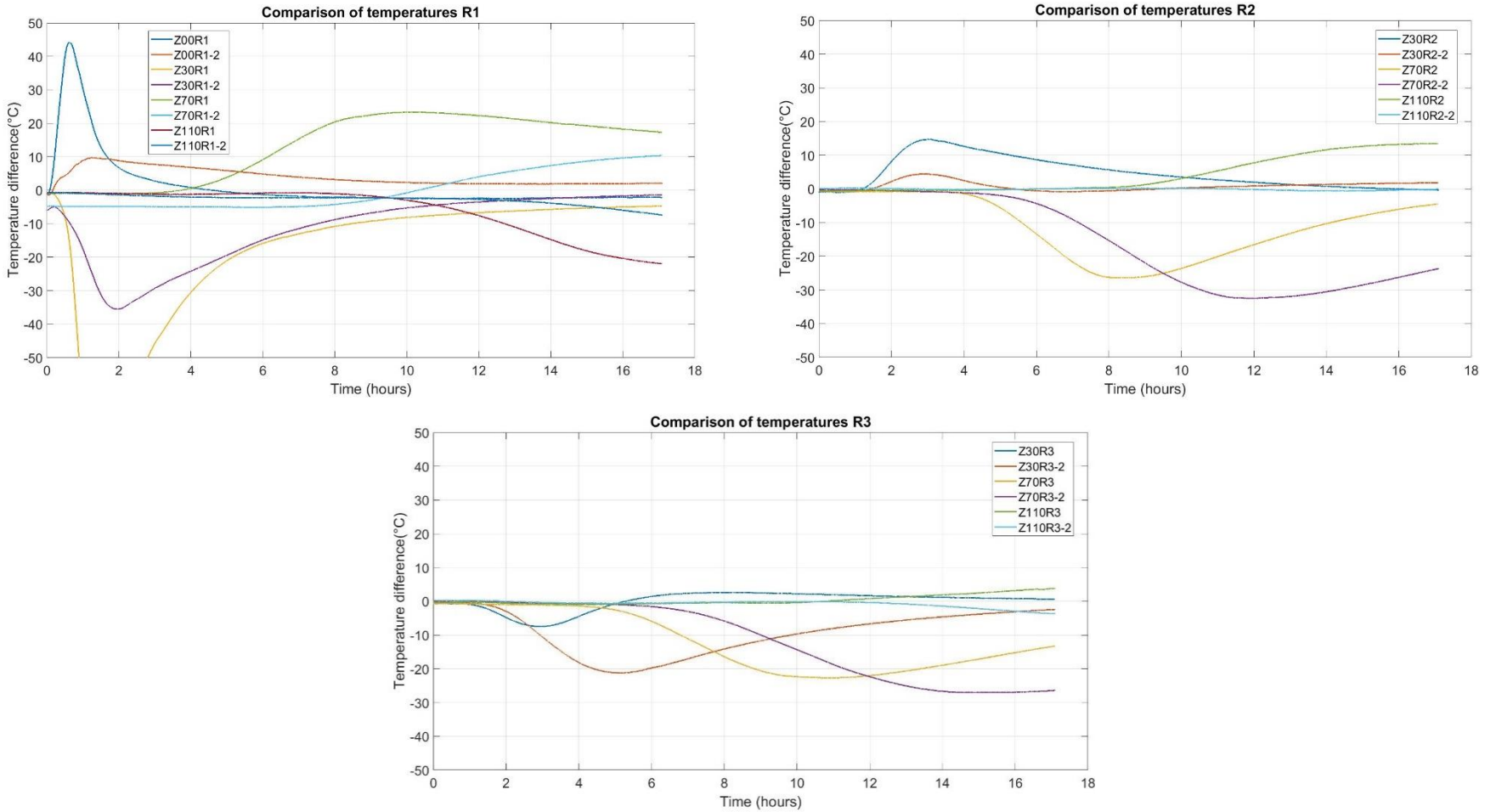

Figure 37 Temperature differences between NW and SW faces for a normal test and a 2-heaters test (indicated with number 2 after the hyphen).

Looking at all the set, the temperature differences between both tests and faces are not big enough, that means that it can be considered that the temperature distribution is equal for all the 360° of the hemisphere. Particularly, in the case of R1, the biggest temperature differences are found in the normal test: less than 5% for Z70 and 11% for Z110. However, for R2 and R3 the biggest differences are in the test performed with one heater off at Z70: 8% and 11%, respectively. It can be said that the biggest divergences occur in Z equal 70.

5.1.3.2 One heater shut off with charge energy held constant

To further test the inlet flow distribution, two tests with the same energy provided were compared. Specifically, two slow charges at 120 m³/h for 24 hours were carried out, but the second one was carried out with one heater off keeping the same total flow rate in this case. The heater switched off was number 1, corresponding to the east thermocouples face.

The main reason of this comparison is to check if the energy stored and recovered are equal for both tests. If it is, it means that the distribution of the hot air inside the bed is balanced for all its volume per each high.

So, next it is shown the performance of the heaters and the flow rate during the charge phase of both tests. In both cases, all heaters were set to and reached 600°C and kept on this value through all the period. The heater number 1 during the second test was switched off, and its temperature increases a bit because of its proximity to the rest of the heaters and to the storing device. Regarding the flow rate it is shown that it is subtly greater in the second test, so it has an impact on the amount of provided power.

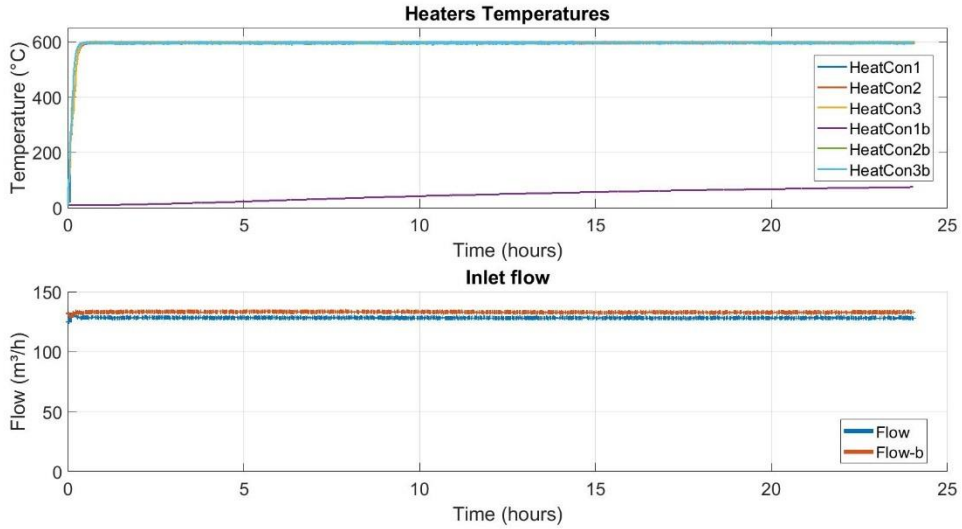

Figure 38 Comparison of heaters temperature and flow rate during the charge phase. Letter "b" indicates the test carried out with only 2 heaters.

It has also been checked the pressure drop of the Droplet for both charges. Like the input flow rate is almost the same, the pressure drop before the heaters increases when one heater is switched off because the inlet air section is reduced by one third. On the other hand, the pressure drop after the heaters is practically the same. Next, both pressures are drawn during the charge for each test and they show the pressure increase before the heater.

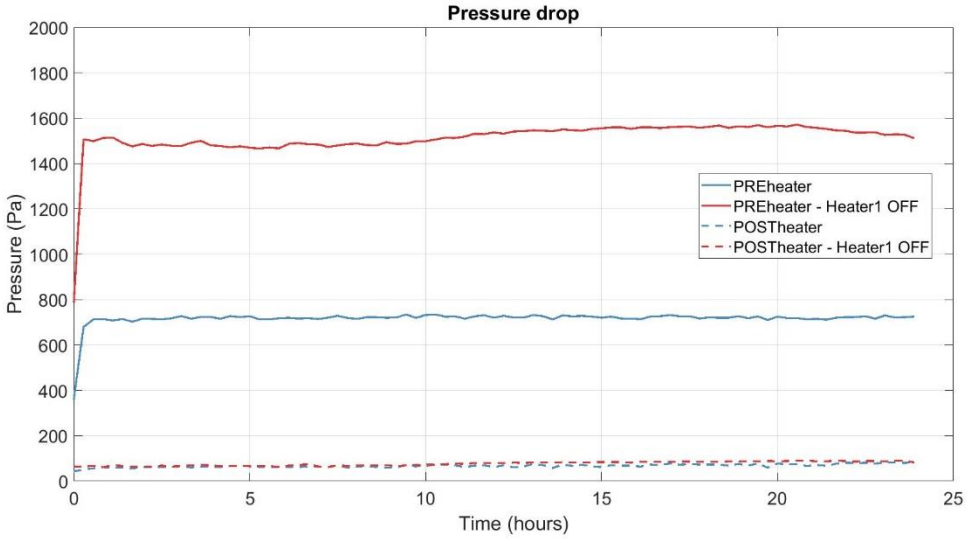

Figure 39 Pressure drop before and after the heaters for both tests.

The mean value of the preheater pressure gauge goes from 719 Pa for the normal test to 1.517 Pa using only two heaters, so the pressure drop is more than doubled in this case as expected, because the pressure drop scales with the square velocity and the air section before the heaters is reduced by one third, so the air flow rate that see every heater is increased by 1,5. The mean value after the heaters should be the same, it is 68 Pa and 76 Pa, respectively for both charges, quite close values.

If we take a look into the temperatures inside the rock bed there is no difference between the values of the three faces of thermocouples and their behavior is essentially the same, except that the Droplet was a little bit colder before starting the charge in the second test, the one only heated by two heaters.

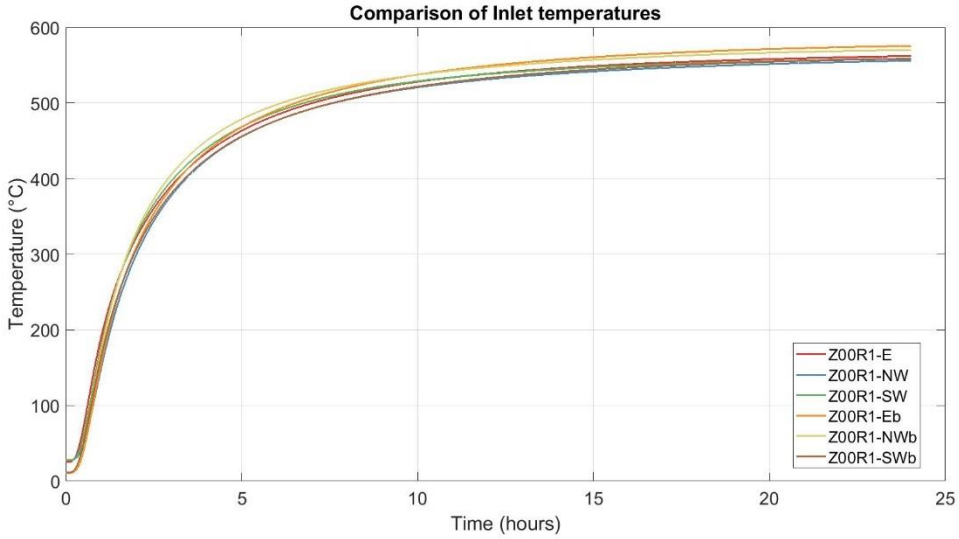

Figure 40 Temperatures on the top of the rock bed for both tests. Letter "b" indicates the test carried out with only 2 heaters.

The following figure shows the energy provided to the rock bed and the energy stored by the rocks along the charge of both tests. As the flow rate of the test performed with one heater off was greater, the energy provided was also higher at each time. The energy stored looks to have the same behavior for both tests.

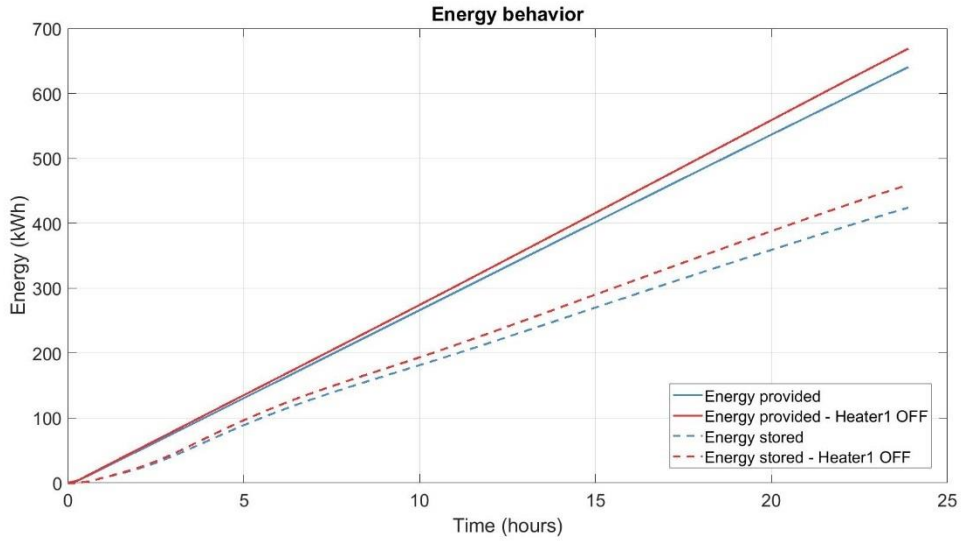

Figure 41 Provided and stored energy evolution during two slow charges.

At the end of the charge the energy values were the following:

Table 3 Energy values for a normal slow charge and one with one heater off.

Test (120m³/h 24h)	Energy provided [kWh]	Energy stored [kWh]	Charge efficiency	State of charge
Slow charge	648,68	424,11	66%	43%
Slow charge Heater1 off	673,95	459,21	68%	46%

Although the energy provided was a 4% higher for the second test compared to the first one, the energy stored was an 8% bigger. The state of charge of the Droplet was also higher for the second test. Despite these differences, we can conclude that both tests had the same charge efficiency, and therefore, the same behavior of the distribution of the air during the charge phase.

Comparing the charge efficiency for the first and second principles against the state of charge of the rock bed it is also noticed that it is higher in the case of the charge with two heaters, but this difference is because of that flow rate discordance. Both curves follow the same profile in a very close way.

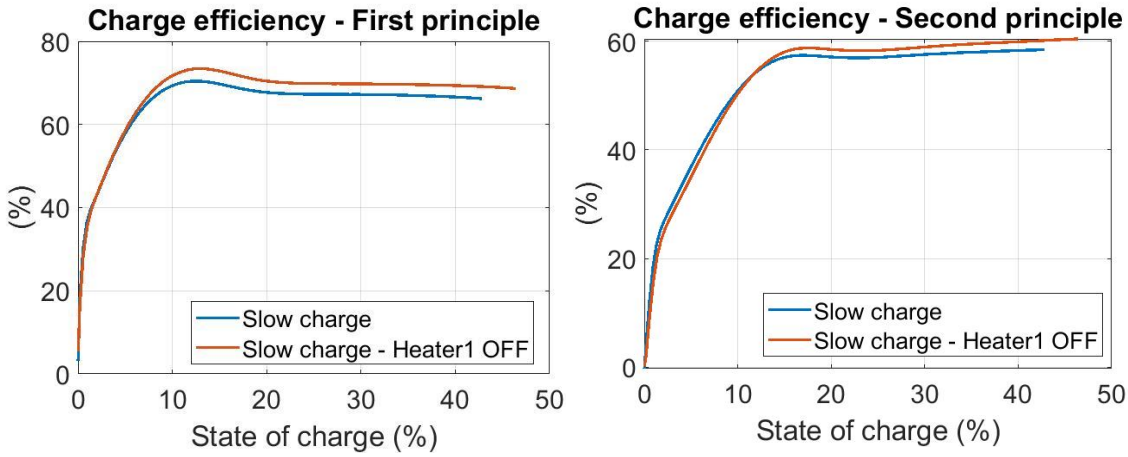

Figure 42 First and second principles charge efficiency of two slow tests.

The discharge of these two tests was done under the same conditions: all the outlet pipes opened and a flow rate of 120 m³/h. Regarding the outlet temperature of the discharge and the recovered power it is noticed that it is smaller in the case charged with all the heaters. Surely this is due to the energy provided that was greater in the second test. Anyway, they have the same behavior and they values are not very different.

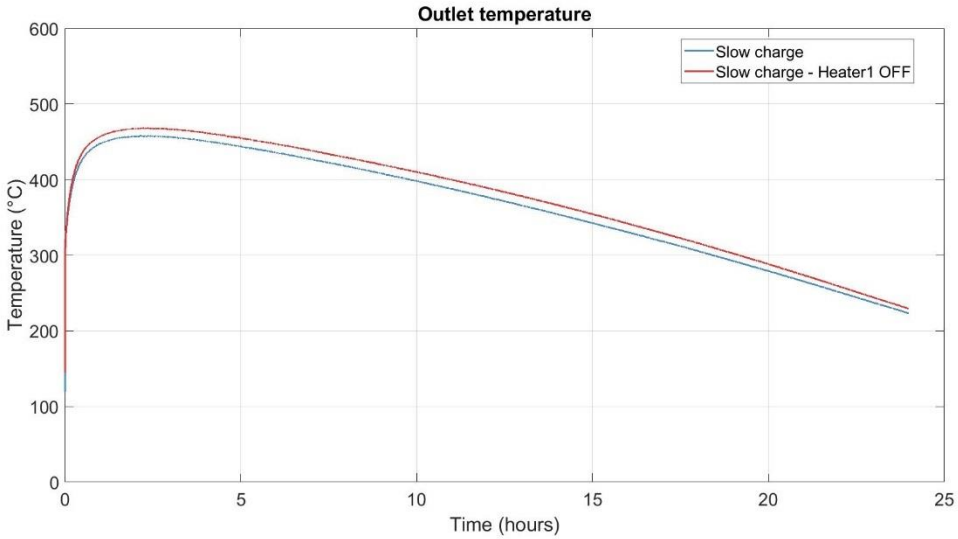

Figure 43 Outlet temperature during the discharge phase.

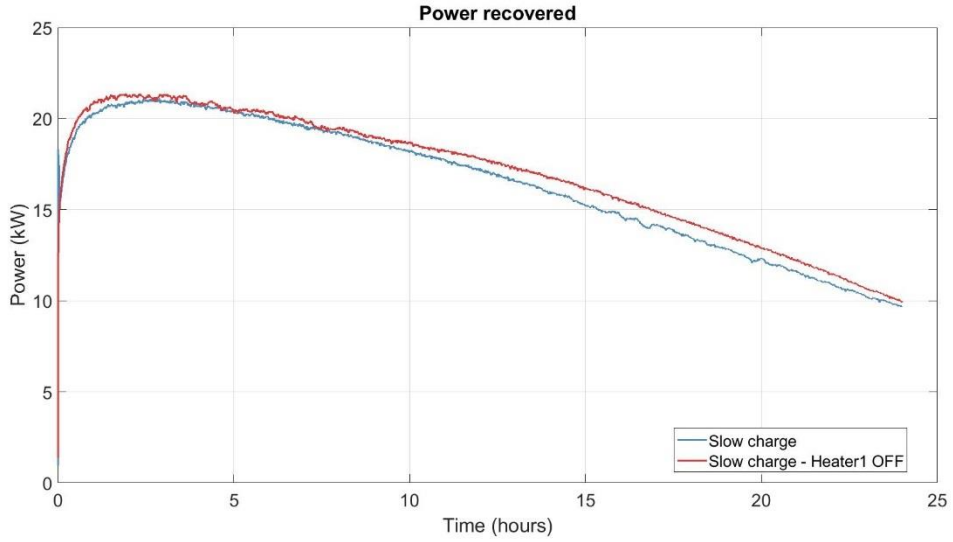

Figure 44 Power recovered during the discharge phase.

The power recovered reached around 21 kW between 1 and 4 hours after starting the discharge in both cases and the power that they still gave after 24 hours was 10 kW.

The energy recovered along the discharge period is very similar in both tests except that after some time the one charged with three heaters recovers less energy because it also was less charged. This fact can be apreciated in the next figure.

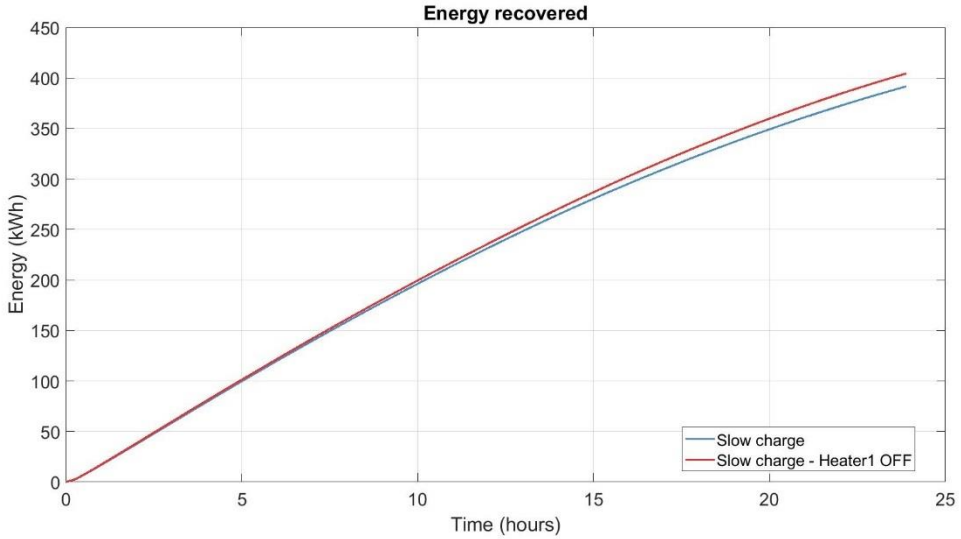

Figure 45 Energy recovered after 24 hours of discharge for every time.

So, the efficiency of the discharge phase is summarised in the next table:

Table 4 Energy values for two slow discharges, one charged with one heater off.

Test discharged at 120m³/h for 24h	Energy stored [kWh]	Energy recovered [kWh]	Discharge efficiency
Slow charge	424,11	394,87	93%
Slow charge Heater1 off	459,21	407,32	88%

The energy recovered is more or less the same, but like the test realized with one heater off started from a more charged rock bed, the discharge efficiency is lower in this case. At the end, although the difference of the provided power between both tests, the roundtrip efficiency was practically the same:

Table 5 Roundtrip efficiency of slow charge and discharge.

Test (120m³/h 24h)	Energy provided [kWh]	Energy recovered [kWh]	Roundtrip efficiency
Slow charge	640,56	394,87	61%
Slow charge Heater1 off	673,95	407,32	60%

As shown above, it is concluded that providing the same amount of energy to the Droplet, either if it is done with all the heaters or only with two, the rock bed has an identical storage and recovery performance. So, the inlet air flow dispersion in the angular direction of the Droplet is well distributed across 360°.

5.1.4 Pressure drop and strain gauges

To ensure the good operation of the Droplet without danger, it is necessary to check the pressure drop inside the rock bed and the strain that it suffers to be sure that the built device will resist.

When increasing the temperature of the rock bed, when the hot air heats the stones, the density decreases, and it causes a pressure increase inside the storage unit. Next it is shown the evolution of the pressure drop before and after the heaters while charging the Droplet with an air flow rate of 200 m³.

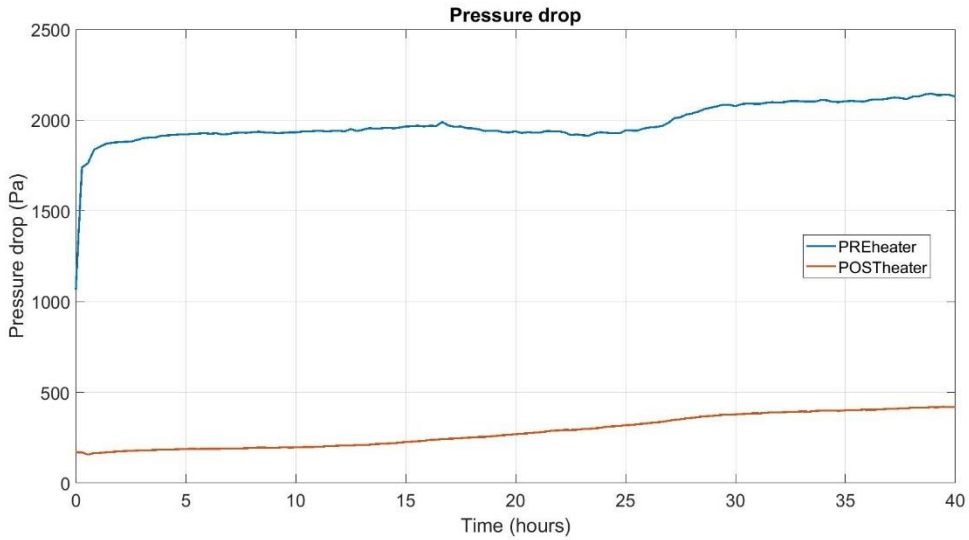

Figure 46 Pressure drop during a charge phase for 40 hours at 200 m³ before and after the heaters.

We must control that the pressure drop never reach a too high value. During all the tests carried out, the pressure drop was small and, therefore, acceptable. The graph above shows that most of the pressure drop of the setup comes from heaters. After 30 hours of charge, it can be seen that the post-heater pressure drop curve tends to stabilize, as the temperature in the rock bed begins to increase more slowly.

For the same reason, due to the high temperature and the pressure drop, there is a force tending to push the rock bed shells. The strain applied to the concrete must be controlled due to it does not behave well under traction and it can be damaged. The four strain gauges located in the concrete reported small values (average of one and a half thousandth part after 40 hours of charge) of unitary elongation what showed that the concrete will resist these high temperatures and effort.

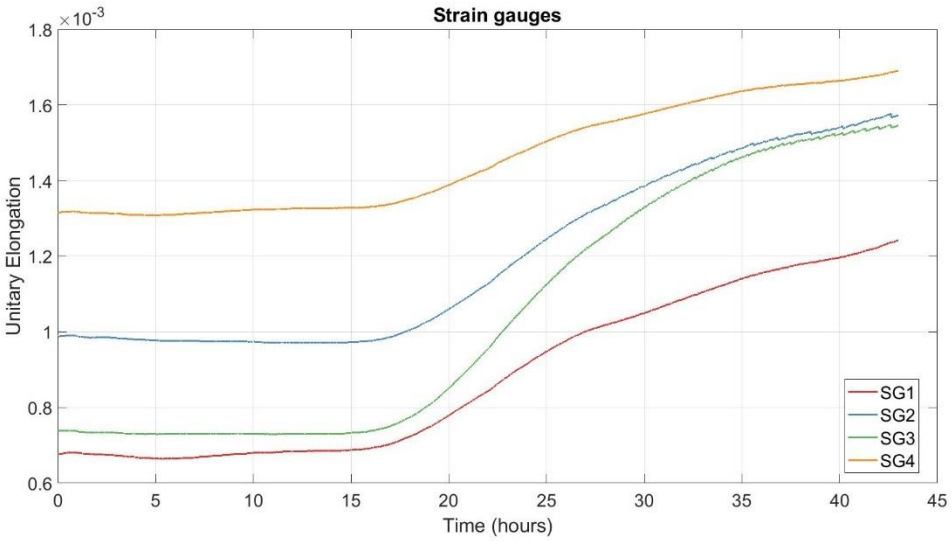

Figure 47 Unitary elongation of the strain gauges located in the concrete.

5.1.5 Power consumption

The only components that consume energy during the charge of the Droplet are the three heaters and the fan of charge. During the discharge phase, there is only the discharge fan consuming energy in order to recover the heat stored.

In most of the performed tests it was used a charge using a heater's power of 30 kW or less. For the tests carried out at maximum heater's power on average the power consumption of the heaters was 44 kW. Comparing the energy meter and the energy provided by the heaters it is found that the efficiency of the heaters is around 97%.

The electric energy input to the heater and to the fan are found as in Eq.49 and Eq.50.

$$E_{heater} = \int_{t_0}^{t_{end}} \dot{m}_f \left(h_f(T_{heater}) - h_f(T_{amb}) \right) dt \qquad \text{(Eq.49)}$$

$$E_{fan} = \int_{t_0}^{t_{end}} \dot{m}_f v \Delta p \, dt \qquad \text{(Eq.50)}$$

Where $\dot{m}_f$ is the mass flow rate of air in the considered pipe, h_f is the specific enthalpy of the air flow, v is the specific velocity of air, Δp is the pressure drop across the rock bed and t is time.

In comparison to the heaters the fans consume very little. In the next graph can be observed the consumed power by one fan depending on the required flow rate.

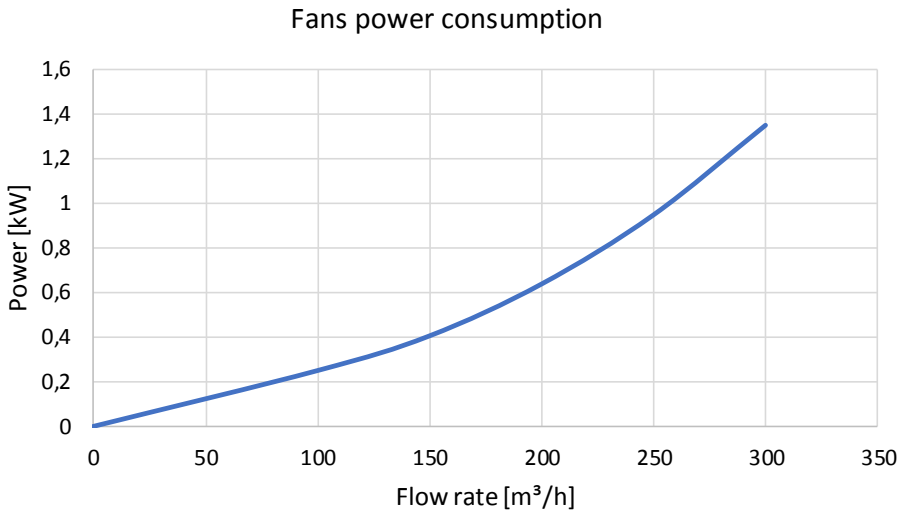

Figure 48 Power consumption of a fan depending of the flow rate. Data extracted from different tests.

Among all the electric energy required to charge the rock bed, more than a 93% is used to heat the air, in all flow rate cases.

5.1.6 Energy storage

The energy behavior through the time has the form of a growing line. The power provided by the heaters is meant to be constant, and so it is the power that enters the rock bed.

If we take a look to a fast charge for less than 17 hours the energy lost through the outlet pipe is minimum. For a charge period of 43 hours, using the same flow rate of charge, the energy lost in the outlet pipe is a 40% of the amount of energy provided. In this case, if we add the energy stored and the lost through the outlet pipe we also got a straight line that follows the energy provided, but we have lost a big amount of energy. The gain of charging more hours the Droplet is not worth it.

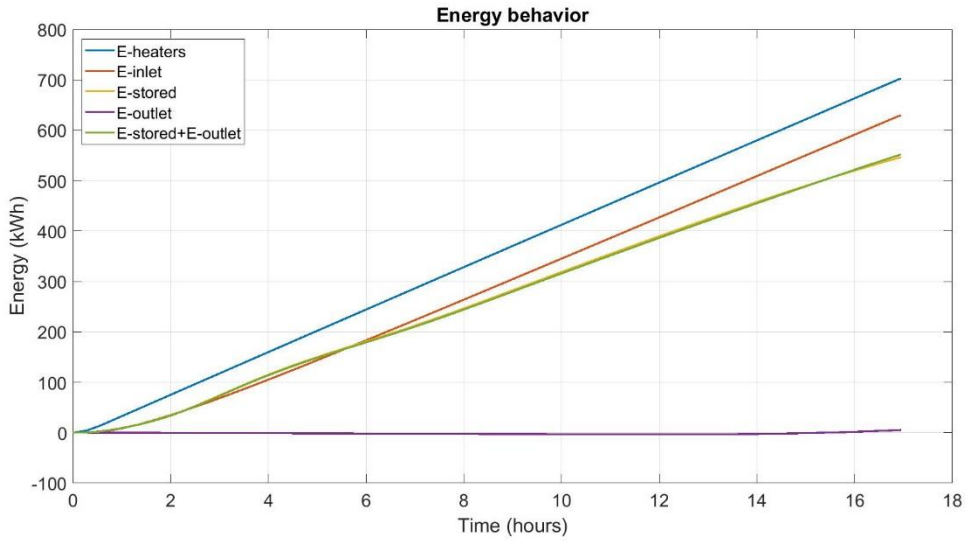

Figure 49 Behavior of the energy stored along the time for a fast charge of 17 hours.

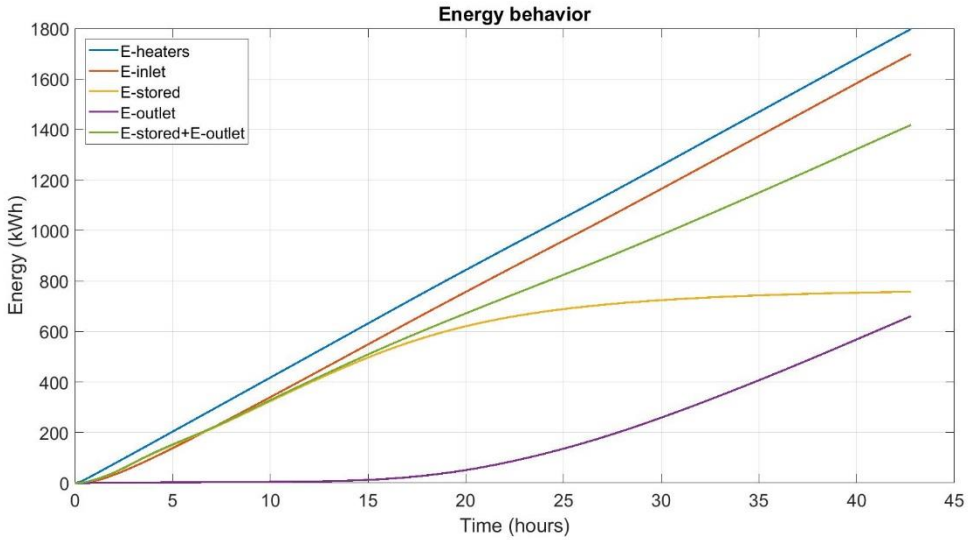

Figure 50 Behavior of the energy stored along the time for a fast charge of 43 hours.

So, every time that we want to do a proper test without having unnecessary losses, one should be aware of stopping the charge right in the moment of maximum optimization of the charge. This time can be calculated depending on the flow rate of charge.

5.1.7 IR measurements thermal losses

To be sure of the good isolation of the experimental setup, it was realized some pictures with infrared camera to check the hottest parts and their temperatures on the surface of the Droplet during a large charge. It was taken pictures after 16, 24 and 42 hours of charge in order to check the temperature evolution on the outer surfaces of the rock bed. Then it is shown IR-images of the facility and their respective temperature ranges after 42 hours of charge.

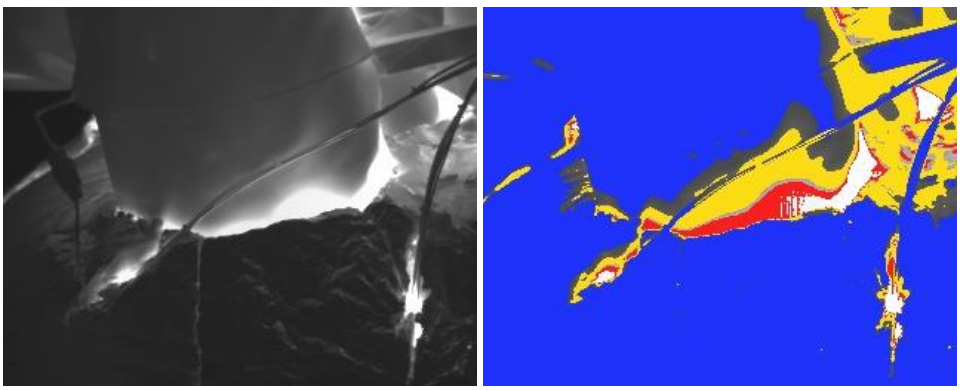

Blue: 0-120°C, Yellow: 120-165°C, Red: 120-192°C.

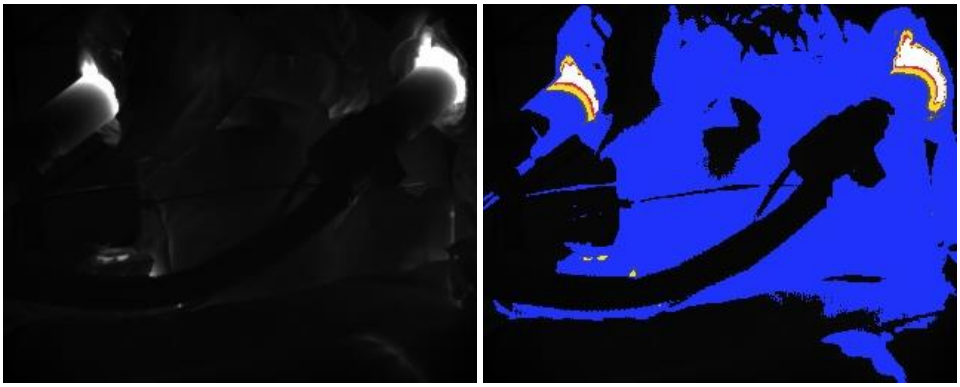

Blue: 0-60°C, Yellow: 60-90°C, Red: 90-110°C.

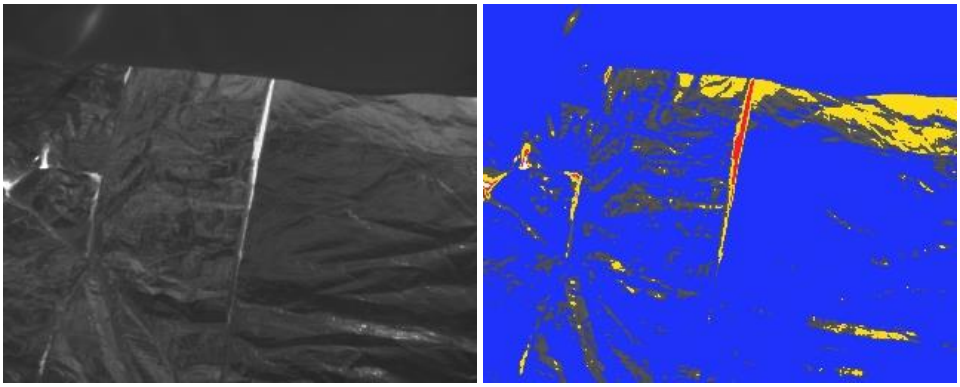

Blue: 0-45°C, Yellow: 45-70°C, Red: 70-90°C.

Figure 51 Infrared images of Droplet' surface after 42 hours of charge. Below each image there is written the range of temperatures of every color.

The hotest part of the Droplet is located near the inlet pipes where was reached 120°C. In the uncovered part of the heaters it is also reached temperatures between 60°C and 110°C. As regards rockwool, it keeps a surface temperature under 45°C. It can be observed that the critical parts are the little openings along the isolating material where the thermocouples are introduced or in the unions, as well as in the discovered part of the heaters. If it was completely well isolated, without openings or discontinuous parts, the maximum temperature of the surface would be much more lower.

For a normal test it will never reach such high temperatures because they are carried out for many less hours. So it is checked that the setup experiment would resist the heat.

5.1.8 Concrete temperature

In every test it is also checked the temperature inside the concrete. We must ensure that it would not reach 60°C, as this is the maximum temperature that can stand the concrete safely.

As it has been calculated previously, the thermal diffusivity of the heat stored inside the Droplet takes 40,5 hours to reach the concrete, so after this period the temperature of the concrete start increasing in a steeper way, as shown in the figure below.

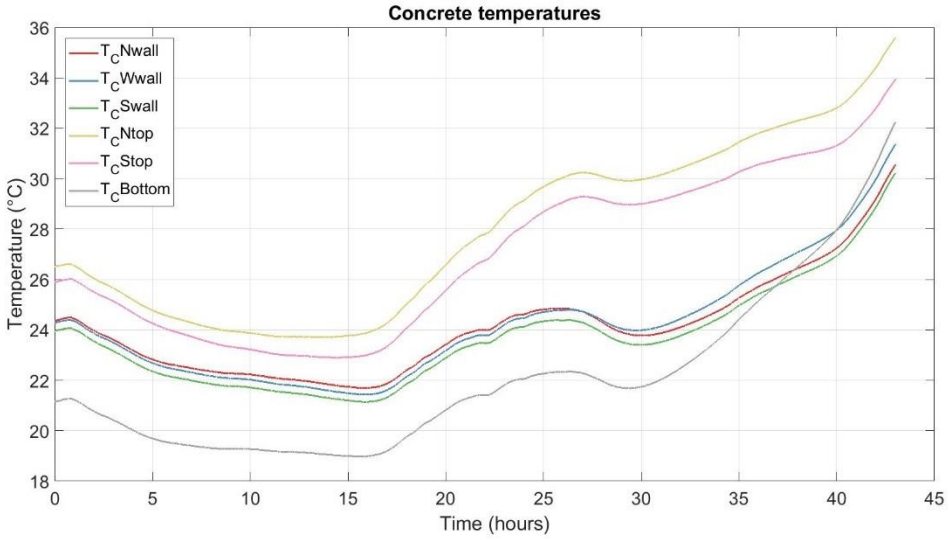

Figure 52 Concrete thermocouples temperature along a fast charge of 43 hours.

The temperature of the concrete has a long period because of the layers of insulation between it and the rock bed itself. It takes some time to start rising the temperature due to the storage of thermal energy inside the rock bed first. As the rock bed gets a higher state of charge, the rise of the concrete's temperature is faster. The top part of the concrete starts increasing its temperature before the wall, but it also colds down faster as can be seen in the next picture. Although at the end of the charge the temperature of the bottom of the concrete is higher than the one on the wall, it colds down very fast once the discharge phase has started because the bottom part of the rock bed is the first one to cool.

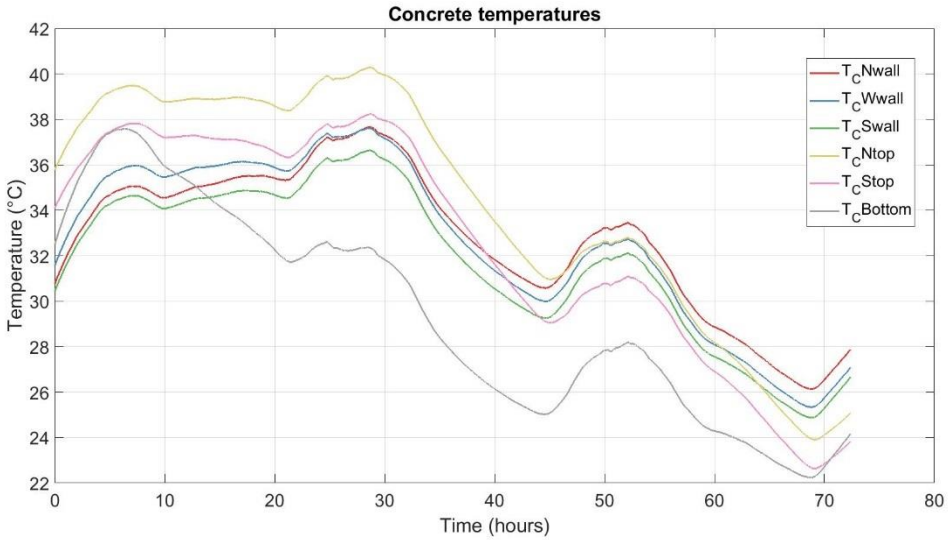

Figure 53 Concrete thermocouples temperature during a discharge period.

During the discharge phase of the rock bed, the temperature continues increasing due to thermal inertia but for a short time. It can be noticed that every about 24 hours there is a hype in the temperature of the concrete, but it tends to decrease as the Droplet is emptied. This fact is caused by the ambient temperature that has a high effect on the concrete's temperature, it slightly

increases during the warmer hours of the day and the ambient temperature helps to cold down the concrete's temperature during the night.

The maximum value that reached the concrete of the Droplet during the tests carried out for more than 40 hours was 40,28°C. The maximum temperature that reaches the concrete depends largely on its initial state. During a slow charge for 26 hours and a fast charge for 43 hours the following values were obtained:

Table 6 Energy and temperature values for different charges.

Test	Time of charge [h]	$E_{provided}$ [kWh]	E_{stored} [kWh]	$T_{top\_concrete}$ at the end of the charge [°C]	ΔT [°C]
Slow charge	26	642,68	476,68	22,20	0,18
Fast charge	16	674,43	517,88	15,16	3,05
Fast charge	24	1.008,28	669,95	24,35	7,41
Fast charge	43	1.797,57	748,07	34,77	8,56

The temperature of the concrete doesn't change much during the charging phase, there has been a maximum increase (temperature at the final state less the temperature at the start) of about 8,5°C for a charge of 43 hours. It has a wider period than the charging time, and the value of the temperature depends on how many hours the Droplet has been stopped without storing any heat, since the concrete will be colder or less. In other words, it depends on its initial temperature. Anyway, the effectivity of the isolation layers has been proved and the concrete is supposed to be able to stand all the tests realized since its temperature variation is small.

5.1.9 Energy balance

Finally, an energy balance is done per four fast charges of 24 hours to validate the calculation procedure of the energy provided, energy stored and heat losses involved in a charge phase. Next table shows the energy values obtained from the experimental data.

Table 7 Energies and heat losses involved in two fast charges of 24 hours.

Test	$E_{provided}$ [kWh]	Inlet losses [kWh]	E_{stored} [kWh]	Outlet losses [kWh]	Wall losses [kWh]	Energy in insulation [kWh]
April 8th	1.063,20	92,61	672,68	135,03	64,06	109,29
April 10th	1.061,50	92,45	678,66	147,91	64,63	134,51
April 24th	1.024,70	98,46	633,71	121,91	64,29	62,50
April 29th	1.031,50	97,42	672,24	110,72	63,00	84,61

Regarding the energy balance, the sum of the energy stored in the rock bed and in the insulation layers plus the heat losses should be equal to the energy provided. The following values are obtained for each test respectively: 1.073,67 kWh, 1.118,16 kWh, 980,87 kWh and 1.027,99 kWh. The values obtained for the energy provided are very close to the sum of the energy stored and heat losses with a maximum difference of 6%, which is a reasonable margin.

5.2 Results of the tests

The goal of this chapter is to describe the operation of the Droplet and find out an efficiency of its performance. First it is studied the behavior of the rock bed during the charge phase together with a detailed analysis of heat losses. Secondly, it is reported a similar analysis for the discharge phase comparing its result starting from the same state of charge. Then, the result of the roundtrip cycle (charge phase followed by discharge phase, without storage period) is shown. Finally, it is proposed a measure to improve the efficiency of the apparatus.

It is important to remark that all charges were started from almost the same start point: empty bed. This means that all the temperatures of the rock bed were more and less at the ambiance temperature, approximately 20°C, so there was almost no energy stored.

5.2.1 Charge phase

All charges have been realized for an input temperature of 600°C. Due to the power of the heaters, the maximum air flow rate that we can make flow through the inlet is 200 m³/h, corresponding to the fast charge, otherwise the heaters are not able to heat the air flow up to 600°C. On the other side, the slow charge is limited by the heat of the heaters, it must be a minimum quantity of air flow to ensure the absorption of the heat provided by the heaters and not get them burned. So, the slow charge corresponds to a flow rate of 120 m³/h.

It is reported the behavior of a slow charge of 24 hours followed by a fast charge carried out for 16 hours, what is equivalent, in both cases, to provide enough energy to charge the Droplet approximately at 65%. The inlet temperature of the air into the rock bed followed the next curve during both charges:

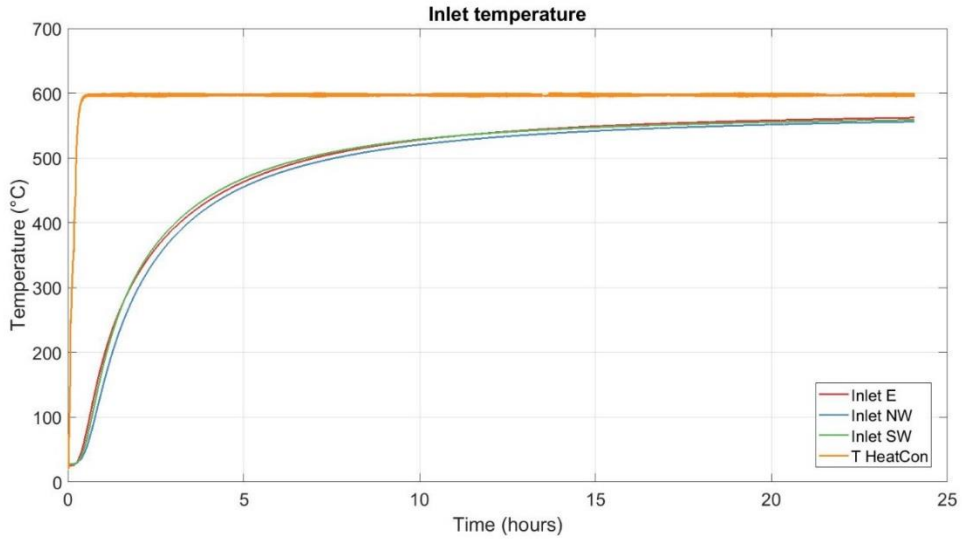

Figure 54 Inlet temperatures of a slow charge of 24 hours.

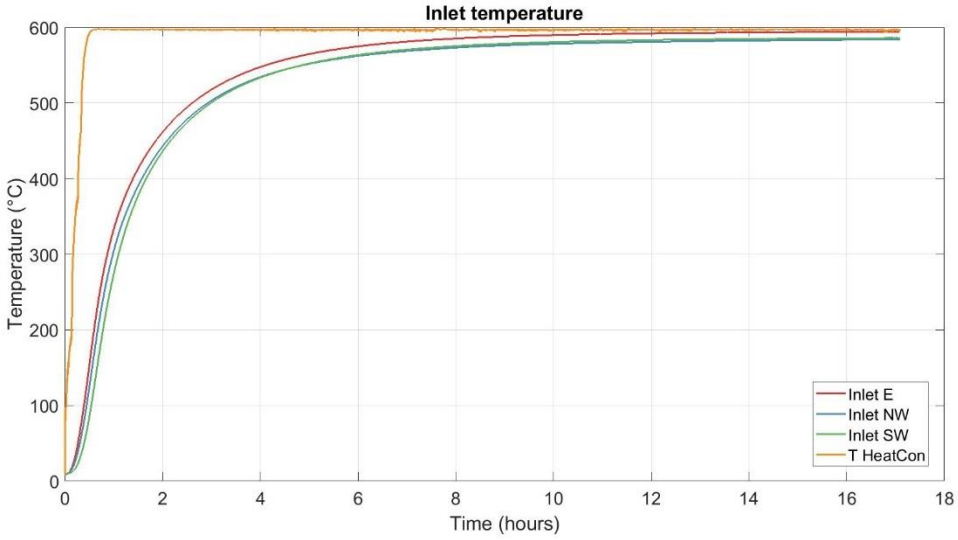

Figure 55 Inlet temperatures of a fast charge during 17 hours.

It can be appreciated that for the fast charge the input air increases faster its temperature and it reaches a higher temperature at the end. While, at the end of the charge, the air enters at 559°C for the slow charge, for the fast one it enters at 587°C.

The evolution of the temperatures inside the rock bed is shown in the next two images; one to compare it throughout the vertical direction and the other one through the radial direction for Z equal 30, 70 and 110, both for the NW face, for slow and fast tests.

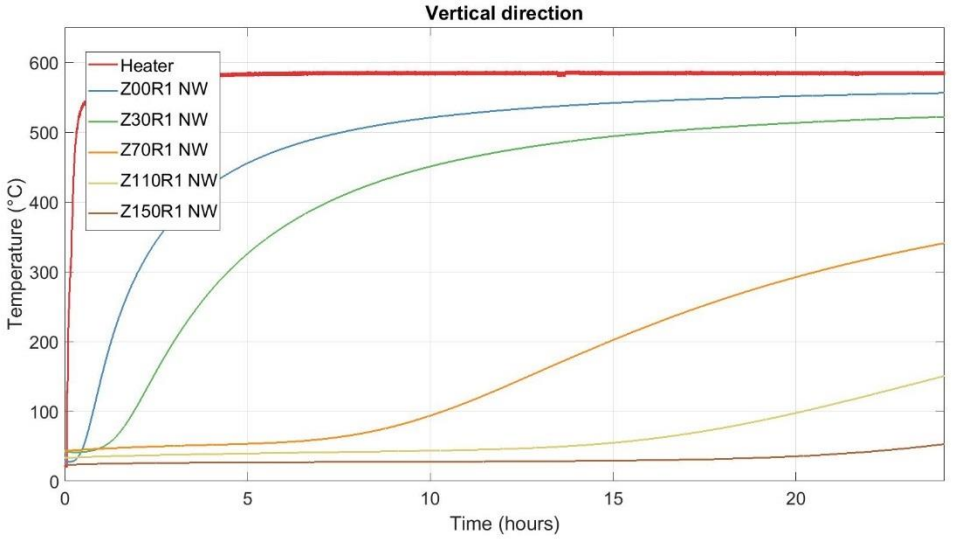

Figure 56 Temperature behavior of thermocouples located in R1 and different height for a slow charge.

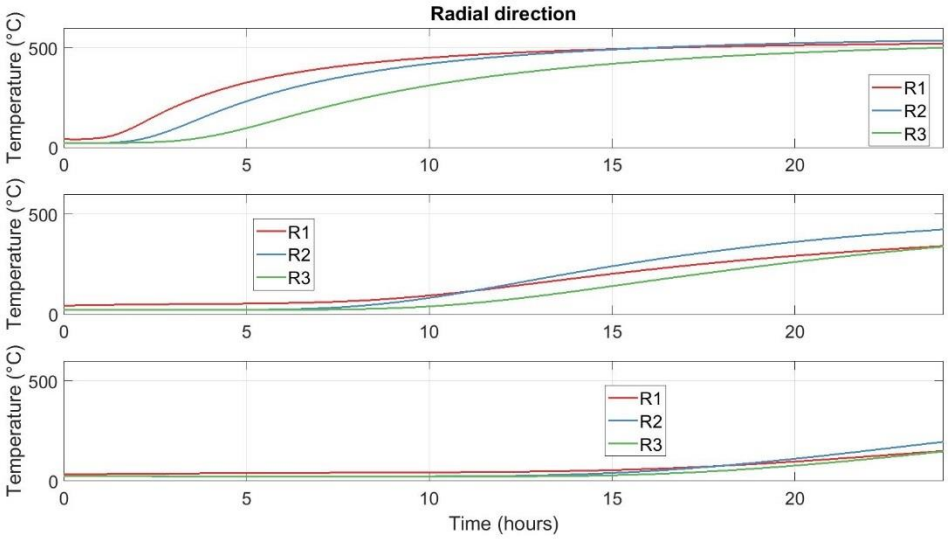

Figure 57 Temperature comparison between the three thermocouples located in each Z for a slow charge.

The previous images show that the temperature of the rock bed start rising in the top and Z00 reaches easily the input temperature. When farther from the air flow entrance, it takes more time to increase the temperature of the stones. The thermocouples located on the bottom (Z150) do not start rising their temperature until after 20 hours of charge.

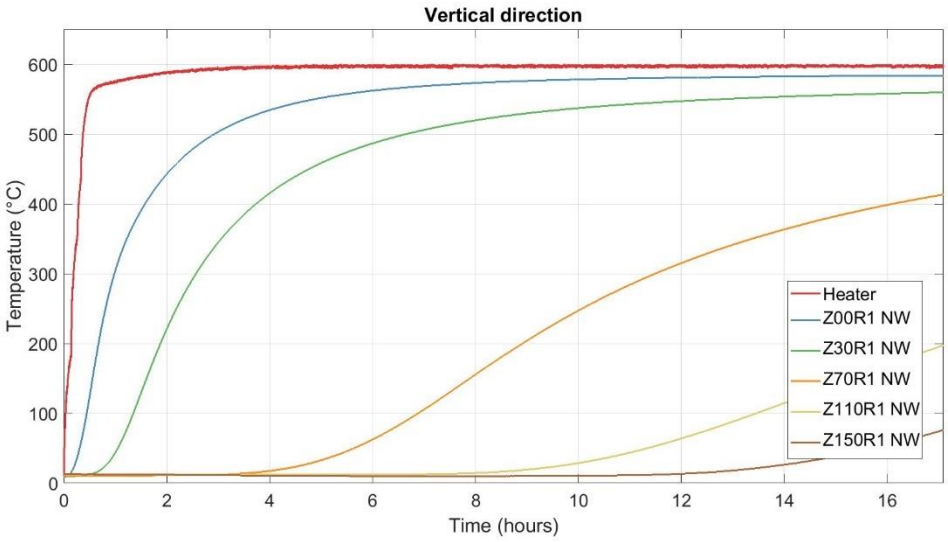

Figure 58 Temperature behavior of thermocouples located in R1 and different height for a fast charge.

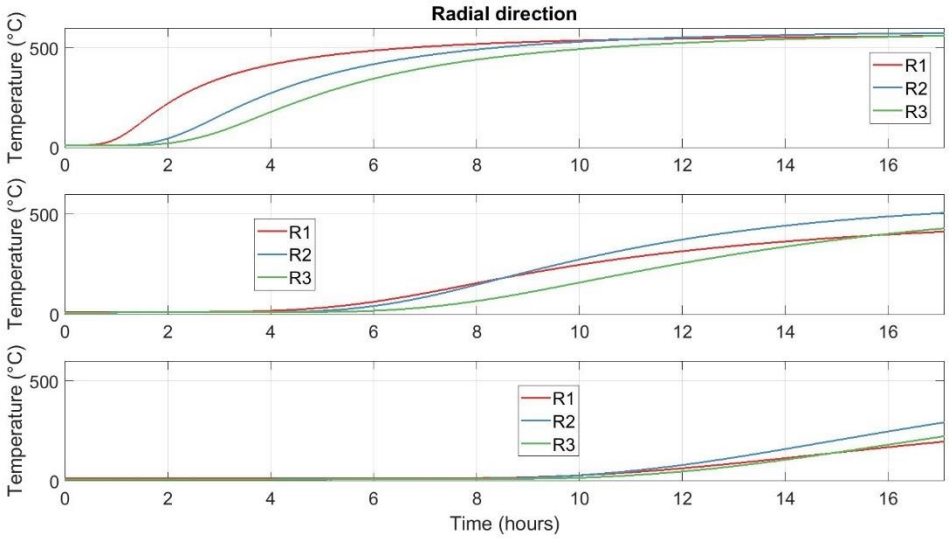

Figure 59 Temperature comparison between the three thermocouples located in each Z for a fast charge.

The fast test follows the same behavior that the slow one but increasing early the temperature of the bed. So, it ends with the same temperature in all its volume with shorter time. In the next two images it is showed the temperatures for the three faces with thermocouples inside the Droplet at the end of each charge what is proportional to the energy stored in the rock bed. It can be appreciated that the second graph presents higher temperatures reaching a state of charge of 51%, when for the slow charge the SOC reached is about 43%. Providing the same amount of energy, the rock bed ends more charged with a faster air flow.

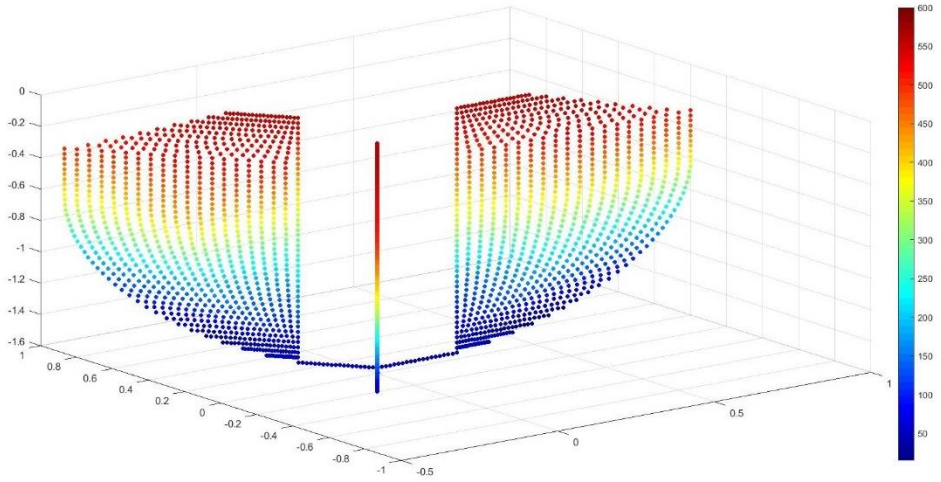

Figure 60 Temperature inside the rock bed for a slow charge after 24 hours.

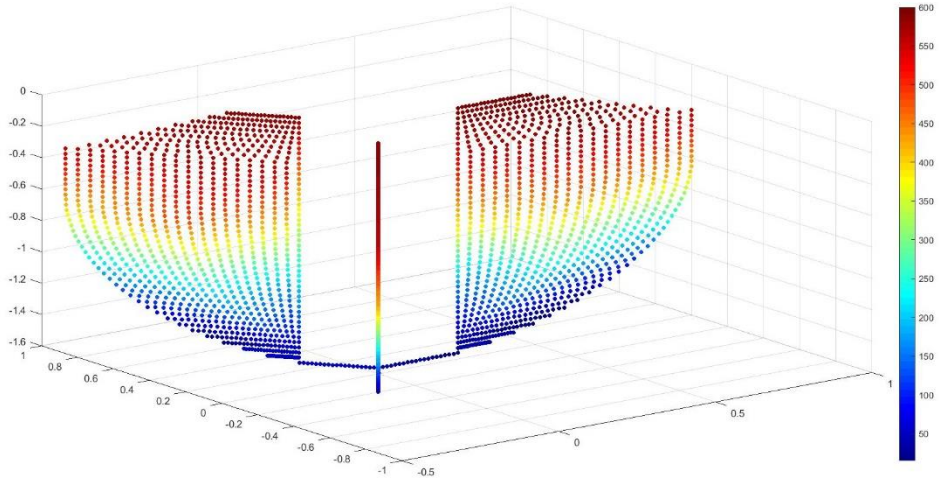

Figure 61 Temperature inside the rock bed for a fast charge after 16 hours.

It is also shown the temperatures inside the rock bed after 24 hours and after 43 hours with a fast charge, what corresponds to a state of charge of 70% and 76%, respectively.

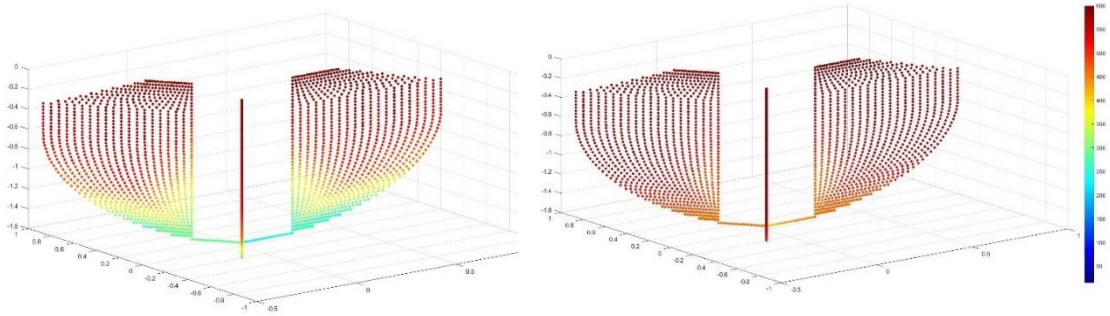

Figure 62 Temperature inside the rock bed for a fast charge after 24 and 43 hours.

The energy provided by the heaters increases linearly along time. The behavior of the energy stored depends on the thermal losses of the device. The evolution of the amount of energy provided with the heaters, stored and extracted through the outlet pipe is shown below.

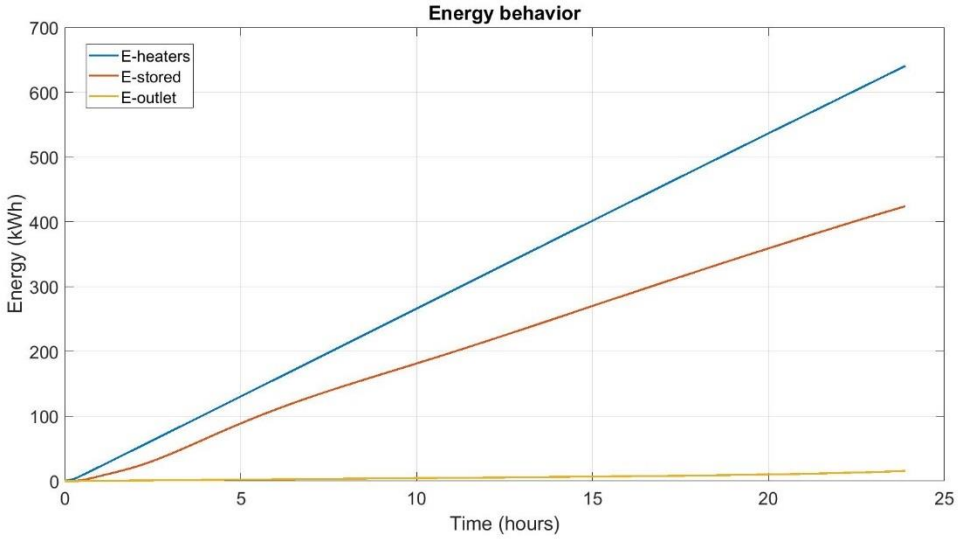

Figure 63 Energy behavior of a slow charge for 24 hours.

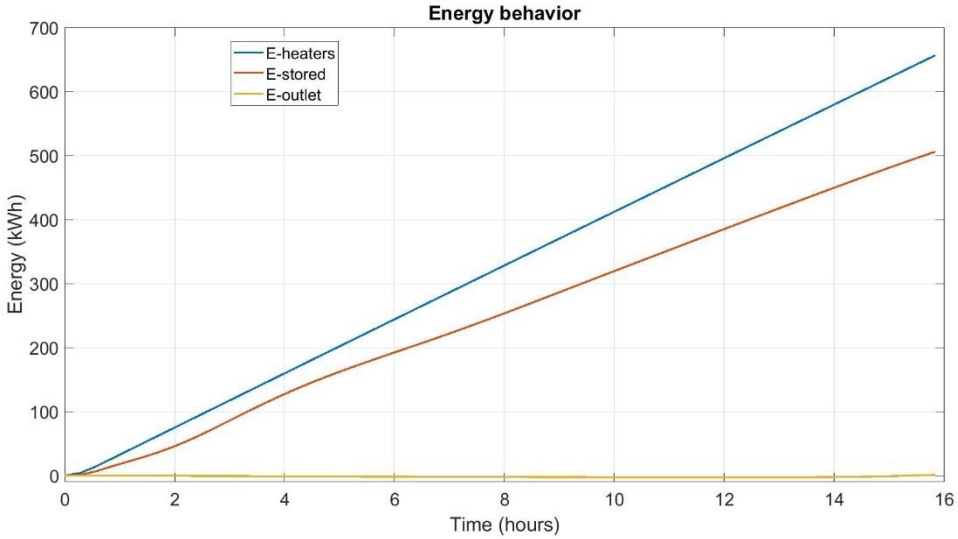

Figure 64 Energy behavior of a fast charge for 16 hours.

Both tests were stopped before having big energy losses, so they almost follow a straight line. Due to the big air flow rate, the energy provided with the fast charge during the same amount of time is almost the double. But, after 15 hours of charge the outlet losses start increasing and so, the gain of energy stored is not that much after the studied period.

Next it is shown the power lost through the outlet pipe and through the isolation walls. Both increase during time, the losses through the outlet pipe in an exponential way and the ones through the walls in a softer way.

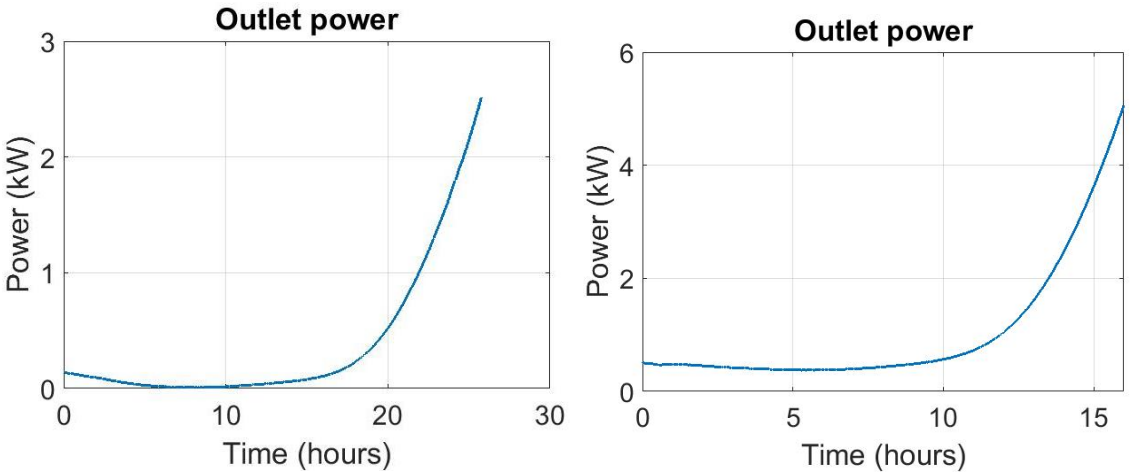

Figure 65 Power lost through the outlet pipe during the slow charge (left) and fast charge (right).

The losses through the outlet pipe are minimum because both tests were stopped at the right moment. For a slow charge after 20 hours and for a fast charge after 10 hours, the thermal losses through the outlet pipe increase rapidly, representing important power losses after more hours. Looking into a fast charge of 40 hours, it can be observed how fast these energy losses increase due to the difficulty to store more energy inside the rock bed until it is reached a stationary state:

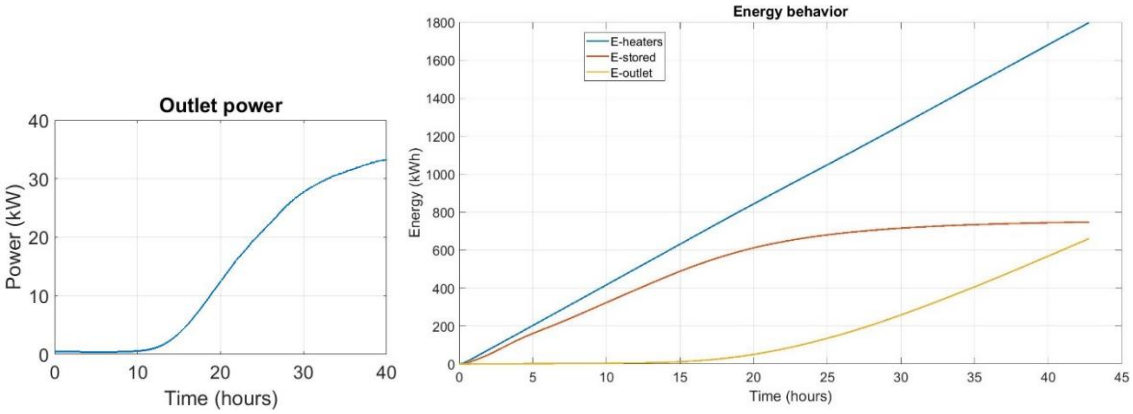

Figure 66 Outlet losses and energy behavior for a charge of more than 40 hours.

On the other hand, looking the losses through the isolating layers, they are not so different respect a slow or fast charge. They increase progressively during time and they reach a value around 3,6 kW at the end of both charges, therefore, they rise a little bit quicker with a fast flow rate.

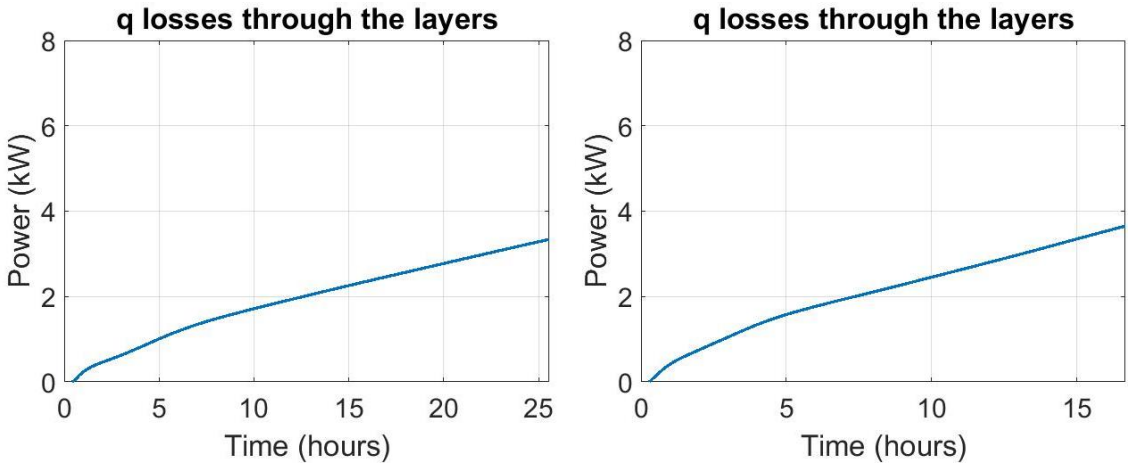

Figure 67 Power lost through the isolation layers during both charges.

At the end of the charge, the following results are obtained for both types:

Table 8 Energy and exergy results of both charges.

Test	$E_{provided}$ [kWh]	$B_{provided}$ [kWh]	U_{stored} [kWh]	B_{stored} [kWh]	T_{rocks}^{max} [°C] (Z30R2)
Slow charge	640,56	295,33	424,11	171,47	539,02
Fast charge	656,48	303,30	505,92	213,24	582,14

Of course, the utilization of a larger flow rate results in a higher provided energy, and so, a larger amount of stored energy for the same amount of time. Then, it is easy to see that the highest temperature of the Droplet will be reached using a larger air flow, even though the charge time was longer for the slow charge. But the important parameter to consider here is the efficiency of the processes what highlight the performance of the setup. So, the efficiency of these two charges and their state of charge are the following:

Table 9 Charge efficiencies for a slow and fast charge.

Test	η_{CH} [%]	$\eta_{II,CH}$ [%]	State of Charge [%]
Slow charge	66,20	58,06	42,83
Fast charge	77,06	70,30	51,10

It can be noticed how the efficiency values of first and second principle are higher for the test carried out at fast charge. There is a better heat exchange between air and rocks at higher flow rate. The fast charge presents a 16% advantage in terms of stored energy and a 21% in the second principle efficiency with respect to the slow charge. This mode of operation also reaches a higher state of charge of the Droplet. Differences between the tests are not only due to the heat transfer inside the rock bed, but also linked to the heat losses. An overview of the energy losses is provided below:

Table 10 Heat losses for a slow and fast charge.

Test	$E_{provided}$ [kWh]	Q_{lost_inlet} [kWh]	$Q_{lost\_through\_walls}$ [kWh]	Q_{outlet_pipe} [kWh]	T_{outlet}^{max} [°C]
Slow charge	642,68	93,80 (14,5%)	49,06 (7,6%)	13,53 (2,1%)	76,48
Fast charge (16 h)	674,43	74,23 (11,0%)	34,72 (5,1%)	5,85 (0,8%)	90,30
Fast charge (24 h)	1.008,28	92,45 (9,1%)	64,63 (6,4%)	138,65 (13,7%)	326,57
Fast charge (43 h)	1.797,57	100,89 (5,6%)	160,98 (8,9%)	668,41 (37,1%)	486,97

The contribution of energy losses is smaller for the fast charge for the same energy provided, so it has a higher efficiency. The amount of energy losses depends to a large extent on the time of charge.

Regarding the losses in the inlet pipe their influence decrease as the time of charge increase, due to the losses through the exterior keep constant and the capacity of energy storage of the inlet has been already covered. For the fast charge there is a higher peak at the beginning because of the higher flow, but then both values stabilize. The difference of inlet losses between the tests is very small and this parameter has a little impact on the result. Its main goal is to determine the thermal energy that enters to the rock bed, defining the heat stored in the insulation material surrounding the inlet and the lost energy to the ambiance.

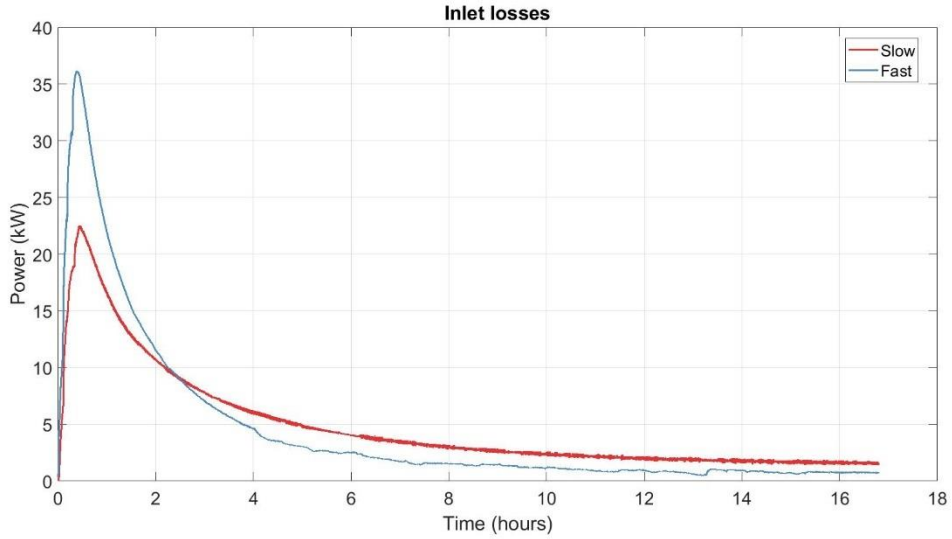

Figure 68 Losses through the inlet pipe for a slow and fast charge.

The power value of losses through the walls remains quite constant after 20 hours of charge, increasing very little, and its contribution is small. For the same state of charge there is not any difference analyzing this parameter.

Energy losses through the outlet pipe are very small at the beginning, but they increase through time as it gets more difficult to store energy, and they become an important loss of the provided

thermal energy. They become more important for the fast charge sooner. For a better comprehension of their behavior it is represented the three types of losses for a charge of 43 hours:

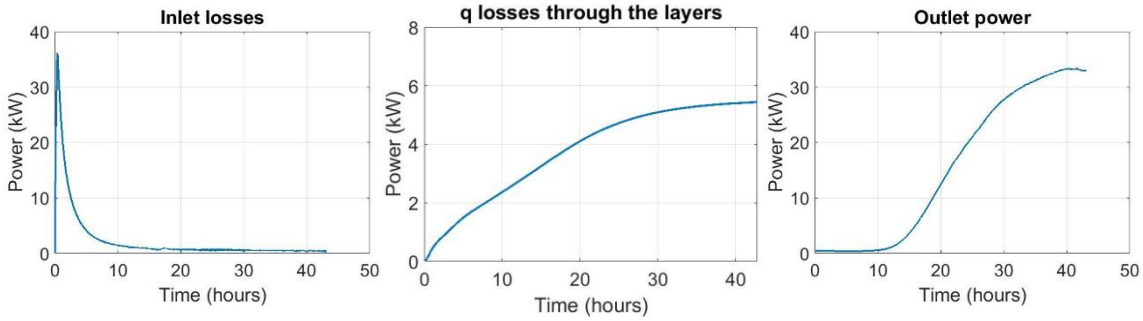

Figure 69 Inlet, walls and outlet losses for a charge for more than 40 hours.

Regarding the heat losses it is more efficient the charge at fast flow due to for the same provided energy it has less losses. If the charge is stopped at the right moment, the losses of the outlet pipe do not represent any inconvenient, as they will be very small. Losses in the inlet pipe are inevitable at the beginning, and then they keep constant.

It has been calculated the energy loss to the ground and ambiance as well. A portion of the energy losses through the isolating layers is sent to the ambiance and so, to the soil. The rest is stored in the isolating layers. The power lost outside the surface of the Droplet follows the following curve:

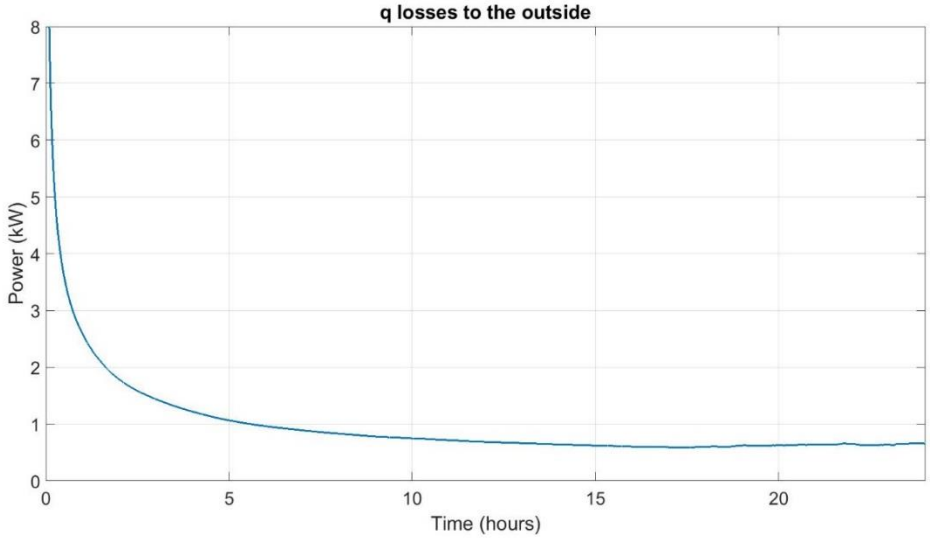

Figure 70 Behavior of the losses to the ground during a fast charge.

During the time this lost energy covers a bigger volume and so the power that receives the soil and the ambiance decrease until achieving a constant value. The losses to the ground are calculated using the semi-infinite body principle and the losses sent to the ambient are found through the external radiative and convective heat transfer coefficients.

Finally, the results of the evolution of the first and second principle efficiencies are presented with respect to the state of charge of the experimental setup as best as we can calculate with our experiment. These profiles result from the ratio between stored and provided power at each time step, whereas overall values in tables are the ratio between the stored and provided energy (exergy for the second principle).

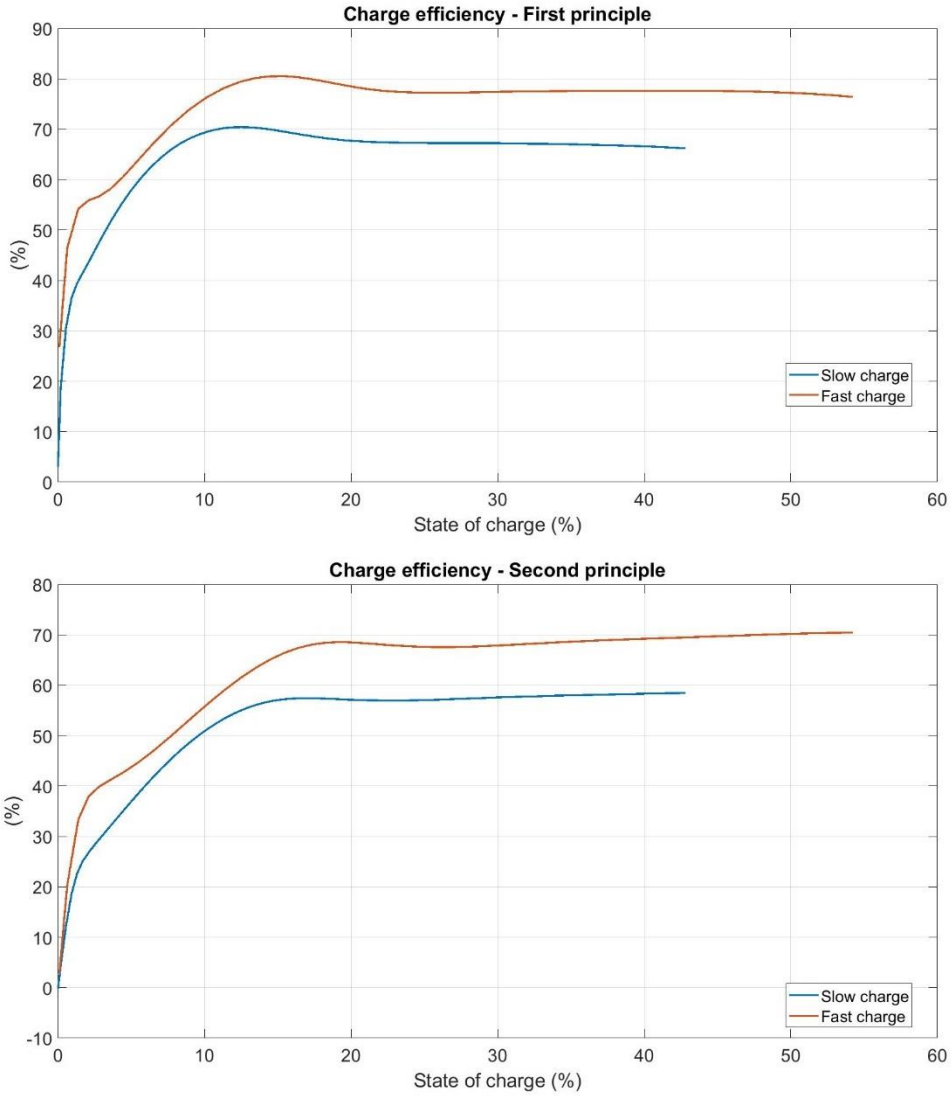

Figure 71 First and second principle efficiency evolution with respect to the state of charge of the rock bed during slow and fast charge.

After an initial transient in which the heat stored presents a peak, the efficiency sets to more constant values, with better performances given by the fast charge, after a state of charge of 15%. In both cases, it is clear how the efficiency suffers a decline after the first hours, coinciding with the moment in which heat losses start to have more impact on the storage unit. Approximately after a SOC of 50% the charge efficiency tends to decrease mainly caused by the heat losses through the outlet pipe, as shows the next graph for a charge of more than 40 hours for a flow rate of 200 m³/h.

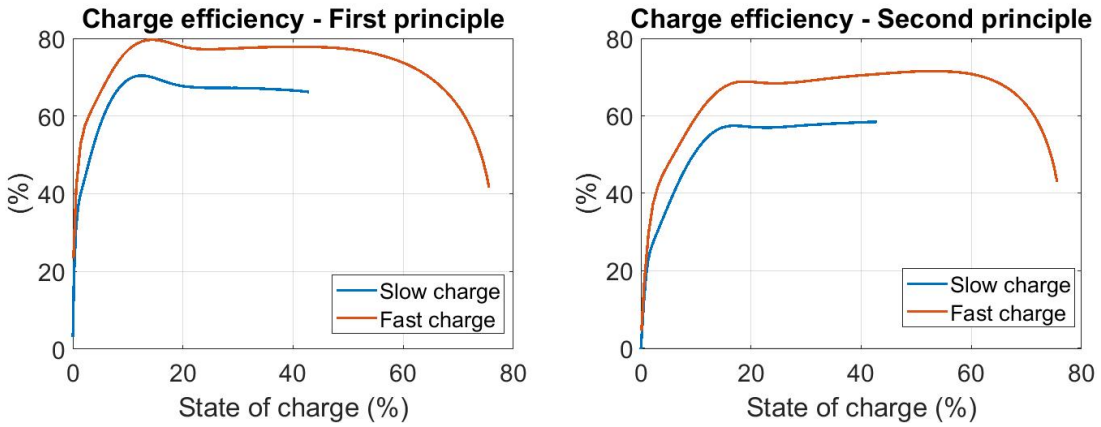

Figure 72 Charge efficiency for first and second principles depending on the state of charge for a slow and a fast charge.

Although there is always uncertainty and taking into account all the considerations, the most accurate charge efficiency of the Droplet for a fast charge, due to it is the most efficient mode of charge, is **78%**, corresponding to a state of charge between 15% and 50%.

5.2.2 Discharge phase

In order to characterize the discharge phase of the rock bed, four different discharge modes were compared starting from the same point of state of charge.

The common charge of these tests was decided to be done at a set temperature of 600°C during 24 hours at 200 m³/h of air flow rate. What corresponds to 44 kW of heaters power, providing 1.056 kWh of energy to the Droplet. Ideally, providing this amount of energy, the Droplet should be able to charge fully its energy storage capacity, but, like it has been already studied, there exists a charge efficiency and the starting point of the discharges was a SOC of almost 70%.

The different discharge tests were realized varying the air flow rate, the only parameter controllable, in steps of 50 m³/h. So, the four tests that are compared were discharged at a flow rate of 150, 200, 250 and 300 m³/h, respectively. The starting state for each test was tried to be the same although the test discharged at 150 m³/h was slightly less charged that the rest. The next table shows the main values of the rock bed before starting every discharge:

Table 11 Parameters of interest before the discharge.

Test	U_{stored} [kWh]	B_{stored} [kWh]	Starting SOC [%]	Energy in insulation [kWh]
150 m³/h	633,71	287,00	64,01	62,50
200 m³/h	678,66	315,94	68,55	134,51
250 m³/h	672,68	308,81	67,94	109,29
300 m³/h	672,24	300,90	67,90	84,61

All the discharge tests were completely discharged, but it was agreed to study and compare them after 24 hours of discharge, corresponding to a full discharge for the test at 300 m³/h. Carried out the four discharges, the following results were obtained after 24 hours:

Table 12 Discharge parameters of interest.

Test	$T_{recovered}^{max}$ [°C]	$E_{recovered}$ [kWh]	$B_{recovered}$ [kWh]	η_{DIS} [%]	$\eta_{II,DIS}$ [%]	SOC_{end} [%]
150 m³/h	509,74	569,91	221,00	81,86	68,06	13,59
200 m³/h	521,10	696,11	271,32	85,60	67,12	4,29
250 m³/h	516,65	730,04	274,05	93,36	72,18	1,49
300 m³/h	527,66	731,71	261,84	96,68	73,90	0,97

Regarding the maximum temperature recovered, it is not possible to recover the air at the maximum storage temperature of approximately 580°C for the considered charge configuration. Even starting the discharge right after the charge process, without a storage period, the air is not recoverable with temperature values close to the maximum storage ones, there exists a difference of about 60°C less.

The efficiency values of the table show that as the air flow rate of discharge increase, better is the performance of the discharge phase and more energy is recovered for the same amount of time. The test discharged at 150 m³/h recover less energy for the same discharge period although it has an efficiency of 80%. Both discharges carried out at 250 and 300 m³/h have an energy efficiency higher than 90%, almost 97% for the discharge at 300 m³/h. Hence, any discharge process of this facility has a good performance due to the good heat transfer between the rocks and the air, providing a high discharge efficiency. Actually, isolating layers also act as storage material from where is possible to recover part of the energy provided.

The energy remaining inside the rock bed after the discharge was less than a 1,5% of the storage capacity for the ones realized at high flow rate, whereas for the discharge at 150 m³/h and 200 m³/h the SOC at the end was around 14% and 4%, respectively, so there was still some energy left available to recover.

Next it is presented graphically the behavior of the air flow recovered during the discharge for each test:

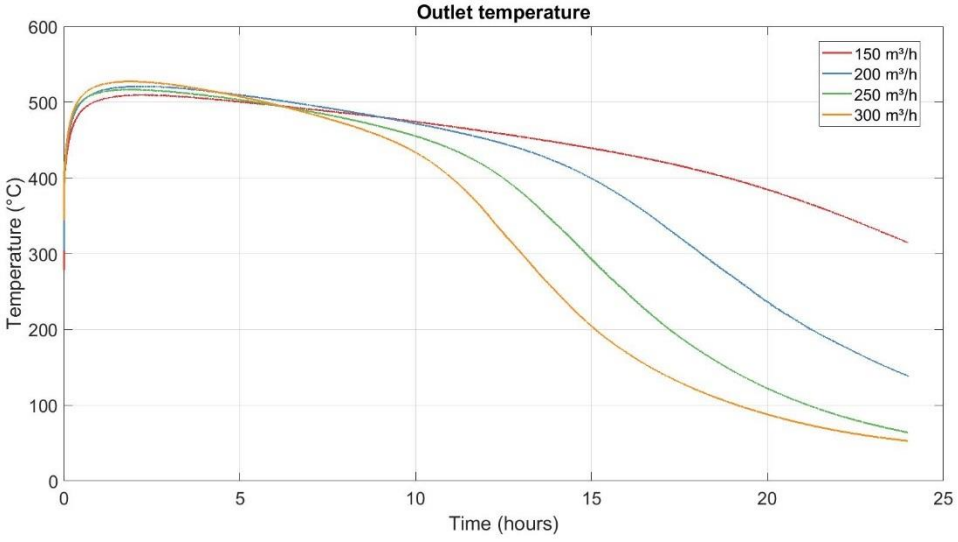

Figure 73 Outlet temperature for the four discharges.

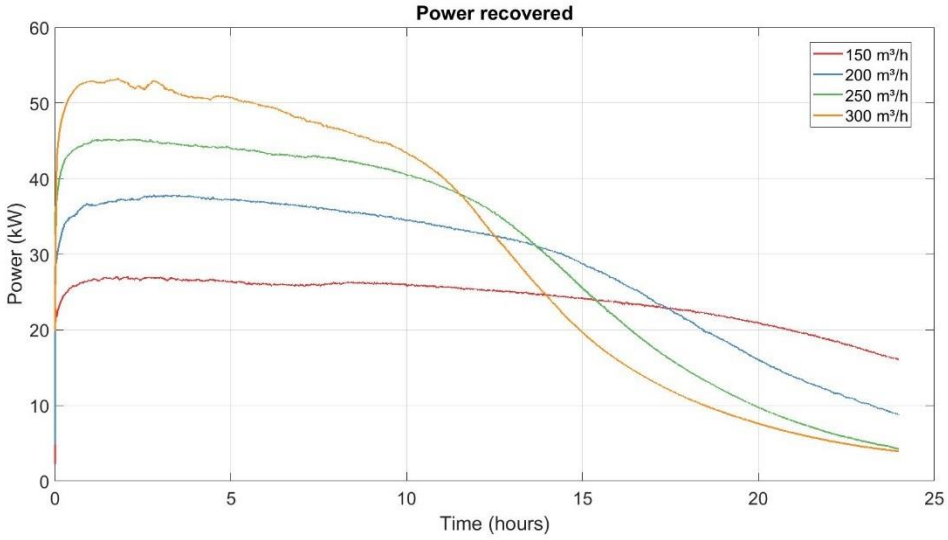

Figure 74 Power recovered during four discharges at different flow rate.

The recovered outlet temperature, in all four cases, reaches more than 500°C during the first hours. For the first 10 hours the air temperature is almost the same for all the studied discharge modes. Then the temperature slowly decreases for the test realized at 150 m³/h and in a steeper way as the flow rate increase.

The recovered power is function of the temperature of the air and the flow rate. So, at the beginning, when all the tests have the same temperature, the power recovered will be higher for higher air flow. If we are interested in a high power, the best discharge option is to carry it out at the maximum flow rate, but if what we need is a stable power during longer time, then better chose a slower range of discharge air flow although it will provide less power.

In real-life, this recovered hot air can be use in several applications that need heat. Particularly, in the end, it is thought that a rock bed storage unit is meant to be sent to a heat recovery steam generator to produce electricity again. What would like to say that discharging at a lower flow rate will be able to provide less power to generate electricity but for longer.

It is remarkable that using this technology of storage, we can easily obtain more than 20 kW of power in 1 minute and more than 50 kW in a little bit more of half an hour using a high flow rate. In a short time, a rock bed storage unit can provide high power, so, it can answer in a quick way the energy needs.

This power results in the following evolution of energy recovered by every discharge test analyzed:

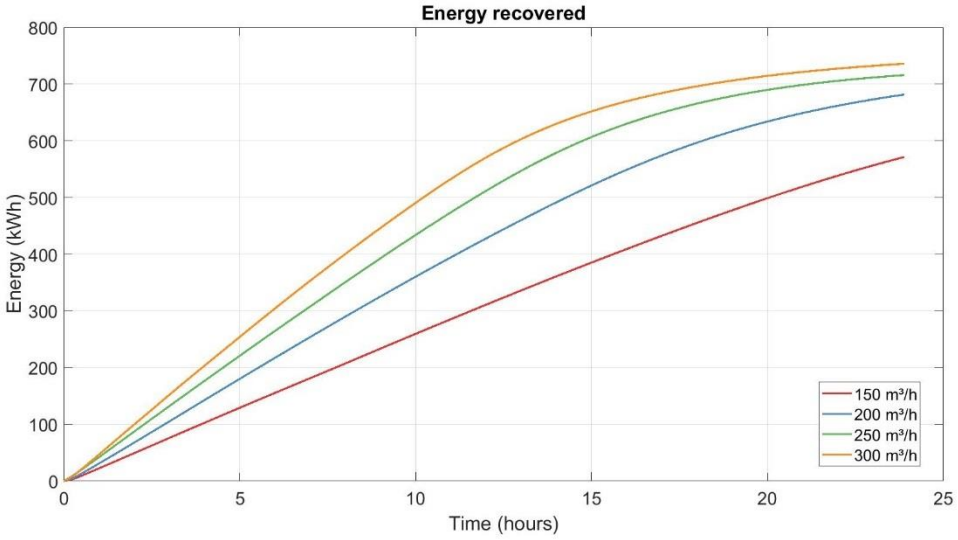

Figure 75 Energy recovered evolution for each discharge test.

As analyzed in the previous table, the curves show that the discharge done at 300 m³/h is the one that recovers more energy in less time. On the other side, the energy recovered by the test realized at 150 m³/h follows a straight line, so it gives a constant power during more time. For the same amount of time, as the discharge air flow rate increase so does the recovered energy.

Again, the best option of discharge mode will depend on the necessities of the facility, depending on how long should be discharged or how much power is needed from the rock bed. Even though, the discharge process with the best performance is done with the highest flow rate, in this case 300 m³/h, equivalent to a discharge efficiency of **97%**.

5.2.3 Roundtrip results

Starting from the performance analysis done on charge and discharge phase separately, it has been obtained an overall characterization of the rock bed storage unit determined by the roundtrip efficiency.

Next are studied the same four tests analyzed previously for the discharge process as they were charged under the same conditions: high flow rate (200 m³/h), heaters temperature at 600°C and for 24 hours. The name of every test corresponds at his discharge flow rate.

The parameters of interest of the charge phases are the following ones:

Table 13 Charge parameters of interest of each test.

Test	$E_{provided}$ [kWh]	$B_{provided}$ [kWh]	U_{stored} [kWh]	B_{stored} [kWh]	SOC [%]	η_{CH} [%]	$\eta_{II,CH}$ [%]
150 m³/h	1.042,70	475,55	633,71	287,00	64,01	60,77	60,35
200 m³/h	1.061,50	490,60	678,66	315,94	68,55	63,93	64,39
250 m³/h	1.063,20	488,95	672,68	308,81	67,94	63,26	63,15
300 m³/h	1.031,50	469,30	672,24	300,90	67,90	65,17	64,11

The charge efficiency values of these tests are lower than the one obtained in the study of the charge phase because these charges were done to get a higher SOC.

Then it is shown the results of the discharge phase:

Table 14 Discharge phase results.

Test	$E_{recovered}$ [kWh]	$B_{recovered}$ [kWh]	η_{DIS} [%]	$\eta_{II,DIS}$ [%]	SOC_{end} [%]
150 m³/h	569,91	221,00	81,86	68,06	13,59
200 m³/h	696,11	271,32	85,60	67,12	4,29
250 m³/h	730,04	274,05	93,36	72,18	1,49
300 m³/h	731,71	261,84	96,68	73,90	0,97

Discharge efficiencies, first and second principle, consider the presence of heat stored in the insulation layers. So, when the rock bed is completely discharged it is possible to have recovered more energy than stored inside the rock bed because it also recovers part of the energy stored in the isolating layers.

At the end, the roundtrip efficiencies calculated as recovered energy over provided (exergy for the second principle) are the following ones:

Table 15 Roundtrip efficiencies for same charged tests but discharged with different flow rates.

Test	η_{RT} [%]	$\eta_{II,RT}$ [%]
150 m³/h	54,66	46,47
200 m³/h	65,58	55,30
250 m³/h	68,66	56,05
300 m³/h	70,94	55,79

The energy efficiency increases as it is utilized a higher flow rate, confirming that either for a charge or a discharge phase it is more efficient the fast process.

So, the most promising setup conditions throughout the whole cycle is to charge it as fast as possible, in this case at 200 m³/h, but up to 50% of SOC and to do the discharge at 300 m³/h (flow rates limited by the actual experimental facility) as they showed to have a higher efficiency in both phases. Acting at a fast flow rate, heat losses have less time to grow and there is a better heat transfer between the rocks and the air. Concluding in a roundtrip efficiency of **75,66 %** (charge efficiency of 78% and 97% as discharge efficiency).

5.2.4 Recirculation

One way to improve the efficiency of the Droplet would be to recirculate the outlet air while charging. The energy that we lose through the outlet pipe depends on the duration of the charge. It is small during the first hours of charge, but it can become very important after about 15 hours.

This air recirculation would consist in to take advantage of the wasted hot air going out from the Droplet and to make it circulate towards the fan of charge to reheat it and bring it to the rock bed again. Like the air of entrance would be already warmer than the ambiance temperature, the heaters wouldn't need to spend so much energy on heating the air. This measure would reduce the energy provided by the heaters to heat the air up to 600 °C.

The next figure shows the amount of energy released by the outlet pipe, and that, therefore, can be saved from recirculating the outlet air for a charge at 200 m³/h.

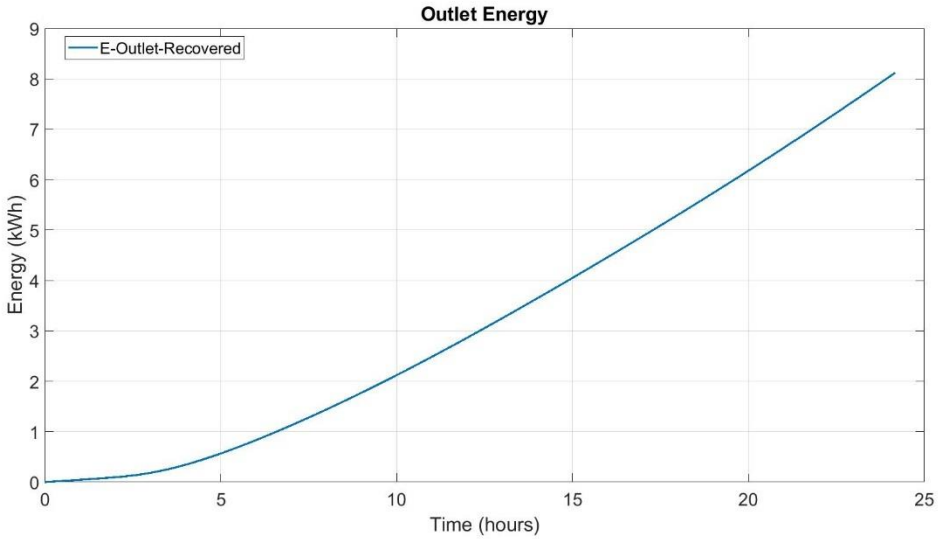

Figure 76 Energy lost through the outlet pipe that can be recovered for a fast charge.

The improvement of the Droplet's efficiency using the outlet air flow recirculation follows the next curve:

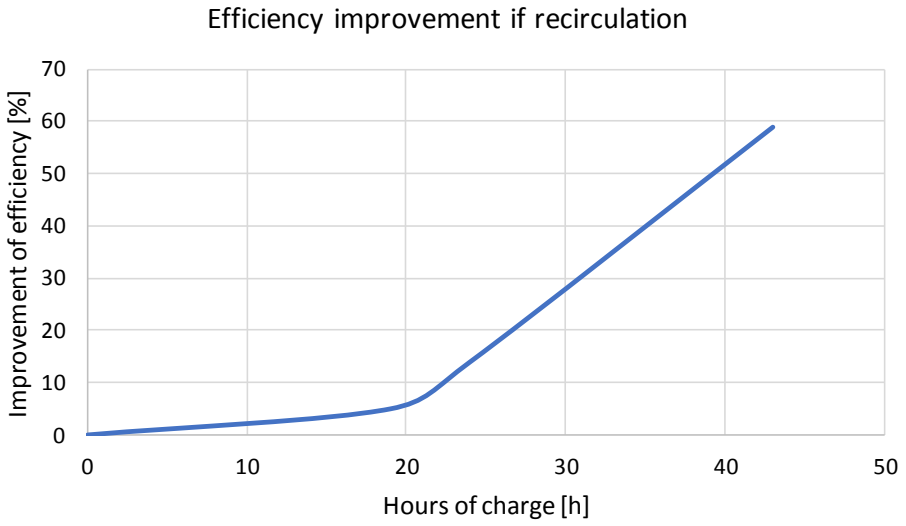

Figure 77 Improvement of rock bed's efficiency if the outlet air is recirculated during the charge.

It must be considered that the energy losses for the output line are not desirable, so it is better to stop the charge at the tight time. But using the recirculation the efficiency of the device will improve in any case.

6 Biomass gasification

Gasification is the process that converts biomass or fossil fuel into gaseous compounds by supplying less oxygen than is needed for complete combustion of the fuel, with a controlled amount of oxygen and/or steam. This is achieved by reacting the biomass matter at high temperatures between 600°C and 1.500°C. The resulting gas mixture is itself a fuel and is called syngas (synthesis gas or synthetic gas) if it is composed of carbon monoxide (CO) and hydrogen (H_2). It is called producer gas, if in addition it contains carbon dioxide (CO_2) and typically a range of hydrocarbons such as methane (CH_4) with nitrogen from the air.

The energy derived from the gasification of biomass (such as wood, bark, branches, leaves, wood chips, etc.) and the combustion of the resulting gas is considered a renewable energy source. The gasification of fossil fuels derived from materials such as plastics is not considered a renewable energy.

The advantage of gasification is that syngas is potentially more efficient than the direct combustion of the original fuel because it can be combusted at higher temperatures or even in a fuel cell. In the last decades the interest in the biomass gasification process has increased due to the growing attention to the use of sustainable energy.

Gasification of biomass resources is already being used to produce bioenergy and bioproducts for use in dual-mode engines to produce power and to produce heat, steam and electricity. Studies are underway to develop biomass gasification technologies to economically produce hydrogen, organic chemicals and ethanol for use as transportation fuel in cars and trucks and to extend its use as a source of electricity [31].

6.1 State of the art overview

The reactors used on an industrial scale to gasify a pre-treated biomass, called gasifiers, essentially differ from one another for the mode of contact between the feed material and the gasifying agent, the mode and rate of heat transfer and the residence time of the fed material into the reaction zone.

Different technological solutions can be implemented in order to obtain different plant configurations; in particular, the mode of contact of the biomass with the gasification agent may be in counter-current, or co-current, or cross flow, and the heat can be transferred from the outside or directly in the reactor using a combustion agent; the residence time can be in the order of hours (static gasifiers, rotary kiln) or minutes (fluidized bed gasifiers).

The gasification process and other biomass conversion technologies such as pyrolysis, and combustion, can provide several primary products, charcoal, liquid, fuel gas and heat that can be processed for obtaining secondary products as electricity, gasoline, diesel, methanol, chemicals and ammonia.

In the last decades, the presence of the gasification process in the European market has increased. In Europe there are 22 gasification plants and 7 companies have the know-how for

their construction. Sixteen are power generation or combined heat and power generation plants, four are co-combustion plants and two plants are dedicated to the production of chemicals.

The biomass gasification plants operating in Europe produce electricity in combined heat and power (CHP) configuration; these plants often do not produce more than 1 MWe. On the other hand, larger plants are often co-combustion plants and only few biomass gasification plants are able to produce biofuels such as methanol or other biofuels.

Biomass gasification has some advantages over traditional combustion processes, in terms of heat and power production and environmental protection [32]:

- Combustion of syngas is cleaner and more efficient respect to the direct combustion of biomass and it is possible to reduce excess air and heat loss into the exhaust gases.

- Combustion in the homogeneous phase allows greater continuity of the process and easier control.

- Volumetric flow rate of the produced fuel gas is much reduced compared to that of the effluent gas of a direct combustion process, resulting in lower costs of the cleaning process.

- Even if the syngas produced is burned on site, there is the possibility of removal of certain impurities after the gasification stage and before the syngas combustion.

- Allows to have more restrictive environmental limits than at the European law for the incineration of waste.

The world's largest biomass gasifier plant, 140 MW of power, is located in Finland and it was integrated with a pulverized coal boiler. This gasifier is fueled with forest residues, stumps and round wood. The plant has been able to lower its CO_2 emissions by approximately 230.000 tonnes per year and SO_2 emissions are also lower.

Nowadays, Denmark can rely on bioenergy for 97 days a year. The biopower sector is currently under scrutiny by EU legislators and may be severely limited by stringent sustainability criteria. This would be short-sighted as biopower could displace environmentally harmful fossil fuels, while providing green electricity as well as heat (in the case of cogeneration plants) [33].

6.2 Biomass gasification mechanism

During gasification process, the fuel (e.g., biomass resources) is heated to a high temperature, which results in the production of volatile compounds (gases) and solid residues (char). The quantity and composition of the volatile compounds depend on the reactor temperature and type, the characteristics of the fuel and the degree to which various chemical reactions occur within the process depending on the operating conditions of the gasifier. [31]

The principal reactions of the gasification are endothermic and the necessary energy for their occurrence is, generally, provided by the oxidation of part of the biomass. The conversion of the fuel to carbon monoxide and carbon dioxide release heat which provides the energy needed to

sustain the other gasification reactions. Gasification is the technology that pulls apart and isolates the processes present in the flame of a burning and it can be distinguished the following main reactions [34]:

- **Drying**: remove part of the moisture contained in the feedstock before it enters to the next process by converting the moisture into steam. The temperature of the complete drying will depend on the moisture percentage of the biomass.

- **Pyrolysis**: application of heat, without the presence of oxygen, to dried biomass to convert it into charcoal. As a result of this burning, the biomass is decomposed or separated into solids (charcoal: solid carbonized fuel), liquids (tar), and gases (flue gases). Once the temperature reaches around 240°C the biomass begins to decompose rapidly.

- **Reduction**: stage where the gasification itself takes place. At higher temperatures and under reducing conditions, when not enough oxygen is available, the following reactions take place forming carbon dioxide, hydrogen, and methane.

$$C + CO_2 \rightarrow 2\,CO$$
$$C + H_2O \rightarrow CO + H_2$$
$$CO + H_2O \rightarrow CO_2 + H_2$$
$$C + 2H_2 \rightarrow CH_4$$

- **Combustion** (oxidation): it is the only exothermic process of the gasification. Air is introduced into the gasifier after the decomposition process. During oxidation, which takes place at about 700–1.400°C, charcoal reacts with the oxygen in the air to produce carbon dioxide and heat. This reaction releases the heat that is used in the endothermic reactions of pyrolysis, gasification (reduction) and drying.

In this specific case, it has been chosen an electrically heated gasifier which means that the heat needed for the different reactions is provided by an electric heater. Hence, the oxidation reaction (combustion) does not occur and the gasifier does not need air because the heater already provides the necessary heat to take place these reactions.

6.3 Electrically heated gasifier

To carry out the present project the coupling of a rock bed thermal storage unit with a two stage electrically heated gasifier has been studied.

In the chosen gasifier each reaction is carried out in a different reactor, this is the reason that it is called two stage. There are three updraft reactors with fixed beds, two where a reaction takes place and another one for the drying. In an updraft reactor (also known as counter-current), the gas enters from below the grate and flows upwards, whereas the fuel flows downwards [34].

Then it is described the operation of the chosen gasifier followed by the flow chart of the process of the two stage electrically heated gasifier, where the heating process for the reduction reactor is made by an electric heater:

- In the first reactor the drying process occurs. It is fed with wood chips and they are dried with the same moisture which has been converted into steam heated by the heat released of the syngas synthesis.

- At the second reactor the dried wood chips are fed at the top and the pyrolysis reaction takes place together with the syngas which is at a higher temperature.

- Following this, the burned material, char, passes through the reduction reactor where gasification occurs, creating syngas, using a mix of pyrolysis gas, steam and syngas heated by an electric heater instead of by the combustion of the biomass.

In this case, as there is no combustion process, it is not necessary to supply air. Steam, pyrolysis gas and syngas are discharged at the top of the reactor of drying, pyrolysis and reduction respectively, and inert ash from the reduction process is extracted from the reactor bottom. The ash produced in the gasification process makes up a low part of the biomass that is fed into the plant and it is so pure that it can be used as fertilizer on farming fields [35].

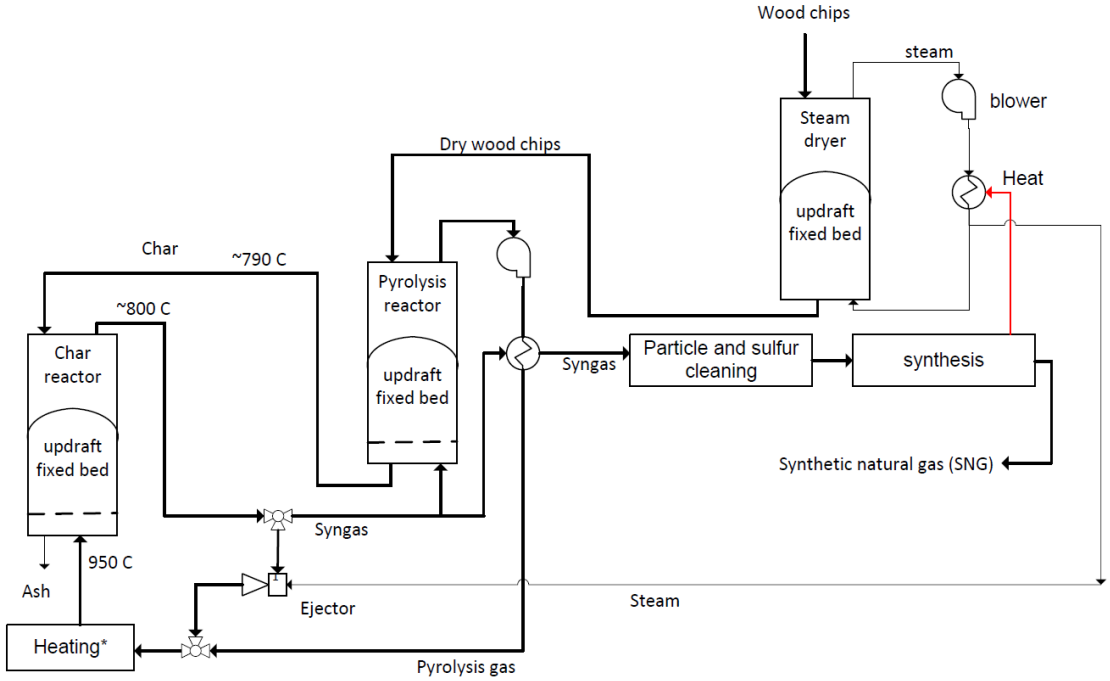

Figure 78 Flow chart of the two stage electrically heated gasifier.

The process breaks down the nonhomogeneous biomass to the molecular level and converts it into a homogeneous fuel: synthetic gas (syngas). This gas needs to be thoroughly cleaned of sulfur and particles, and after it is synthesized to obtain synthetic natural gas (SNG). This gas can be used to create a variety of valuable products or be burn in a gas engine, which allows to produce more electricity than any other available technology, or it can be injected to the natural gas network.

Avoiding the intake of air, it is avoided the dilution of syngas with N_2 and therefore to have to separate them before the methanation process. Sometimes steam is added before the ejector with the goal of produce more H_2, to have a richer gas in H_2 which is used to produce methane. So, the final gas is extracted only from the biomass, plus the steam that can be added to it.

7 Theoretical analysis of the coupling of a rock bed with a biomass gasifier

A biomass gasification plant continuously needs a heat source in order to carry out its endothermic reactions. As already said, the biomass gasifier selected utilizes the electricity of the grid as the energy input of the process.

It is believed that there are several configurations that could bring benefits while coupling a biomass gasifier with a rock bed thermal energy storage. Therefore, synergies can be formed between both technologies because they can work together in a better way, more efficiently or providing economic benefits.

The synergy proposed in this work is to supply part of the heat needed for the reduction reaction with the hot air stored in a rock bed. The main concept of this synergy is that the rock bed will be charged using the electricity produced during the periods where there is more production than energy demand, so the electricity is cheap. During these periods, the gasifier will be heated by a backup heater because it does not make sense to charge and discharge the rock bed at the same time.

Then the electricity consumed by the heaters of the rock bed will be stored in the rock bed in the form of heat at the desired temperature. When needed, this energy will be recovered and exchanged with the gases of the gasifier to heat them up.

If these gases are not hot enough before entering the reduction reactor they will be heated by the backup electric heater. Otherwise, the gases will have the desired temperature to enter the reactor and the backup heater will not switch on.

To use the rock bed helps to not waste the surplus of energy produced during low periods of electricity demand and it lets us take advantage of the low electricity price periods, which are generally caused by high renewable energy production, by storing this energy to use later. It also avoids using the electric heater of the gasifier to work during high electricity prices periods, and thus saves on the cost of heating the reactor.

7.1 Previous studies

Different coupling configurations between a gasifier and a rock bed are possible. The one more developed is a system that combines an unglazed transpired solar collector, a rock bed and a biomass gasifier stove with a heat exchanger. During charge periods, a charging blower forces ambient air into the rock bed through the biomass stove-heat exchanger unit. The system operates as follows: the collector supplies the complete hot air demand when the available solar radiation is enough to meet the demand; during daytime fluctuations in solar radiation, a part of the rock bed supplies the deficient energy; and heat stored in the rock bed is extracted during the night, ensuring uninterrupted supply of hot air at the required temperature [36].

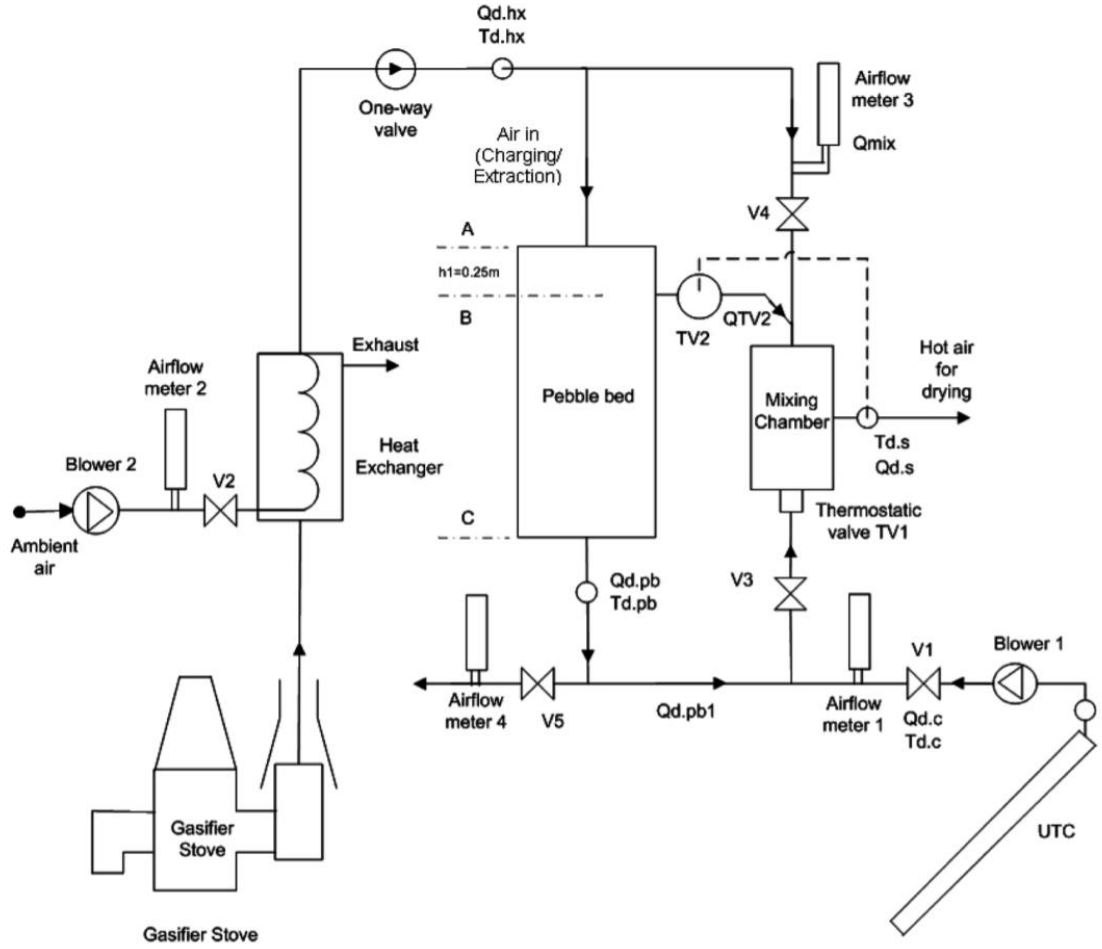

Figure 79 Schematic configuration of the solar-biomass-rick bed storage drying system [36].

One of the main constraints of biomass fuel utilization in a small-scale drying system is the operating difficulties related to the adjustment of combustion/feeding rate. Use of thermal storage may reduce the problem since combustion operation can be accomplished in a much shorter time and then the use of heat can be regulated by simply adjusting the air flow [20].

7.2 Coupling model description

Two relations between the rock bed and the electrically heated gasifier have been studied: the first one is a recirculation of the air after it has transferred the power needed to the gasifier to the entrance of the discharge pipe of the rock bed, and the second one before the air comes back to the rock bed it is used to produce electricity in a HRSG (Heat Recovery Steam Generator) coupled to a traditional power plant. The interactions between both technologies are shown in the following diagrams where the flow chart of the gasifier has been simplified:

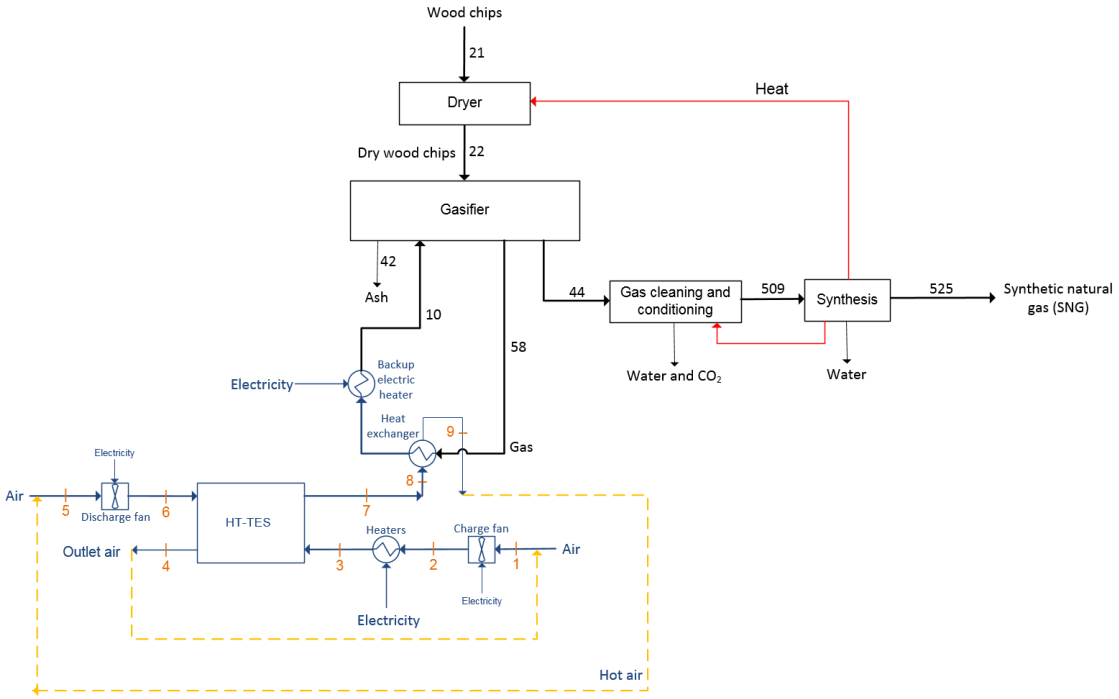

Figure 80 Diagram of the coupling for the air complete recirculation configuration.

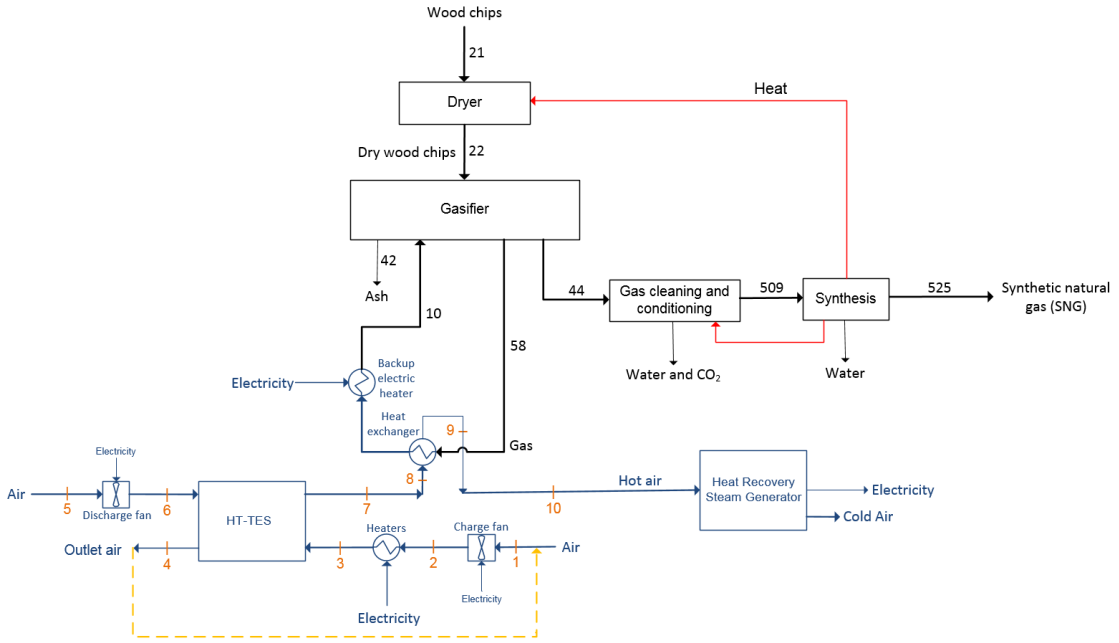

Figure 81 Diagram of the coupling with an HRSG configuration.

In both cases the outlet air during the charge phase is recovered and sent again to the inlet pipe of the rock bed while doing its recirculation.

A HRSG is a heat exchanger that recovers heat from exhaust gases to an extreme degree. The heat is recovered in the form of steam which is served as the power source of a power-generating steam turbine. This equipment makes the combine cycle the most efficient power generation system available today.

7.3 Model methodology and inputs

In this section it is described all the parameters and methodology used to model the coupling announced before.

7.3.1 Start conditions

The thermal power needed by the biomass gasifier to maintain their reactions is 16 MW. This power will be supplied either by the HT-TES or by the backup electrical heater depending on the electricity prices.

As commented above, both, the rock bed and the backup heater, stay operating when the price of the electricity is low. The backup heater heats the gasifier and the rock bed is in charge mode. When prices get higher, the backup heater is switched off and the rock bed changes to discharge mode until there is not enough energy stored or prices go down again. If the electricity price keeps high and the rock bed is empty, so it does not have enough energy to provide the needed power to the gasifier, there is no other option than to heat the reactor using the backup heater.

To differentiate from low or high prices, there is an input value that determines the reference price point that can be changed for each desired test. Below this set point price, it is considered to have low electricity prices and above it, high ones.

As shown in the gasifier's flow chart, the gases that enter to the reduction reactor need to be at a temperature of 950°C. It means that the outlet air of the rock bed must reach a temperature of about 1.000°C to be able to exchange its heat with the gases that enters the heat exchanger at around 760°C and make them reach the desired temperature. For this reason, rock bed materials must be resistant to thermal cycling between ambient and high temperature (1.000 - 1.200˚C), which needs to be tested in accelerated experiments to demonstrate durability. It also must be studied which type of rock would be the best option. But these two aspects are not part of this project. The model has been done considering an optimal performance of all the elements and materials that are part of the rock bed.

In order to provide the power to the gasifier (16 MW) between these such high temperatures, the power provided to the rock storage, which starts from air at ambient temperature, must be much higher. This fact impacts on a very large air flow. In this case, the mass flow of discharge is determined by the power that needs the gasifier and by the difference of temperatures that needs to provide. As seen in the droplet, the rock bed energy storage provides more power and energy in less time for a higher flow rate of discharge.

Next equation, the energy balance in the heat exchanger between the gasifier and the outlet air of the rock bed, allows to calculate the mass air flow needed to provide the power required by the gasifier:

$$\dot{m} = \frac{P_{gasifier} 3{,}6 \cdot 10^9}{(h_8 - h_9)} \qquad \text{(Eq.51)}$$

where $\dot{m}$ is the mass flow of the rock bed in kg/h, the power required by the gasifier, $P_{gasifier}$, which is 16 MW and h_8 and h_9 are the air enthalpies at 1.000°C and 780°C, respectively, in J/kg.

The power of the heater of the rock bed depends on the price point set, as it is shown later. Its power is a function of the number of hours where the price is higher and lower than the set point,

and of the power needed to provide. The goal is to be able to charge the rock bed with the same amount of energy that the gasifier will need for one year.

The fan power is determined by the velocity of the air and the pressure drop. It has been taken the same air velocity that in the Droplet case and the pressure drop has been calculated doing the proportional part regarding the volume of the storage unit, calculated from Eq. 52. The mass flow is constant through all the system while charging and discharging processes, but the storage volume changes in every test because the storage volume of stones needed vary depending on the price point set. The price point determines the capacity of storage that must have the rock bed. The pressure drop through the rock bed is then scaled based on the volume of the rock bed as shown below.

$$V_{storage} = \frac{E_{max} 3.600}{(1-\varepsilon)\rho_r c_{p,r}(T_{heater} - T_{amb})} \quad \text{(Eq.52)}$$

$$r = \frac{V_{storage}}{V_{droplet}} \quad \text{(Eq.53)}$$

$$\Delta P = r^{1/3} \Delta P_{droplet} \quad \text{(Eq.54)}$$

$$P_{fan} = \frac{v \Delta P}{\eta_{fan} 3{,}6 \cdot 10^9} \quad \text{(Eq.55)}$$

where E_{max} represents the energy capacity in kWh of the storage; ε is the porosity of the rock bed, equal to 0,45; $V_{storage}$ is the volume of the rock bed in m³; ρ_r is the rock density at the operating temperature, i.e. 3.002 kg/m³; $c_{p,r}$ is the specific heat capacity of the rocks at the operating temperature, with a value of 1,12 kJ/(kg·K); T_{heater} is the storage temperature, assumed uniform and constant at 1.050°C; T_{amb} is the inlet ambient air during discharge, considered 15°C for this purpose. r is the volume relation between every model and the Droplet, ΔP is the pressure drop of the rock bed in Pa, where $\Delta P_{droplet}$ is 418 Pa. It has been considered a fan efficiency of 0,8 and an air velocity $v = 5{,}9683e{+}04\ m/h$ to calculate the fan power.

As analyzed before, in the results of the Droplet, the best roundtrip efficiency is 75,66%. In this case the storage unit is bigger, and from an isolation standpoint it does not make any difference. The thickness of the isolation would be the same in a bigger rock bed since the inside temperatures near the walls will not change. Hence, it will have higher efficiency (lower losses) which has been estimated to be 85%.

And finally, for the HRSG has been set the temperatures between it is supposed to work with, so it is considered that the discharge air, after the heat exchanger with the gasifier, will arrive to the HRSG at 770°C and it will leave the heat recovery at ambient temperature. The energy balance of this heat exchanger gives us the power provided to the HRSG which is almost 50 MW.

The coupling of these two technologies is not more efficient than to use them separately, there are more heat losses because it involves more processes. But, it is supposed to be economically beneficial due to it let you buy more electricity at low price and use the heat stored when the electricity price increase.

7.3.2 Electricity price

The utilization of this system has been simulated according to the current electricity price and projections in the West Danish region. The performance of the coupling has been studied mainly in two situations: using the hourly prices of the year 2018 and for the predicted prices in the year 2035.

The scenario for the year 2035 includes much more wind and solar power in all Europe, so there will be more hours of low and high electricity prices because of the fluctuation of these sources [37].

In the next two images it can be noticed the influence of having more renewable sources, what would make vary more the price of the electricity depending on the weather conditions mainly. The hourly price rank in the year 2018 was centered around 328 DKK/MWh, in comparison with the mean value of 353 DKK/MWh for the year 2035. Although the mean price is predicted to increase, there will be more hours at low price and so, a greater availability to charge the rock storage.

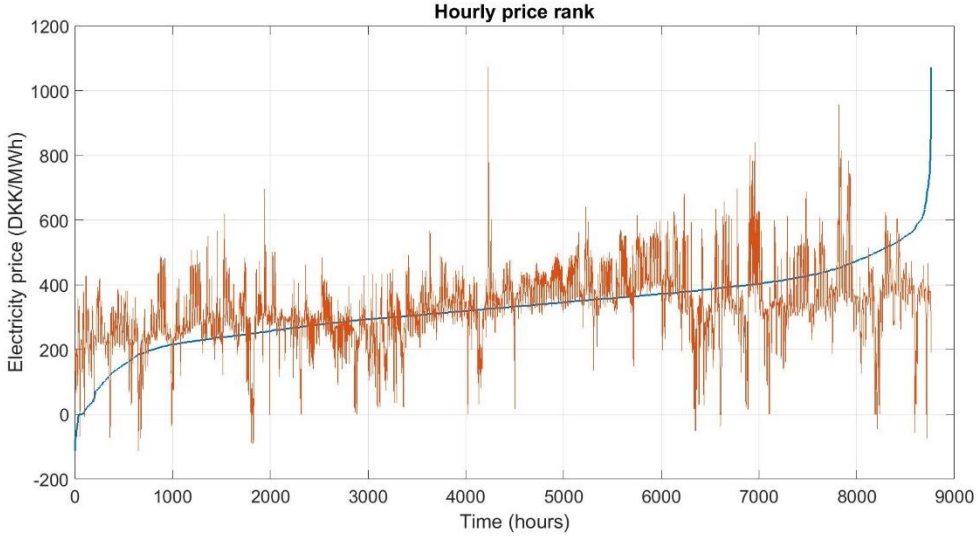

Figure 82 Hourly electricity price rank for year 2018. Blue line: sorted values.

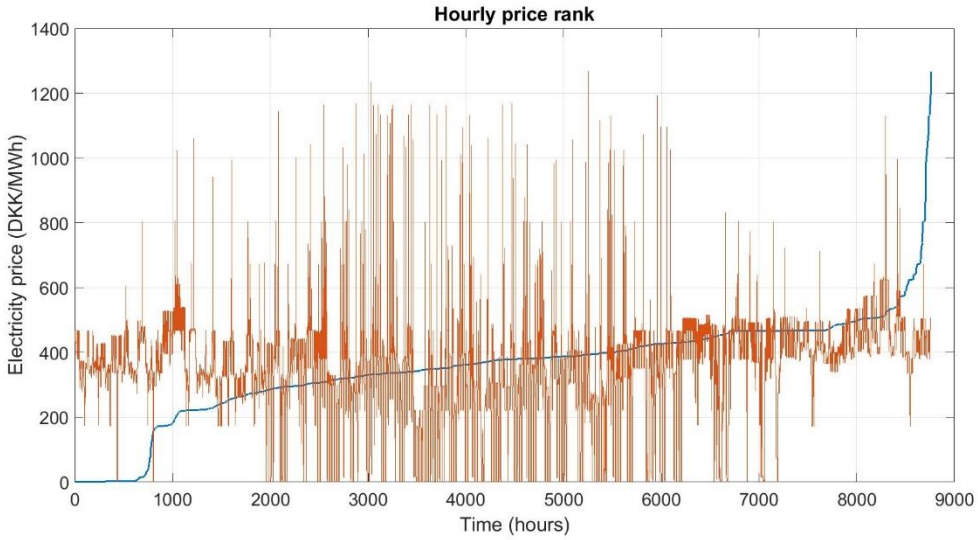

Figure 83 Hourly electricity price rank for year 2035. Blue line: sorted values.

For the 2035 scenario is predicted that for more than 750 hours the electricity price will be less than 50 DKK/MWh.

The power needed of the heaters depends on the set point of the price. This point distinguishes the hours of the year that would be considered high or low price. Every year we would like to provide as much energy as possible of the total needed by the gasifier with the rock bed. Sometimes there will not be any other option than to use the backup heater if the discharge period is too long.

So, the heaters power is calculated as a function of the hours of charge and discharge modes that depend on the hourly electricity prices of each year, the power needed by the gasifier and the operation efficiency of the rock bed (found during the analysis of the Droplet) which results from Eq. 56.

$$P_{heater} = \frac{h_h P_{gasifier}}{h_l \eta_{rb}} \quad \text{(Eq.56)}$$

where h_h and h_l are the number of hours at high and low price, respectively, $P_{gasifier}$ is the power that the rock bed must provide to the gasifier in MW and η_{rb} is the efficiency of the rock bed. In the recirculation case $P_{gasifier} = 16\ MW$, whereas for the HRSG mode the power that must provide the droplet to the gasifier is the result of the next equation:

$$P_{gasifier} = \frac{\dot{m}(h_8 - h_{amb})}{3{,}6 \cdot 10^9} \quad \text{(Eq.57)}$$

where $\dot{m}$ is the mass flow of the rock bed in kg/h and h_8 and h_{amb} are the air enthalpies at 1.000°C and ambient temperature (15°C), respectively, in J/kg.

In short, the following two curves are obtained for the years 2018 and the predicted scenario of the year 2035 for the recirculation mode to see the great impact that electricity prices have in the heater's power needed. Or from the other point of view, the right choice of the heater's power is very import because depending on the electricity prices that will take place in the future, unknown but predictable, it can save more or less money.

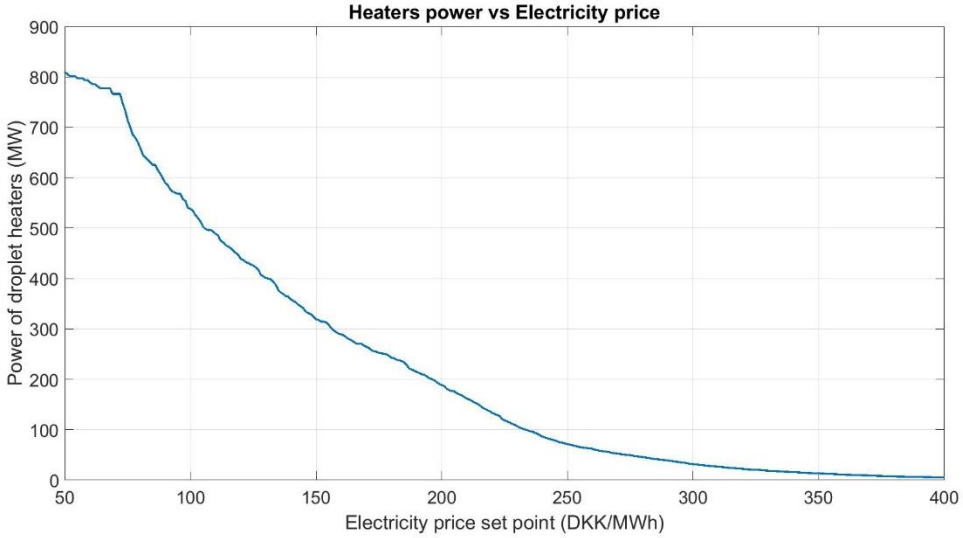

Figure 84 Heaters power based on the set price for year 2018 electricity prices.

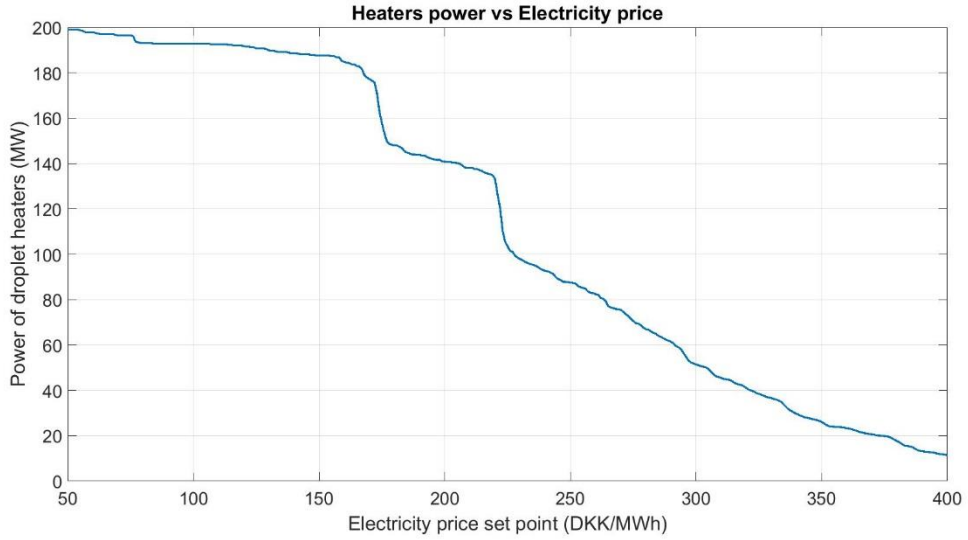

Figure 85 Heaters power based on the set price for year 2035 electricity prices.

For an electricity price set point between 50 and 400, the year 2018 shows a steep slope that drops from a heater of 800 MW when the set price is 50 DKK up to 200 MW or lower if the price point is higher than 200 DKK. However, the curve for 2035 is staggered due to the big hourly price differences but the heaters power needed is much lower in any case, 200 MW for a set price of 50 DKK.

Then, the same graphs are reported to see the evolution during the last six years of the hourly electricity price and the heaters power depending on the price point.

Figure 86 Sorted hourly electricity prices per different years.

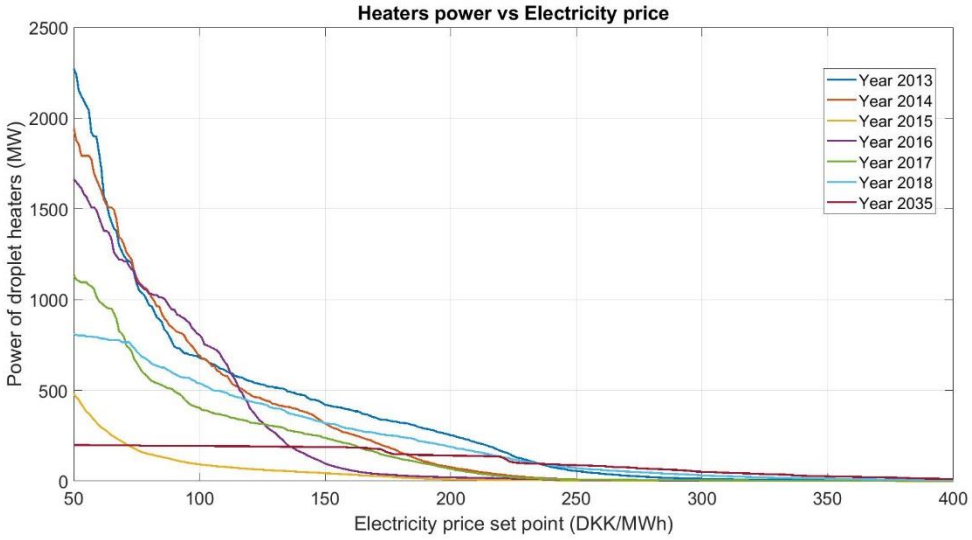

Figure 87 Heaters power based on the set price per different years.

There is not a clear evolution because the electricity price depends to a large extent on the renewable energies production and therefore on atmospheric agents. It can be noticed that on year 2015 the prices were lower than the rest, so the power needed of the heaters could be smaller because it could run during more hours per year using the same price point.

A difference of behavior is found in the predicted values for the year 2035. The power needed of the heaters is very much lower for price points under 150 DKK/MWh because it has a longer period of low prices.

7.3.3 Methodology

To model the coupling between the HT-TES and the electrically heater gasifier, the experimental characterization of the Droplet was used. The experimental results were analyzed in the previous chapters and the Droplet behavior has been extrapolated to operate at 1.000°C and to provide the power needed by the gasifier. Regarding the values of the gasifier, they were provided by the mechanical department of DTU [38] which has done several modeling of different types of biomass gasifiers.

The power needs and values resulted from the biomass gasifier model were the following for an input of wood chips of 100 MWth:

- High temperature heat input to gasifier (electricity and/or heat from rock bed): 16,0 MW.
- Auxiliary power: steam compressor to feed the ejector (not on sketch) plus the two blowers): 2,2 MW.
- Syngas output: 109,1 MWth.

Therefore, the conversion efficiency from biomass plus electricity to syngas is: 92,3%.

The auxiliary power to convert the syngas to SNG (Synthetic Natural Gas), includes two compressors, one of the syngas to 10 bar and its product is compressed to 80 bar to produce the SNG. They both consume 7,9 MW. The resulting SNG output power is 90,4 MW, what ends in an overall efficiency of the gasifier of 71,7%.

The modeling of the coupling has been designed for these specific necessities of the gasifier. The procedure to find the energy stored in the rock bed at each hour of the year has been calculated in terms of power.

The rock bed charges if the electricity price is lower than the chosen price point. In this case, the rock bed stores the power of the heaters every hour. For the discharge mode, if there is not enough energy inside the rock bed, the backup heater provides the power to the gasifier and the rock bed is stopped, so it is neither in charge nor discharge mode. If the rock storage is charged, at every hour of discharge mode it is subtracted the power that needs the gasifier, taking into account the rock bed efficiency, if the configuration is in recirculation mode. Otherwise, if the configuration uses a HRSG, it is also extracted from the bed, the energy that uses the HRSG to produce electricity. Finally, for every hour of charge or discharge it is counted the power consume of the charge or discharge fan, respectively.

Using this methodology, we can easily calculate the yearly cost of the coupling system by multiplying the hourly prices and the different powers of every hour. It is a best case of the coupling due to we already know the electricity prices for all the year and the optimum heater's power can be calculated.

The electricity produced by the HRSG is calculated as constant for every hour of discharge mode of the rock bed, being calculated from the enthalpy difference between its work temperatures, the mass flow and the efficiencies of the HRSG itself and the power plant. The electricity power generated while discharging is 25,40 MW, resulting from next equation:

$$P_{HRSG} = \frac{\dot{m}(h_{10} - h_{amb})}{3{,}6 \cdot 10^9} \eta_{HRSG} \eta_{pp} \qquad \text{(Eq.58)}$$

where $\dot{m}$ is the mass air flow in kg/h, h_{10} and h_{amb} are the enthalpies of the air at 770°C and ambient temperature (15°C) in J/kg, respectively, and η_{HRSG} and η_{pp} are the efficiencies of the HRSG and of the power plant to convert thermal energy into electricity, corresponding to 85% and 60% respectively.

In this model, the initial energy stored in the rock bed has been designed to match the amount of energy stored at the end of the year for each simulation. There is not a maximum storage capacity of the rock bed, it is supposed to be unlimited although, for every initial condition (price point and year of electricity prices) the minimum capacity needed changes and it effects the volume of storage material. Therefore, the fans power needed also change as they depend on the rock bed dimensions.

8 Theoretical coupling to a biomass gasifier results

In this chapter the results of the coupling between the electrically heated gasifier and a packed rock bed storage unit are presented and analyzed. For this reason, different situations of operation mode depending the set price point chosen are compared and they are reported per several years as well.

First, to check the correct performance of the model, the energy stored inside the rock bed was compared with the yearly curve of the price during one random week. Looking the following image, extracted from a set price of 200 DKK/MWh (indicated by dished line), it can be confirmed that when the price of the electricity is lower than the set price point, the rock bed stores energy and the other way around, the rock bed is in discharge mode when the price of the electricity is higher than the set point.

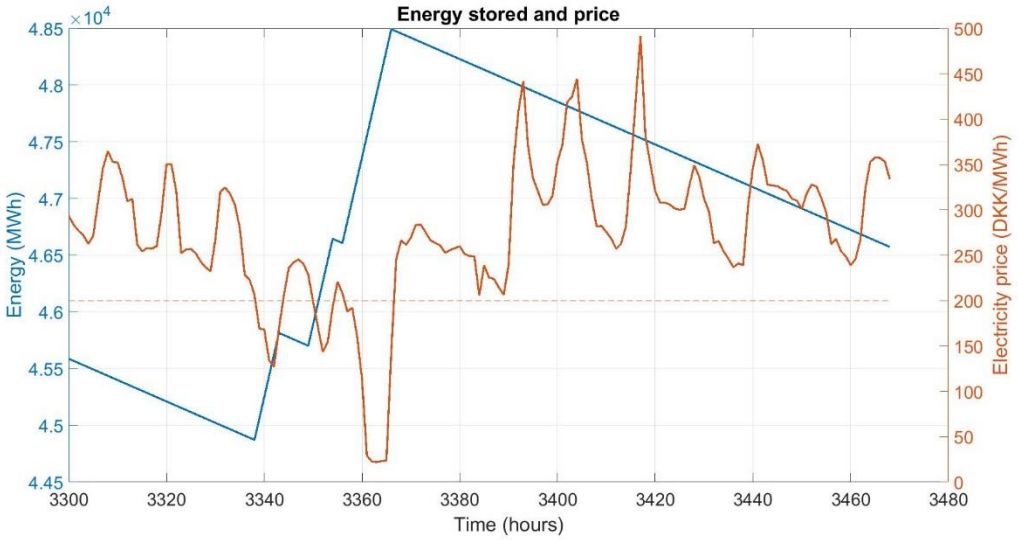

Figure 88 Energy stored inside the rock bed and hourly electricity price for the year 2018.

The behavior of the rock storage using the electricity prices predicted for the year 2035 is totally different. The price fluctuation is much more peaked and so, discharge periods are not as long as in the case of the year 2018. A bigger heater is needed to store the same amount of energy, in less time; 188 MW of heater using 2018 prices and 140 MW for year 2035.

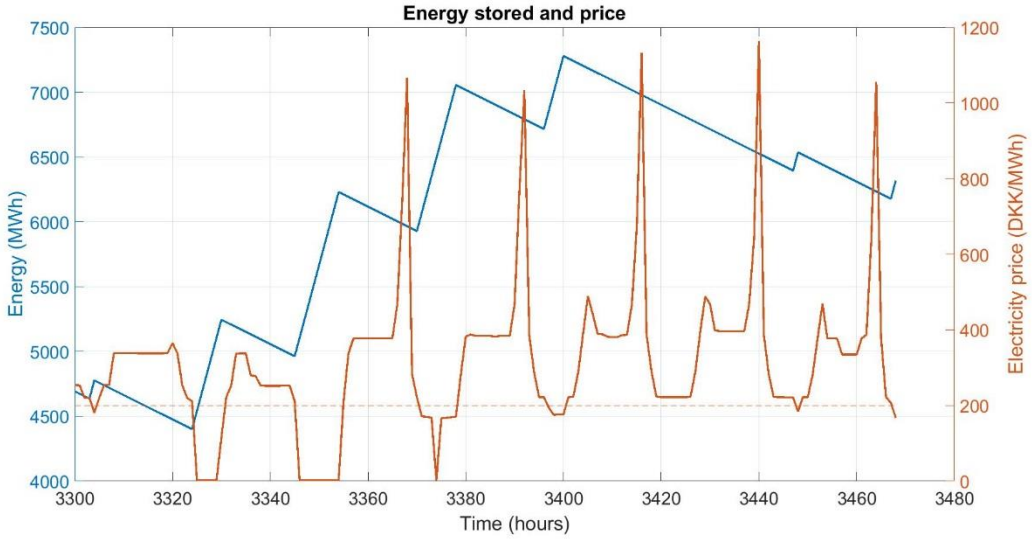

Figure 89 Energy stored inside the rock bed and hourly electricity price for the year 2035.

Looking at these two representations, it is confirmed the good performance of the calculation of the energy storage through the time.

8.1 Rock bed cycles

It is important to know how many cycles of charge and discharge will have to stand the rock bed in order to control the chemical and physical properties of the rocks and to be sure that they will resist and keep adequate characteristics to carry out their function.

The number of cycles (charge and discharge) depends on every year electricity prices and on the chosen price point, they are exactly the same for both configurations studied. To have an idea of cycles dimensions, it is shown the cycles characteristics for a set price point of 200 DKK/MWh.

Table 16 Rock bed cycles information for a set price point of 200 DKK/MWh per year analyzed.

Year	N° cycles	Charge average [h]	Discharge average [h]	Longest charge [h]	Longest discharge [h]
2013	116	5,24	70,89	41	688
2014	239	7,25	28,63	79	551
2015	294	19,73	9,79	253	138
2016	280	14,91	16,49	309	572
2017	258	7,44	26,63	49	571
2018	135	6,17	59,44	40	801
2035	153	6,79	49,16	40	982

The rock bed, following the years analyzed, will be exposed under an annual average of 210 cycles of charge and discharge. In all the cases, the minimum charge and discharge period is 1 hour. Most of years show smaller periods of charge and longer discharge periods, so big heaters are necessary. The only year that would have smaller discharge periods than the charge ones is the 2015, because its mean electricity price value is lower than 200 DKK/MWh.

All the years show some very large discharge periods. The viability of the rock bed to provide during all the time the energy needed by the gasifier at the desired temperature should be verified experimentally. If the set price point is increased, charge periods increase as well, and so, discharge periods are shorter. If contrary, if the price point is reduced, bigger heaters will be needed as the charge hours will be reduced.

If the chosen price point is near the mean value, the number of cycles is higher than if the set price point is close to the extreme prices, in this case the number of cycles will be greatly reduced.

8.2 Gasifier operation cost

The normal operation cost of the electrically heated gasifier for one year depend on every hour price of electricity. If the gasifier works 24 hours per day and 365 days a year, the yearly cost of the electricity needed to run the heater and the auxiliary devices of the plant is the following:

Table 17 Operation cost of the electrically heated biomass gasifier per year.

Year	Operation cost gasifier [DKK]
2013	41.395.435
2014	33.591.047
2015	25.593.655
2016	30.692.006
2017	33.327.594
2018	46.011.864
2035	49.586.345

Although the last years the use of renewables energies has increased, and so there exists periods with very low prices or even negatives, there are also peaks of higher prices and the average value is higher. At the end, the total cost spent on the electricity needed by the gasifier plant is not seen reduced. The predicted prices for the year 2035 show an increase of this expense, as it has already happened in 2018.

Making use of a rock storage unit the total cost spent on electricity can be reduced taking advantage of the hours where the price is low.

8.3 Coupling characterization

The year 2018 has been chosen to show deeper the operation of the coupling model to be the most recent year. Next, the two different configurations are studied for different set price points. It is reported some remarkable values of the needed storage unit per each case, the electricity costs and the curve of the energy stored inside the rock bed, which accords with the charge and discharge phases.

- Price point equal to 100 DKK/MWh:

The choice of a low price point like 100 DKK/MWh requires a big heater because there are not so many hours in which the electricity price is lower, so the charge of the rock bed has to be done very fast and it means higher heater's power.

Table 18 Results of the coupling at 100 DKK/MWh price point for the year 2018.

Year 2018 - 100 DKK/MWh	Recirculation	HRSG
Heaters power [MW]	538,25	2.237,95
Max. Energy stored [MWh]	52.754,79	219.656,22
Total energy stored [MWh]	2,26E+08	9,45E+08
Storage volume [m³]	99,23	413,16
Fans power [MW]	0,027	0,044
Annual electricity costs [DKK]		
Fans	78.237	125.904
Backup heater	4.040.755	
Rock bed heater	4.867.228	20.237.054
Revenue	-	72.825.940
Operation expense	8.986.219	-48.422.228
Savings	**37.025.645**	**94.434.092**

The power needed of the heaters and the energy stored is four times bigger for the HRSG configuration. This is because the system requires more energy to produce electricity instead of recovering it again to provide it to the gasifier. So, the rock storage volume must be bigger too.

In this case, the price point set is so low that the rock bed must charge very fast and it has long periods of discharge (see *Figure 90* and *Figure 91*), so, it is a good opportunity to generate a lot of energy and sell it at higher prices. With a HRSG configuration, the energy that can be produced is so much that its benefits are higher than the operation expenses.

For a set price point of 100 DKK/MWh, using electricity prices of 2018, the operation savings of the gasifier would have been 37 MDKK using the rock bed in the recirculation configuration and 94 MDKK in the HRSG mode.

Next two images show the evolution of the energy stored inside the rock bed. It can be easily distinguished the charge and discharge periods. Take into account that the amount of energy stored at the start of the year was forced to match the energy stored at the end for each modeling, which depends on the different charge periods.

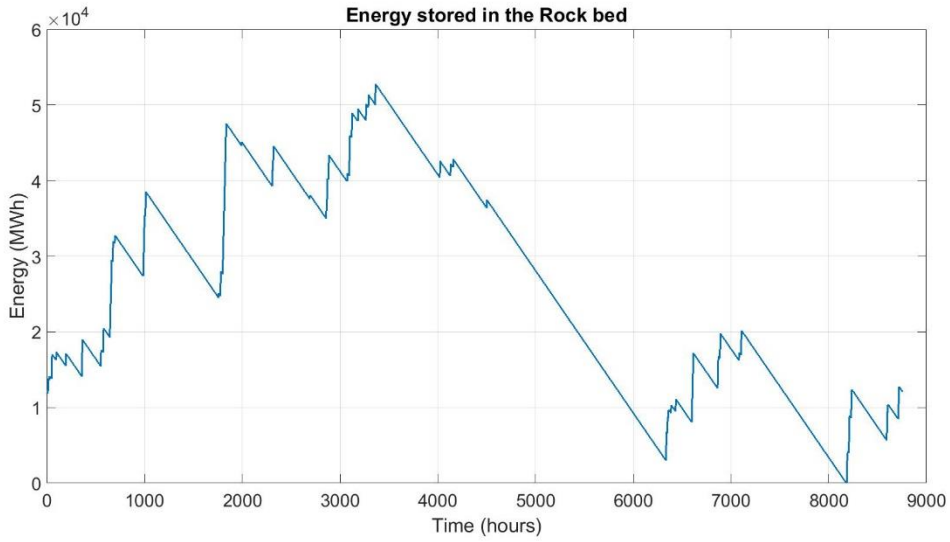

Figure 90 Energy stored in the rock bed for a price point of 100 DKK/MWh with 2018 electricity prices and recirculation configuration.

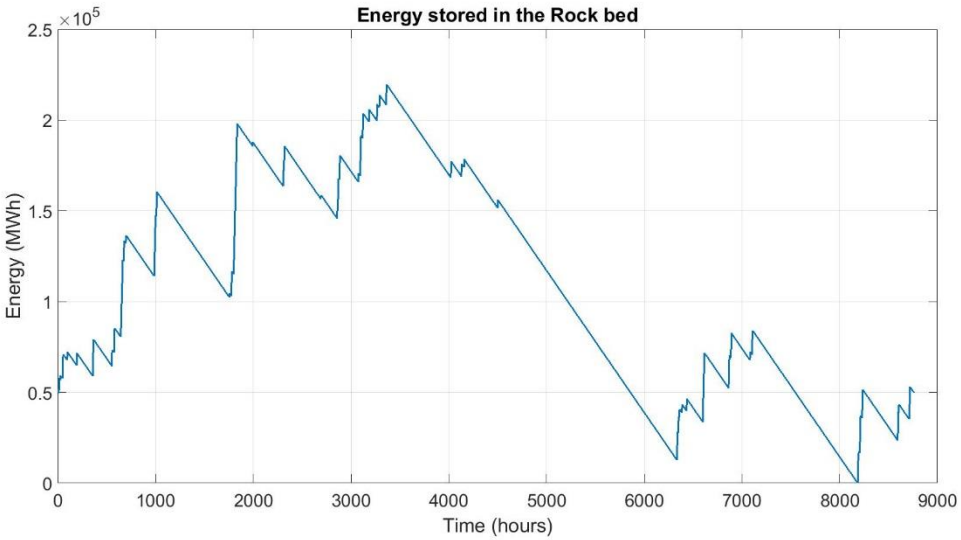

Figure 91 Energy stored in the rock bed for a price point of 100 DKK/MWh with 2018 electricity prices and HRSG configuration.

The behavior of the energy stored in the rock bed is exactly the same in both configurations due to the charge and discharge mode depends only on the electricity prices. In addition, heaters powers are proportional to the power subtracted from the rock storage in each case. So, the backup heater is used during the same hours, therefore the yearly price of its utilization is the same in both cases. The only difference regarding the energy stored is the amount of heat which is bigger in the HRSG configuration because more energy is required during the discharge phase.

So, in next price points examined, only one plot of the energy stored is shown since they have the same curve for both configurations even though with different amounts of energy.

- Price point equal to 300 DKK/MWh:

Table 19 Results of the coupling at 300 DKK/MWh price point for the year 2018.

Year 2018 - 300 DKK/MWh	Recirculation	HRSG
Heaters power [MW]	31,68	131,71
Max. Energy stored [MWh]	59.989,06	249.530,66
Total energy stored [MWh]	2,60E+08	1,08E+09
Storage volume [m³]	112,83	469,34
Fans power [MW]	0,028	0,046
Annual electricity costs [DKK]		
Fans	81.647	131.341
Backup heater	22.184	
Rock bed heater	22.941.943	95.388.450
Revenue	-	54.641.740
Operation expense	23.045.774	40.900.236
Savings	**22.966.090**	**5.111.629**

For a higher price point, heaters power is considerably lower because there are more hours during the year in which the rock bed is charged, and, in this specific year, choosing a price point of 300 DKK/MWh, the bed is basically only charging during the first half of the year. Hence, the storage volume needed is higher and so it is the energy stored. In this situation the curve of the energy stored (*Figure 92*) is fairly different.

As already seen in the previous case, the cost of the backup heater is independent of the chosen configuration. The operation cost of the charge and discharge fans is higher, and the backup heater is used during less hours. Global operation costs are superior and the revenue in the HRSG configuration is lower. In total, the economical savings are almost 23 MDKK in the recirculation configuration and 5 MDKK in the HRSG mode, lower than choosing as a price point 100 DKK/MWh. Unlike the previous case, the savings are higher for the recirculation mode.

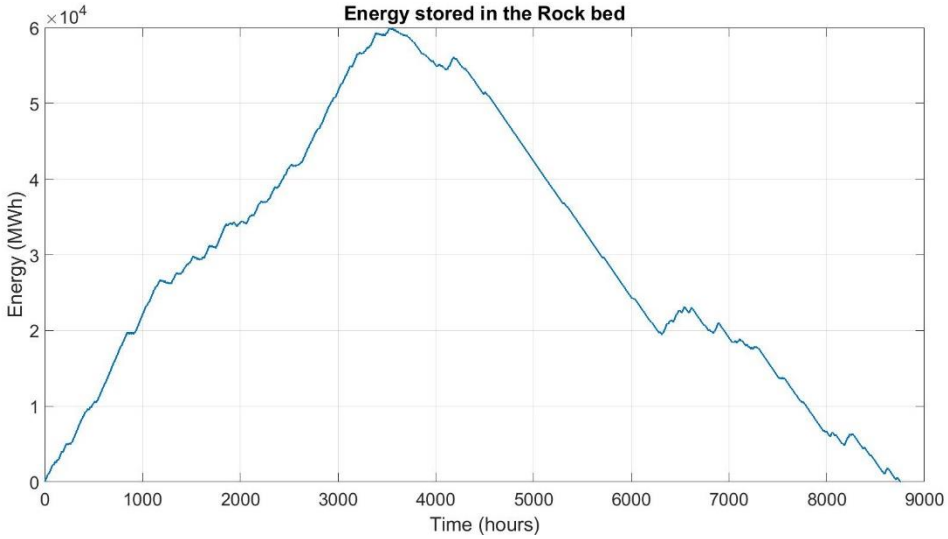

Figure 92 Energy stored in the rock bed for a price point of 300 DKK/MWh, recirculation mode and year 2018.

- Price point equal to 500 DKK/MWh:

Table 20 Results of the coupling at 500 DKK/MWh price point for the year 2018.

Year 2018 - 500 DKK/MWh	Recirculation	HRSG
Heaters power [MW]	1,27	5,31
Max. Energy stored [MWh]	6.266,88	26.367,18
Total energy stored [MWh]	2,64E+07	1,12E+08
Storage volume [m³]	11,79	49,59
Fans power [MW]	0,013	0,022
Annual electricity costs [DKK]		
Fans	38.436	62.097
Backup heater	226.930	
Rock bed heater	3.273.268	13.609.657
Revenue	-	7.984.630
Operation expense	3.538.634	5.914.054
Savings	**42.473.230**	**40.097.810**

Choosing a price point higher than the mean value like 500 DKK/MWh, the power of the heaters and the storage volume are greatly reduced, as well as the energy stored and fans power. In this year, during almost all the first half of the year the rock bed would have been in charge mode.

In this specific case, both configurations guarantee a similar amount of savings with respect to the operating cost of the gasifier alone, 42 MDKK for the recirculation mode and 40 MDKK with the HRSG configuration. The revenue for the generation of electricity is not so significant but the operation costs are lower in both cases.

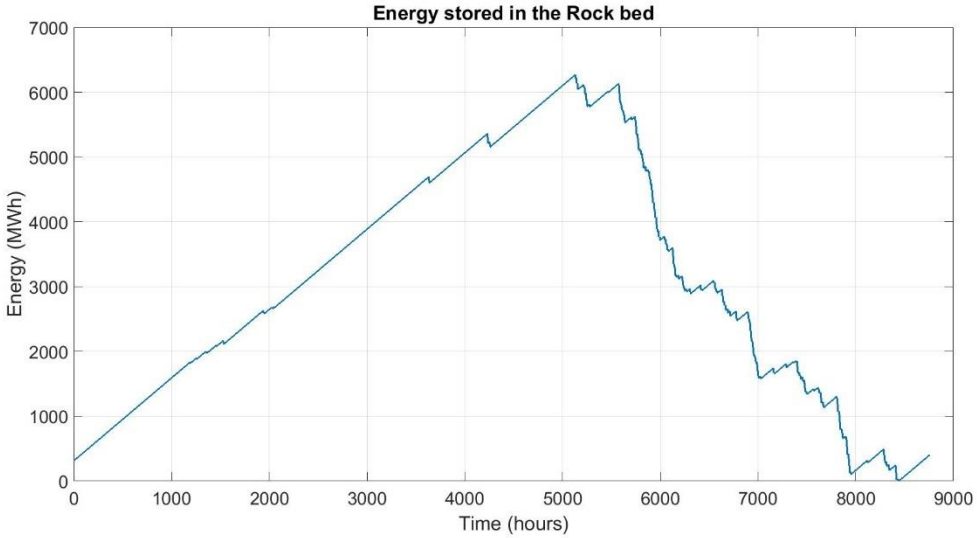

Figure 93 Energy stored in the rock bed for a price point of 500 DKK/MWh with 2018 electricity prices and recirculation configuration

In general, as the price point is increased, the size of the storage unit needed is reduced in both configurations, and so it does the heaters power, as shown before.

Both configurations present equal mass air flow of discharge because both must provide the same power to the gasifier. HRSG configuration requires bigger heaters power, storage volume and, so, fans power, because it has a higher consume of the energy stored: 16 MW to the gasifier plus the energy that goes to the HRSG. The operation costs of the fans and rock bed heaters are higher in the HRSG configuration because of their power, but they work during the same hours than in the recirculation case. The backup heater would work for 24 hours with a price point set of 500 DKK, while with a price point of 300 DKK and 100 DKK the operation hours of the backup heater would be 909 hours and 1.901 hours, respectively. The higher the set price point, the less hours the backup heater works per year, although it also depends on the hourly price distribution.

Next it is shown three of the most important parameters to consider for each configuration and per different price points: heaters power, minimum energy storage needed (maximum required) and yearly economic savings with 2018 electricity prices.

Table 21 Heaters power, Max. energy stored and savings for 2018 electricity prices.

RECIRCULATION				HRSG			
Price point [DKK/MWh]	Heater's power [MW]	Max. Energy stored [MWh]	Savings [DKK]	Price point [DKK/MWh]	Heater's power [MW]	Max. Energy stored [MWh]	Savings [DKK]
5	1.854,97	72.905,48	40.228.472	5	7.712,64	303.440,45	124.141.237
50	809,79	50.858,93	37.329.622	50	3.366,96	211.775,90	107.493.740
100	538,25	52.754,79	37.025.645	100	2.237,95	219.656,22	94.434.092
150	319,07	50.726,69	32.647.896	150	1.326,65	211.221,63	70.934.784
200	188,59	48.493,20	27.320.790	200	784,12	201.938,34	45.237.190
250	71,47	62.062,65	22.617.833	250	297,20	258.356,14	14.087.046
300	31,68	59.989,06	22.966.090	300	131,71	249.530,66	5.111.629
350	13,30	36.250,90	28.223.987	350	55,30	150.867,71	11.522.203
400	5,07	16.243,46	35.663.054	400	21,08	67.849,14	26.218.889
450	2,33	9.997,47	40.129.691	450	9,68	41.879,25	35.580.465
500	1,27	6.266,88	42.473.230	500	5,31	26.367,17	40.097.810
550	0,58	2.905,11	44.301.817	550	2,41	12.390,79	43.367.396
600	0,22	1.229,27	45.285.297	600	0,94	5.424,42	45.030.669

In the table above, you can see how the heaters power and the storage capacity required diminish as the price point set increase. In any year, the relation between the savings and the chosen price point is not direct because the number of charges and they duration change according to the hourly electric price.

By the year 2018, the economic savings are more constant for the recirculation configuration whereas for the HRSG one, below a set price point of 200 DKK/MWh savings increase drastically, savings are lower than in the recirculation mode around the mean value of the electricity price, and for high price points savings are similar for both configurations. It is represented in the graph below.

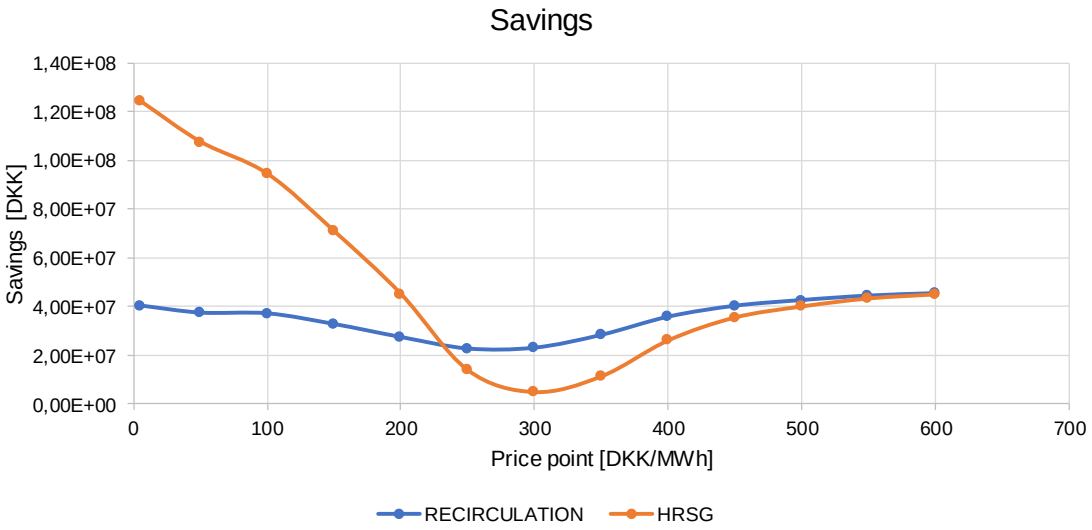

Figure 94 Yearly savings per 2018 electricity prices by implementing a rock storage depending on the price point and configuration.

The big difference between both configurations savings at low price points is due to the generation of electricity with the HRSG. For low price points a lot of energy is stored in a short time at cheap price and then, after the storage period, this energy is converted again into electricity and sold at higher prices. With a low set price point, most time of the year the facility is in discharge mode, and so, producing electricity. It must be considered that for low price points, and especially for the HRSG configuration, the heaters power needed is very high and it also requires a big storage unit.

Next, it is shown two box plot graphs with the savings that would have represented the utilization of the rock bed for each configuration and several price points. The yearly savings correspond to the difference between the cost of the utilization of the biomass gasifier and the operation expenses of its cost using the rock bed. Each box represents one price point set and its width is caused by the savings difference between the analyzed years (from 2013 to 2018 and 2035).

Figure 95 Savings box plot for all years (2013-2018, 2035) for a recirculation configuration per different price points.

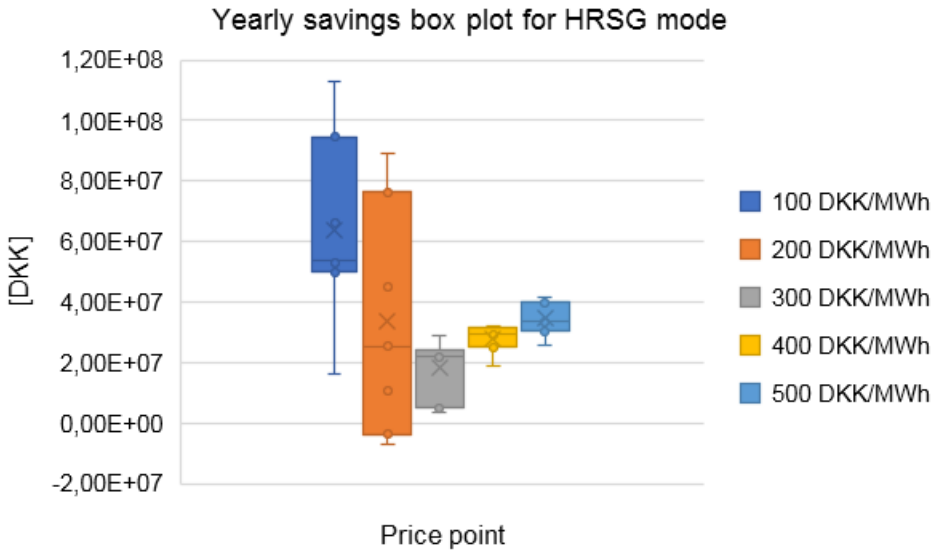

Figure 96 Savings box plot for a HRSG configuration per different price points.

Every year the hourly price curve is different, and it depends on many unpredictable factors. So, it is not easy to determine the best configuration and characteristics to use because they vary per year.

Analyzing the results obtained between the chosen price points and for the years that were analyzed, the recirculation configuration always give economically benefits with respect to the operation of the gasifier alone. Whereas, for a price point of 200 DKK/MWh, negative values were obtained in two years for a HRSG configuration. In these two cases, the coupling would not be beneficial.

100 DKK/MWh and 200 DKK/MWh price points show a very wide range, so lots of variance in savings in both configurations. Although in some years savings can be very high, in others they can be the lowest. On the other side, for a price point of 300 DKK/MWh and 400 DKK/MWh the yearly savings are quite constant independently of the year used for the electricity prices and of the configuration.

This proves that the most secure way to choose the characteristics and dimensions of the coupling is doing it thinking in a price point near 300 - 400 DKK/MWh since it will be easier to predict the yearly savings and therefore, to estimate the economic benefits of the coupling corresponding to the necessary investment. In this case, the mean value of the calculated savings for the years studied is higher for the recirculation configuration, specifically for a price point of 400 DKK/MWh.

Otherwise, for a set price point of 500 DKK/MWh and HRSG configuration there is also a narrow range and with a higher average of savings that the case proposed above. Despite this, the price point is fairly high and there would be few discharges periods or shorter ones. This fact is not a problem, but the gasifier would be working normally for most part of the time, so it would not make so much sense the coupling with the Droplet, even though savings are obtained.

It has been proved to be economically beneficial the use of a rock bed thermal energy storage in most of the cases. However, for the HRSG configuration the energy that must be stored in the rock bed is much higher than the one needed by the gasifier throughout the year.

It must be emphasized that without the recirculation of the air or its use to reconvert this outlet heat into electricity through a HRSG, this coupling would not provide any economic benefits.

Finally, next test was realized to show the importance of choosing the most suitable installation dimensions: rock bed characteristics and dimensions needed for a recirculation mode with a price point of 400 DKK/MWh for 2013 electricity prices were fixed (heater's power: 2,34 MW, storage volume: 10,96 m³ and fans power: 13,05 kW) and they were simulated for an operation with the hourly electricity prices of the following years. The results obtained are reported below:

Table 22 Savings and difference using a rock bed optimized for 2013 electricity prices and a price point of 400 DKK/MWh.

Year	Savings using current year prices [DKK]	Savings with 2013 facility [DKK]	Difference [DKK]
2014	32.413.884	28.897.914	-3.515.970
2015	24.961.632	21.982.866	-2.978.766
2016	28.845.112	26.150.722	-2.694.390
2017	31.891.000	28.727.104	-3.163.896
2018	35.663.054	33.275.271	-2.387.783
2035	32.072.290	25.744.003	-6.328.287

Using the facilities optimized for the operation with 2013 hourly electricity prices would have a negative impact regarding the savings of the rest years, although savings will still be obtained anyway. The yearly average of savings obtained is almost 27,5 MDKK, and the values have a standard deviation of 3,8 MDKK. So, the model predicts that the yearly savings would be compressed between 23,6 MDKK and 31,3 MDKK.

If any configuration designed for a price point with a greater variability of savings had been chosen, the difference of the annual savings achieved would be much greater and, consequently, economic losses would be much higher compared to the optimized savings for each year. The range in which savings could be found would be much wider as well.

It is remarkable that for the previsions of year 2035, when the hourly electricity price curve will be fairly different that the one of last years, the facility would be even less adequate, and it would give less economically savings than it could do with an optimized sizing.

The choose of the best suitable characteristics of the setup to maximize the savings every year is tricky because of the electric price uncertainty for future years. Looking at this model, the choose of a setup designed for a price point of 400 DKK/MWh in a recirculation configuration seems a safe choice with high savings. It will not have a wide difference between yearly savings and the loss of yearly savings will not represent a big impact for the different years. So, any dimension sized for a price point of 400 DKK/MWh could be a good option to choose.

9 Conclusions

In the present thesis a feasibility analysis of the coupling of a thermal energy storage based on rocks with an electrically heated biomass gasifier has been carried out. A big part of the work has been the experimental characterization of the HT-TES rock bed of 3,2 m³ at a theoretical maximum storage temperature of 600°C.

A rock bed storage unit is a very attractive solution because the stones and the insulation used are relatively inexpensive, compared to other storage types like batteries. It has been shown that rock beds like the Droplet are not as fast as batteries, but, they can provide air at high temperature (≈530˚C) in a few minutes and generate electricity when coupled to a traditional power plant.

Throughout the entire period of development of the project more than 25 charge and discharge tests have been realized with the experimental setup. Most tests were done for a slow (120 m³) or fast (200 m³) charge and discharge phases were realized for multiple flows. The energy provided to the Droplet is determined by the chosen air flow rate and the duration of the charge.

The different tests analyzed had led to the following final outcome values for the rock bed configuration studied: first law efficiency values for the fast charge phase can range between 77% and 79%, whereas second law values between 68% and 71% for states of charge between 15% and 50%, otherwise the charge is less efficient. On the other hand, slow charge showed a lower efficiency in all the cases, reaching a maximum first law charge efficiency of 70%.

Results related to discharge cycles, were found to be 97% and 74% for the first principle analysis and second principle one, respectively. These values were obtained for a discharge phase at 300 m³/h flow rate. Leading to the most efficient roundtrip cycle with an overall efficiency of almost 76%, according to the first principle of thermodynamics, and around 52% according to the second one. It all proved that the Droplet presents a good performance for storing energy in the form of heat and the air flow velocity was found to affect the charging efficiency largely.

Compared to the horizontal rock bed previously studied at DTU Energy, during the charge phase the heat tends to distribute in a stratified way while injecting hot air from the top, where the hottest layers are the upper ones due to buoyancy phenomena. As the state of charge increases, the hot front moves downward. And during the discharge, the heat recovery is improved because the air flow is injected from the bottom to the top (hottest region), and then the hot front simply moves upward as discharge goes on due to buoyancy. This behavior is reflected into a higher overall efficiency of the rock bed with a vertical configuration.

The final goal of this work was to understand if a theoretical coupling of the rock storage unit with an electrically heated biomass gasifier is feasible from an economical point of view. The results showed that this coupling itself is not profitable unless the system can take advantage of the hot outlet air of the rock bed after it has passed through the heat exchanger of the gasifier. So, two solutions were proposed: a full recirculation of this air to the entrance of the rock bed, like this, the air already enters to the rock bed at a high temperature and it is easier to reach the maximum stored temperature, and to generate electricity starting from this hot air with a heat recovery steam generator. In both cases the outlet air during the charge phase was meant to be recirculated as

well, in order to require less power from the heaters to warm up the inlet air of the rock bed up to the desired temperature.

Regarding the predictions made about the operation of the coupling between a HT-TES rock bed and a biomass gasifier the results of the modeling carried out for both coupling configurations analyzed give good economic values in most of the cases. The final solution has been chosen mainly for economic safety reasons throughout the years. The best coupling of operation between the rock HT-TES and the specific electrically heated biomass gasifier, is to size the rock bed according to an electric price point of 400 DKK/MWh in a configuration of recirculation with the gasifier. This coupling will allow the system to take advantage of the electricity prices fluctuations during the year and obtain a quite precise range of economic savings per year. This solution is also one of the cheapest in investment of the different results found because it requires smaller heaters and fans and less storage volume, apart from that the recirculation configuration does not need the installation of a HRSG and its location does not have to be near an already existing power plant.

If the size of the scaled rock bed to match the energy needs of the gasifier is optimized according to 2013 prices, it would require a heater's power of 2,34 MW, a fans power of 13,05 KW and it would occupy a volume of 10,96 m^3. With this characterization, the yearly average of savings obtained thanks to the coupling of the gasifier with the rock bed storage would be near 27,5 MDKK, what represents a 60% of the total operating cost of the gasifier according to 2018 prices.

In few years, a storage unit will be needed in the Danish energy system since most of the electricity will come from renewable sources and a rock bed could be a good solution. On the other side, it has been proved that the utilization of a rock bed unit, thanks to its high efficiency and despite the heat losses through all the process, is economically profitable only by buying the electricity at low price, storing it in the form of heat and generating electricity again to sell it at high prices. Besides, in regions where district heating is used, the waste heat from the generation process of electricity can be utilized for district heating, and thus, improve the overall energy efficiency and economy considerably.

9.1 Future work

It has been shown that the actual studied experimental setup has a better performance than the first horizontal testing facility analyzed and that the vertical flow responds in a better way and take advantage of the buoyancy forces. Despite this, there are still some aspects that can be improved, such as the position of some valves or gauges that were missed when carrying out the tests in order to obtain more information.

The storage mode of the Droplet has to be studied over a wider range of operating conditions to be sure that it is able to store the needed heat during a particular period. Moreover, a relevant aspect which can be investigated is the influence of a repetitive cycling activity on the charge and discharge phases without discharging the rock bed completely. This would actually be a way to redefine the potential of the Droplet in real-life applications and the next step of this project is to understand the feasibility of a large-scale applications. Higher storage temperature is wanted to be tested as well.

During the next years, a PhD project is going to work further on this subject to understand the operation of the coupling between a rock bed thermal energy storage and a biomass gasifier together with a traditional steam power production cycle connected to district heating operating over a full year.

List of figures

List of tables

Nomenclature

A	*Surface area (m^2)*
b	*Specific exergy (kWh/kg)*
B	*Exergy (kWh)*
c_p	*Specific heat capacity (kJ/kg ·K)*
C_{th}	*Thermal capacity (kWh)*
E	*Energy (kWh)*
g	*Gravitational constant ($m \cdot s^{-2}$)*
h	*Specific enthalpy (kWh/kg)*
h_{conv}	*Convective heat transfer coefficient ($W \cdot m^{-2} \cdot K^{-1}$)*
h_{rad}	*Radiactive heat transfer coefficient ($W \cdot m^{-2} \cdot K^{-1}$)*
k	*Thermal conductivity ($W \cdot m^{-1} \cdot K^{-1}$)*
L	*Characteristic length (m)*
m	*Mass (kg)*
$\dot{m}$	*Mass flow rate (kg/h)*
Nu	*Nusselt number*
p	*Pressure (Pa)*
P	*Power (kW)*
q	*Specific heat flux (W/m^2)*
Q	*Heat flux (W)*
r	*Volumes relation*
$r_{1,2}$	*Radial coordinate (m)*
R	*Thermal resistance (K/W)*
Ra_L	*Rayleigh number*
s	*Specific entropy ($kWh \cdot kg^{-1} \cdot K^{-1}$)*
SOC	*State of charge*
t	*Time (h)*
T	*Temperature (K)*
u	*Specific internal energy (kWh/kg)*
v	*Fluid velocity (m^2/h)*
V	*Volume (m^2)*
$\dot{V}$	*Volumetric flow rate (Nm^3/h)*
x	*Spatial coordinate (m)*

Greek letters

ε	*Porosity*
ϵ	*Emissivity*
η	*Efficiency*
μ	*Dynamic viscosity (Pa·s)*
ν	*Kinetic viscosity (m^2/s)*
ρ	*Density (kg/m^3)*
σ	*Stefan-Boltzmann constant*
δ_t	*Penetration depth (m)*

Bibliography

[1]. NASA (2019, March). Global Climate Change. Retrieved from https://climate.nasa.gov/.

[2]. European Commission of Energy, Climate change and Environment (2019): Climate strategies & targets. Retrieved from https://ec.europa.eu/clima/.

[3]. Danish Energy Agency: “The Danish Energy Model”. Retrieved from https://ens.dk/en.

[4]. A. S. Pedersen, K. Engelbrecht, S. Soprani, M. Wichmann, J. Borchsenius, F. Marongiu, K. Dinesen, T. Ulrich, L. Algren, K. Capion, O. Alm, L. Christensen, S. N. Rasmussen (2018): “High-Temperature Thermal Energy Storage for electrification and district heating”.

[5]. DTU Chemical Engineering. Thermal Gasification and Pyrolysis of Biomass. https://www.kt.dtu.dk/english/research/chec/research-areas/gasification.

[6]. F. Marongiu, S. Soprani and K. Engelbrecht (2019): “Modeling of High Temperature Thermal Energy Storage in Rock Beds – Experimental comparison and parametric study”. Under Review.

[7]. P.Taylor, R.Bolton, D.Stone and P.Upham (2013): “Developing pathways for energy storage in the UK using a coevolutionary framework”, *Energy Policy* vol. 63, pp. 230-243.

[8]. P.Denholm, E.Ela, B.Kirby, and M.Milligan (2010): “The role of energy storage with renewable electricity generation”. National Renewable Energy Laboratory. Technical Report.

[9]. Al.S.Pedersen, B.Elmegaard, C.H.Christensen, C.Kjoller, and F.Elefsen (2014): “Status and recommendations for RD&D on energy storage technologies in a Danish context”. Danish Energy Research Programme, Danish Energy Agency. Technical Report.

[10]. R. Tiskatine, R.Oaddi, R.Ait El Cadi, A. Bazgaou, L. Bouirden, A. Aharoune, A. Ihlal (2017): “Suitability and characteristics of rocks for sensible heat storage in CSP plants”, *Solar Energy Materials and Solar Cells* vol. 169, pp. 245-257.

[11]. A. Gil, M. Medrano, I. Martorell, A. Lázaro, P. Dolado, B. Zalba, L. F. Cabeza (2010): “State of the art on high temperature thermal energy storage for power generation. Part 1-Concepts, materials and modellization”, *Renewable and Sustainable Energy Reviews* vol. 14, pp. 31-55.

[12]. K.G.T. Hollands (1981): “Rock bed thermal storage”. Solar Energy Conversion II (Edited by A. F. Janzen, R. K. Swartman), pp. 121-130. Pergamon Press, Oxford.

[13]. Jain D. (2007): “Modeling the performance of the reversed absorber with packed bed thermal storage natural convection solar crop dryer”, *Journal of Food Engineering* vol. 78, pp. 637–647.

[14]. S. Aboul-Enein A. A. El-Sebaii, M. R. I. Ramadan and H. G. El-Gohary (2000): “Parametric study of a solar air heater with and without thermal storage for solar drying applications”, *Renewable Energy* vol. 21, pp. 505-522.

[15]. Tambunan A. H., L. P. Manalu and Kamaruddin A. (2010): “Exergy Analysis on simultaneous Charging and Discharging of Solar Thermal Storage for Drying Application”, *Drying Technology,* vol. 28, pp. 1107-1112.

[16]. G. Zanganeh, A. Pedretti, S. Zavattoni, M. Barbato and A. Steinfeld (2012): “Packed-bed thermal storage for concentrated solar power – Pilot-scale demonstration and industrial-scale design”, *Solar Energy* vol. 86, pp. 3084 – 3098.

[17]. K. G. Allen, T. W. von Backström and D. G. Kröger (2014): “Packed rock bed thermal storage in power plants: design considerations”, *Energy Procedia* vol. 49, pp. 666 – 675.

[18]. K. G. Allen, T. W. von Backström, E. Joubert and P. Gauché (2016): “Rock bed thermal storage: Concepts and costs”, AIP Conference Proceedings 1734.

[19]. M. Cascetta, G. Cau, P. Puddu and F. Serra (2014): “Numerical investigation of a packed bed thermal energy storage system with different heat transfer fluids”, *Energy Procedia, vol.* 45, pp. 598-607.

[20]. L. O. Nelwan, D. Wulandani and I. D. M. Subrata (2017): “A Preliminary Study on Rock Bed Heat Storage from Biomass Combustion for Rice Drying”, *Earth and Environmental Science* vol. 147, pp. 012-027.

[21]. K. G. Allen, T. W. von Backström, D. G. Kröger, A. F. M. Kisters (2014): “Rock bed storage for solar thermal power plants: Rock characteristics, suitability, and availability”, *Solar Energy Materials and Solar Cells* vol. 126, pp. 170-183.

[22]. T. E. W. Schumann (1929): “Heat transfer: A liquid flowing through a porous prism”, *Journal of the Franklin Institute* vol. 208, no. 3, pp. 405–416.

[23]. E. Alannís, L. Saravia, and L. Rovetta (1977): “Measurement of rock pile heat transfer coefficients”, *Solar Energy* vol. 19, no. 5, pp. 571–572.

[24]. C. G. Furnas (1930): “Heat Transfer from a gas Stream to bed of Broken Solids”, *Industrial and Engineering Chemistry* vol. 22, no. 1, pp. 26–31.

[25]. P. Chandra and D. H. Willits (1981): “Pressure drop and heat transfer characteristics of air-rockbed thermal storage systems”, *Solar Energy* vol. 27, no. 6, pp. 547–553.

[26]. Shitzer and Levy (1983): “Transient behavior of a rock-bed thermal storage system subjected to variable inlet air temperatures: analysis and experimentation”, Trans. ASME. *Journal of Solar Energy Engineering* vol. 105, no. May, pp. 200–206.

[27]. S. Soprani, F. Marongiu, L. Christensen, O. Alm, K. D. Petersen, T. Ulrich and K. Engelbrecht (2018): “Design and Testing of a Horizontal Rock Bed for High Temperature Thermal Energy Storage”, *Applied Energy* vol. 251, pp. 113-345.

[28]. L. Evangelisti, C. Guattari, P. Gori and F. Bianchi (2017): “Heat transfer study of external convective and radiative coefficients for building applications”, *Energy and Buildings* vol. 151, pp. 429-438.

[29]. F. P. Incropera, D. P. Dewit, T. L. Bergman, A. S. Lavine (2005): “Fundamentals of Heat and Mass Transfer”, Sixth edition.

[30]. G. Nellis and S. Klein (2009): “Heat Transfer”, Semi-infinite 1-D Transient Problems.

[31]. S. Sadaka, (2017): “Gasification, Producer Gas and Syngas”, Agriculture and Natural Resources.

[32]. A. Molino, S. Chianese, D. Musmarra (2016): “Biomass gasification technology: The state-of-the-art overview”, *Journal of Energy Chemistry* vol. 25, pp. 10-25.

[33]. Bioenergy Europe (2019): “Biomass for power generation”. Retrieved from https://bioenergyeurope.org/.

[34]. Ministry of New and Renewable Energy of New Delhi. Biomass Portal: “Biomass Gasification”.

[35]. J. R. Pels, D. S. de Nie, J. H.A. Kiel (2005): “Utilization of ashes from biomass combustion and gasification”, European Biomass Conference & Exhibition.

[36]. M. Augustus Leon & S. Kumar (2008): “Design and Performance Evaluation of a Solar-Assisted Biomass Drying System with Thermal Storage”, Drying Technology, pp. 936-947.

[37]. Energinet (2018): “System perspective 2035. Long-term perspectives for efficient use of renewable energy in the Danish energy system”.

[38]. DTU Department of Mechanical Engineering. https://www.mek.dtu.dk/english.

Appendix A Dissemination

The analyzed project in this master thesis has had a lot of mediatic repercussion in social media and interest from external people. During the development of the thesis, apart from the realization of the work itself, visits have also been made to school groups and university students who had to carry out a school project related to the subject. Thus, explanatory talks and guided visits to the experimental setup in Risø Campus took place. Among these dissemination activities, the Danish Minister for Higher Education and Science Tommy Ahlers was the one who inaugurated the built facility.

- Interview with two students of journalism to follow my day's work routine on DTU Energy in Risø Campus. They made a video for a tv-feature assignment which will presumably be published on the media site medietorvet.dk.

- Visit of a group of students from Roskilde University (RUC) to show them the facility and answer some questions about energy storage and to explain the operation of the Droplet.

In addition, Fabrizio Mayta and I accompanied our supervisor Kurt Engelbrecht to show the experimental setup to a seventh course class and on June 13th a school class of 10 years old kids will also visit our installation.

Appendix B Data sheets

B.1. Materials

METALLURGICA VENETA
ACCIAI SPECIALI

Azienda Certificata

AISI 304

Qualità materiale	**X5CrNi18-10** AISI 304	**Austenitico**
Norma di riferimento	**EN 10088-3: 2005**	
Numero	**1.4301**	

Composizione chimica

C% max	**Si%** max	**Mn%** max	**P%** max	**S%** max	**Cr%**	**N%** max	**Ni%**	Scostamenti ammessi per analisi di prodotto
0,07	1,00	2,00	0,045	0,030	17,5-19,5	0,11	8,0-10,5	
± 0.01	+ 0.05	± 0.04	+ 0.005	± 0.005	± 0.20	± 0.01	± 0.10	

Temperature in °C

Temperatura di fusione	**Deformazione a caldo**	**Solubilizzazione**	**Stabilizzazione**	**Indurimento**	**Saldatura**	
					preriscaldo	distensione
1400-1420	1180-950	1000-1120 acqua	900 aria	incrementabile con **trafilatura**	non richiesto	raffreddamento lento
		atmosfera controllata				

Proprietà meccaniche

Laminato EN 10088-3: 2005

sezione mm		Prova di trazione in longitudinale e resilienze long. / tang. a +20 °C							
		R	**Rp** 0.2	**A**%	**A**%	**Kv** +20 °C	**Kv** +20 °C	**HB** a)	
oltre	fino a	N/mm²	N/mm² min	min L	min T	J min L	J min T	max	
	160	500-700	190	45	--	100	--	215	solubilizzato
160	250	500-700	190	--	35	--	60	215	solubilizzato

a) solo per informazione

Trafilato +C EN 10088-3: 2005 (si consiglia: materiale solubilizzato prima della trafilatura)

sezione mm		Prova di trazione in longitudinale a +20 °C						
		R	**Rp** 0.2	**A**%	**A**%	**Kv** +20 °C	**Kv** +20 °C	
oltre	fino a	N/mm²	N/mm² min	min L	min T	J min L	J min T	
	35	700-850	350	20	--	--	--	livello di resistenza 700
	25	800-1000	500	12	--	--	--	livello di resistenza 800

Barre **lavorate a freddo** EN 10088-3: 2005 in condizione 2H, 2B, 2G, 2P

sezione		**R**	**Rp** 0.2	**A**%	**A**%	**Kv** +20 °C	**Kv** +20 °C
oltre	fino a	N/mm²	N/mm² min	min L	min T	J min L	J min T
	10 a)	600-950	400	25	--	--	--
10	16	600-950	400	25	--	--	--
16	40	600-850	190	30	--	100	--
40	63	580-850	190	30	--	100	--
63	160	500-700	190	45	--	100	--
160	250	500-700	190	--	35	--	60

a) nella gamma 1 mm ≤ d < 5 mm i valori sono validi solo per i tondi - le proprietà meccaniche delle barre non tonde con spessore < 5 mm devono essere concordate al momento della richiesta e dell'ordine

Tabella di incrudimento mediante **Trafilatura**

R	N/mm²	600	700	850	960	1100	1200	1340	1480	1650
Rp 0.2	N/mm²	300	560	720	850	960	1080	1200	1310	1440
A	%	35.0	25.0	10.0	9.0	8.0	7.0	6.0	5.5	5.0
C	%	72	70	68	60	55	47	44	40	38
Riduzione	%	**0**	**10**	**20**	**30**	**40**	**50**	**60**	**70**	**80**

Fucinato EN 10250-4: 2001 materiale solubilizzato

Prova di trazione in longitudinale a +20 °C

diametro / *spess.*		**R**	**Rp** 0.2	**A**%	**Kv** +20 °C	**Kv** +20 °C	**Kv** -150 °C	**Kv** -196 °C
oltre	fino a	N/mm²	N/mm² min	J min L	J min L	J min T	J min L	J min L
	675/450	500-700	190	30	100	60	60	60

METALLURGICA VENETA
ACCIAI SPECIALI

Azienda Certificata

AISI 304

Valore minimo di snervamento a caldo su materiale solubilizzato EN 10088-3: 2005 EN 10250-4: 2001													
Rp 0.2	N/mm²	--	155	140	127	118	110	104	98	95	92	90	**laminato** solubilizzato
Rp 0.2	N/mm²	--	157	142	127	118	110	104	98	95	92	90	**fucinato** solubilizzato
Prove a **°C**		**50**	**100**	**150**	**200**	**250**	**300**	**350**	**400**	**450**	**500**	**550**	

EUROPA EN	**ITALIA** UNI	**SPAGNA** UNE	**GERMANIA** DIN	**FRANCIA** AFNOR	**UK** B.S.	**SVEZIA** SS	**USA** AISI/SAE
X5CrNi18-10	X5CrNi18-10	F3504	X5CrNi18-10	Z5CN18-09	304S15	2332	304

X5CrNi 18-10 AISI 304

Espansione termica	[m/(m•K)] •10^{-6}	--	17.2	17.6	17.8	18.0	18.2	18.6	--	--
Modulo elastico	longitudinale N/mm²	193000	--	186000	179000	172000	165000	154000	127000	--
Modulo elastico	tangenziale N/mm²	86200	--	83000	80000	76800	73700	60000	50000	--
Resistività elettrica	Ohm•mm²/m	0.72	0.78	0.86	--	1.00	--	1.11	1.21	1.26
Conduttività	Siemens•m/mm²	1.39	1.28	1.16	--	1.00	--	0.90	0.83	0.79
Calore specifico	J/(Kg•K)	500	--	510	--	550	--	585	630	--
Coefficiente di dilatazione lineare	10^{-6}/°K	--	16.8	--	--	17.8	--	18.8	20.2	--
Prove a **°C**		**20**	**100**	**200**	**300**	**400**	**500**	**600**	**800**	**900**

Densità Kg/dm³	**Conducibilità termica** W/(m•K)							**Permeabilità magnetica**	**Resistenza alla corrosione intergran.** in condizioni di	
	20 °C	**100** °C	**200** °C	**400** °C	**500** °C	**600** °C	**800** °C	μ_r	fornitura	sensibilizzazione
7.93	15	16.3	17.5	19.9	21.5	22.5	25.1	1.008	si	no

Tratt. termico	Temperature (+ ...°C) - valori minimi												Comportamento a **fatica**
	20	**100**	**200**	**300**	**350**	**400**	**500**	**550**	**600**	**650**	**700**	**750**	
+AT 2)	190	155	127	110	104	98	92	90	80	--	70	--	Rp 0.2 N/mm²
+AT 2)	--	--	--	--	--	--	--	190	130	85	55	35	Creep rupture, 10.000 h N/mm² 1)
+AT 2)	--	--	--	--	--	--	--	140	90	50	30	15	Creep rupture, 100.000 h N/mm² 1)
+AT 2)	267	--	--	--	--	--	--	--	--	--	--	--	Resistenza allo snervamento ciclico, σ_y N/mm² con basso numero di cicli
+AT 2)	0.29	--	--	--	--	--	--	--	--	--	--	--	Esponente di tensione ciclica, n' con basso numero di cicli
+AT 2)	1628	--	--	--	--	--	--	--	--	--	--	--	Coefficiente dei cicli a fatica, K ' N/mm² con basso numero di cicli
+AT 2)	986	--	--	--	--	--	--	--	--	--	--	--	Coefficiente di resistenza a fatica, σ_f ' N/mm² con basso numero di cicli
+AT 2)	- 0.12	--	--	--	--	--	--	--	--	--	--	--	Esponente di resistenza a fatica, b con basso numero di cicli
		--	--	--	--	--	--	--	--	--	--	--	
+AT 2)	0.17	--	--	--	--	--	--	--	--	--	--	--	Coefficiente di duttilità a fatica, g_f ' con basso numero di cicli
+AT 2)	- 0.40	--	--	--	--	--	--	--	--	--	--	--	Esponente di duttilità a fatica, c con basso numero di cicli
		--	--	--	--	--	--	--	--	--	--	--	

1) carico unitario di rottura per scorrimento 2) +AT trattamento termico di solubilizzazione, 1000-1080 °C

SkamoInnerWall Brick

Kvalitet	Værdi	Enhed
Bruttodensitet (D1)	700	kg/m³
Længde (tolerance T2: ±4 mm)	228	mm
Bredde (tolerance T2: ±3 mm)	108	mm
Tykkelse (tolerance T2:±2 mm)	54	mm
Trykstyrke: Liggeflade middel	6	N/mm²
Trykstyrke: Liggeflade normaliseret	4,6	N/mm²
Vedhæftning styrke (EN 998-2, anneks C)	0,15	N/mm²
Aktive opløselige salte		S0
Varmeisolering (S2) (gennemsnit) $\lambda_{10,dry}$	0,155	W/(mK)
Brandklasse	Klasse A 1	
Frostbestandighed	F 0	

Disse data er gennemsnitlige resultater af tests gennemført i henhold til standardprocedure med forbehold for udsving. De anførte data er tilvejebragt i god tro som en teknisk service og kan ændres uden varsel. Der tages forbehold for fejl og trykfejl.
Revisionsnummer: 19-02-2018

Skamol
Østergade 58-60, 7900 Nykøbing Mors, Danmark
Tel.: +45 97 72 15 33
www.skamol.com

HASLE REFRACTORIES

Technical Data

Low Cement Castable. Easy Flow

		D39A-EF
Max recommended temperature (°C)		1500
Main component		Chamotte
Density (kg/m³)	EN ISO 1927-6	2200
Max grain size (mm)		5
Average water addition (%)		8-9
Chemical composition (%)		
Al_2O_3		39
SiO_2		56
SiC		-
Fe_2O_3		1.3
CaO		2.0
Thermal conductivity (W/mK)		
800°C	EN 993-15	1.65
1200°C		1.90
Cold MOR/CCS after heating (MPa)		
110°C	EN ISO 1927-6	11/70
500°C		11/70
1000°C		13/90
1500°C		14/100
Permanent linear change (%)		
500°C	EN 993-10	0.0
1000°C		-0.2
1500°C		-0.4
Other physical properties		
Reversible linear expansion at 1000°C (%)	EN 993-8	0.45
Hot MOR at 900°C (MPa)	EN 993-7	24
Open porosity at 1000°C (%)	EN 993-1	17-18
Abrasion at 1000°C, test angle 90° (cm³ loss)	ASTM C 704	4.8
Resistance to alkali attack (scale 0-10, 0 is best)	CEN/TS 15418	0
Resistance to thermal shock	EN 993-11	Low

The technical data provided represent average reference values established by ASTM- DIN- and EN-test procedures. The values are determined in a laboratory and serve to give general information. Values are liable to natural deviations and are not to be cited as guaranteed properties or guaranteed values

WE PROTECT YOUR PROCESS

HASLE Refractories A/S · Kanegaardsvej 1 · DK-3700 Roenne · P: +45 5695 1800 · F: +45 5695 3181
SE No: DK20223707 (import) · DK20223944 (export) · Reg. No: 204805 · CVR No: DK20223707
Bank: Danske Bank Acc. No: 4720-4720951495 · BIC/SWIFT: DABADKKK· IBAN: DK5330004720951495
hasle@hasle-refractories.com · www.hasle-refractories.com

Revision: 1.Feb 2017

Data sheet

Superwool® blanket

ENGLISH

Metric information - Page 2
Imperial information - Page 3

Description

Superwool® Plus and Superwool® HT blanket offer the same benefits as the other members of the Superwool fibre family but with improved handling strength and enhanced thermal properties. Superwool® Plus and Superwool® HT blanket are manufactured from pure raw materials using a new manufacturing technology. In addition to enhanced thermal properties, large nuisance dust particles have been effectively eliminated making the product soft to the touch and less irritating during use.

Superwool® Plus blanket are made of Superwool® Plus long fibres
Superwool® HT blanket is made of Superwool® HT long fibres

Both Superwool® Plus and Superwool® HT blanket exhibit outstanding insulating properties at elevated temperatures. Superwool® Plus and Superwool HT blanket have excellent thermal stability and retains their original soft fibrous structure up to its maximum continuous use temperature. Superwool® Plus and Superwool® HT blanket are needled from both sides and possesses high strength before and after heating. Superwool® Plus blanket and Superwool® HT blanket contain neither binder nor lubricant and does not emit any fumes or smell during the first firing. They are flexible, easy to cut and shape and easy to install.

Type

Blanket made from high temperature insulation wool.
CAS number: 329211-92-9

Classification temperature

Superwool® Plus blanket: 1200°C (2192°F)
Superwool® HT blanket: 1300°C (2372°F)

The maximum continuous use temperature depends on the application. Unaffected by most chemicals except strong alkalis, phosphoric acid and molybdenum. For further advise please contact your local Morgan Thermal Ceramics partner.

Typical applications

- Power generation especially HRSG duct insulation
- Chimney insulation
- Process heater linings
- Pipe wrap
- Annealing furnace linings
- Furnace and kiln back-up insulation
- Storage heater insulation
- Domestic oven insulation
- Automotive exhaust heat shields
- Aluminium transfer launder covers
- Welding stress relief

Benefits

- Exceptional thermal insulating performance compared with industry standards
- Free of binder or lubricant
- Immune to thermal shock
- Low heat storage
- Good resistance to tearing
- Flexible and resilient
- Good sound absorption
- Superwool® fibre meets the requirements specified under NOTE Q of European Regulation 1272/2008. All Superwool® fibre products are therefore exonerated from labelling requirements in Europe
- No requirement for warning labels under Globally Harmonised System (GHS) for the classification and labelling of chemicals.

SDS:
EU: 144/138
NA: 350
GHS: n/a

Data sheet

Superwool® blanket

Metric information

	Superwool Plus blanket					Superwool HT blanket			
Classification temperature, °C	1200					1300			
Colour	White					White			
Density, kg/m³	64	80	96	128	160	64	96	128	160
Thermal conductivity, ASTM C-201, **W/m K**									
@200°C	0.06	0.06	0.05	0.05	0.04	-	0.05	0.04	-
@400°C	0.11	0.09	0.09	0.08	0.07	-	0.10	0.08	-
@600°C	0.18	0.15	0.14	0.12	0.11	-	0.19	0.14	-
@800°C	0.29	0.24	0.21	0.18	0.16	-	0.32	0.23	-
@1000°C	0.42	0.36	0.29	0.25	0.23	-	0.48	0.34	-
@1200°C	-	-	-	-	-	-	0.69	0.48	-
Tensile strength, EN 1094-1, **kPa**	30	45	55	75	90	30	50	75	95
Permanent linear shrinkage, ENV 1094-1, **%** after 24 hours isothermal heating, %									
@1200°C	1					-			
Chemical composition, %									
SiO_2	62 - 68					70 - 80			
CaO+MgO	-					18 - 25			
CaO	26 - 32					-			
MgO	3 - 7					-			
Other oxides	<1					<3			

Availability and Packaging

Superwool® HT Blanket are packed in cartons, 1260 x 940mm pallet + stretchable film.
Marks (o) and width 1220mm upon request (subject to minimum order requirements).

Superwool® Plus blanket

Thickness mm	Density kg/m³					Length mm	Width mm	Carton m²
	64	80	96	128	160			
6				•		4 x 5500	610	13.42
10			•	•		18500	610	11.28
13		•	•	•	•	14640	610	8.93
19	•	•	•	•	•	9760	610	5.95
25	•	•	•	•	•	7320	610	4.46
38	•	•	•	•		4880	610	2.98
50	•	•	•	•		3660	610	2.23

Superwool® HT blanket

Thickness mm	Density kg/m³				Length mm	Width mm	Carton m²
	64	96	128	160			
6		•	•	o	4 x 5500	610	13.42
10		•	•	•	18500	610	11.28
13		•	•	•	14640	610	8.93
19	o	•	•	•	9760	610	5.95
25	o	•	•	•	7320	610	4.46
38	o	•	•	o	4880	610	2.98
50	o	•	•	o	3660	610	2.23

Contact

Europe:
Telephone:
+44 (0) 151 334 4030

E-mail:
marketing.tc@morganplc.com

North America:
Telephone:
+1 (706) 796 4200

E-mail:
northamerica.tc@morganplc.com

South America:
Telephone:
+54 (11) 4373 4439

E-mail:
marketing.tc@morganplc.com

Asia:
Telephone:
+65 6595 0000

E-mail:
asia.mc@morganplc.com

Data sheet

Superwool® blanket

Imperial information

	Superwool Plus blanket		Superwool HT blanket	
Classification temperature, °F (°C)	2192 (1200)		2372 (1300)	
Continuous use temperature, °F (°C)	1832 (1000)		2102 (1150)	
Color	White		White	
Density, pcf (kg/m³)	6 (96)	8 (128)	6 (96)	8 (128)
Thermal conductivity, ASTM C 201, **BTU•in./hr•ft²•°F** (W/m•K)				
@500°F (260°C)	0.46	0.39		0.41
@1000°F (538°C)	0.81	0.73		0.85
@1500°F (816°C)	1.26	1.28		1.57
@1800°F (982°C)	1.57	1.73		-
@2000°F (1093°C)	-	-		2.54
Chemical analysis, %				
SiO_2	62 - 68		70 - 80	
CaO + MgO	29-39		18 - 25	
Other oxides	<1		<3	
Leachable chlorides	trace		-	

Availability and Packaging

Thickness, in (mm)	Density, pcf (kg/m³)				Length, in (mm)	Width, in (mm)	ft²/carton for 24 in width rolls (m²)
	4 (64)	6 (96)	8 (128)	10 (160)			
1/4 (6)			•		240 (6095)	24, 48 (610, 1220)	160 (15)
1/2 (13)		•	•	•	600 (15240)	24, 48 (610, 1220)	100 (9)
1 (25)	•	•	•	•	300 (7620)	24, 48 (610, 1220)	50 (5)
1-1/2 (38)	•	•	•		180 (4575)	24, 48 (610, 1220)	30 (3)
2 (50)	•	•	•		150 (3810)	24, 48 (610, 1220)	25 (2)

This is packaging for items purchased from within North America, items for export may have different details and order requirements.

Contact

Europe:
Telephone:
+44 (0) 151 334 4030

E-mail:
marketing.tc@morganplc.com

North America:
Telephone:
+1 (706) 796 4200

E-mail:
northamerica.tc@morganplc.com

South America:
Telephone:
+54 (11) 4373 4439

E-mail:
marketing.tc@morganplc.com

Asia:
Telephone:
+65 6595 0000

E-mail:
asia.mc@morganplc.com

SeaRox SL 660

NEW NAME

HC Firebatts 150

Firesafe Insulation

Product description

SeaRox SL 660 is a slab made of stone wool. The product is specially developed to provide maximum fire protection. SeaRox SL 660 can be supplied with reinforced alu foil.

Application

SeaRox SL 660 is used for hydrocarbon fire protection of bulkheads, decks and firewalls.

Product Properties

	Performance				Norm
Thermal conductivity	T (°C)	10	100	300	EN 12667
	λ (W/mK)	0,035	0,043	0,073	
Nominal density	150 kg/m³				EN 1602 / IMO
Compressive strength	-				EN 826
Fire classification	Non-combustible Approved for H constructions Low Flame-Spread Properties				Acc. IMO FTP code
Water absorption (short term)	< 1 kg/m²				EN 1609 AC
Max. Application Temperature	Wool: 750°C Facing: 80°C				-
Sound absorption directly mounted	α_w = 0,90 Thickness: 2x50 mm				ISO 354 (approximated) Evaluated after ISO 11 654
Facings (on request)	Reinforced alu foil				IMO A.653(16) (low flame - spread)

Dimensions

SeaRox SL 660:
Thickness (mm): 30, 50 mm Length (mm): 1000 mm Width (mm): 600 mm

SeaRox SL 660 ALU:
Thickness (mm): 30, 50 mm Length (mm): 1000 mm Width (mm): 600 mm

Local variations in standard dimensions might occur.

0575/

Rockwool Technical Insulation reserves the right to make necessary product changes at any time. Technical specifications are thus stated subject to change.

ROCKWOOL®
TECHNICAL INSULATION

Rockwool Technical Insulation
DK-2640 Hedehusene
Tel: +45 46 56 16 16
Fax. +45 46 56 16 04
export@rockwool.com
www.rockwool-rti.com
Part of Rockwool International A/S

B.2. Setup components

SV 300/1

Side channel blowers
- single stage, air-cooled
- with pedestal

Seitenkanal-Verdichter
- einstufig, luftgekühlt
- mit Standfuß

Soufflantes à canal latéral
- mono-étagées, refroidies par air
- avec pied

Soffianti a canale laterale
- monostadio, raffreddate ad aria
- con piedistallo

Compresores de canal lateral
- una etapa, refrigerado por aire
- con pie

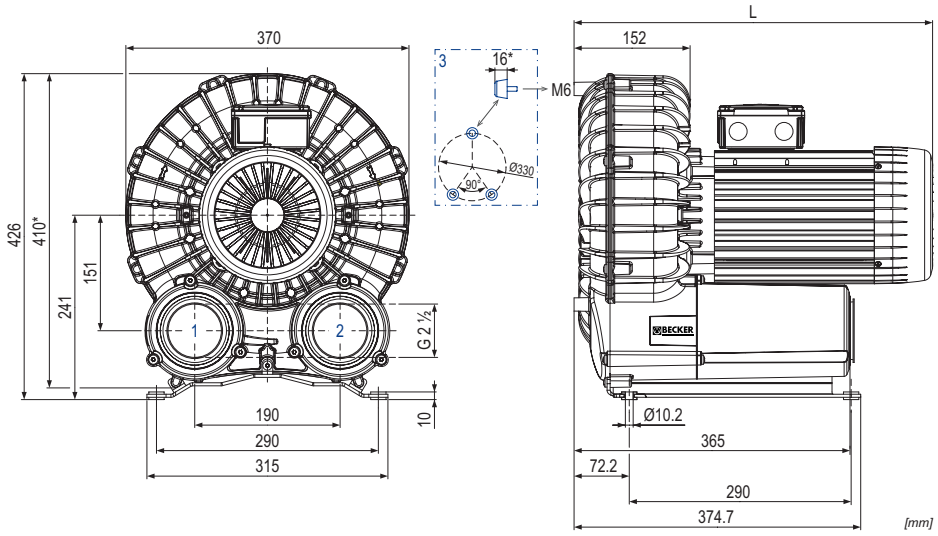

1 Vacuum connection
Sauganschluss
Raccord vide
Raccordo aspirazione
Conexión de vacío

2 Pressure connection
Druckanschluss
Raccord pression
Raccordo pressione
Conexión presión

3 Rubber buffer position (optional)
Gummipufferposition (optional)
Position de tampon en caoutchouc (optionnel)
Posizione del respingente in gomma (optionale)
Posición del tope de goma (opcional)

m³/h		mbar rel.		kW 3~		Ⓜ	L	kg	dB(A) 1)	
50 Hz	60 Hz	50 Hz	60 Hz	50 Hz	60 Hz		mm		50 Hz	60 Hz
325	390	+165	+140	2.2	2.65	1-2	469	40.0	66.9 (+115 mbar)	68.9 (+95 mbar)
		+250	+230	3.0	3.6	3-5	494	42.5	71.1 (+165 mbar)	69.4 (+155 mbar)
		+370	+340	4.0	4.8	6-8	538	54.5	72.8 (+255 mbar)	73.4 (+235 mbar)

Ⓜ			50 Hz kW	50 Hz V ±10%		50 Hz min⁻¹	50 Hz A	60 Hz kW	60 Hz V ±10%		60 Hz min⁻¹	60 Hz A	№ IP55 • ISO F • bimetal	№ SV 300/1
1	2.2/2.65kW	3~	2.2	Δ230/Y400	IE3/UL/CSA	2910	7.7/4.45	2.65	Δ265/Y460 Δ230/Y400	IE3/UL/CSA –	3510 3460	7.6/4.4 8.3/4.6	42289201603001GD	G023732
2		3~			–			2.65	YY230/Y460 208	IE3/UL/CSA –			42389207603000GD	G023785
3	3.0/3.6kW	3~	3.0	Δ230/Y400	IE3/UL/CSA	2890	10.6/6.1	3.6	Δ265/Y460 Δ230/Y400	IE3/UL/CSA –	3500 3460	10.6/6.1 11.6/6.7	42489201603000GD	G023725
4		3~			–			3.6	YY230/Y460 208	IE3/UL/CSA –	3510 3480	6.2 13.0	42589207603000GD	G023838
5		3~	3.0	Δ200/Y350	IE3			3.6	Δ220/Y380-400 Δ200/Y350	IE3 –			42489285603000GD	G023846
6	4.0/4.8kW	3~	4.0	Δ230/Y400	IE3/UL/CSA	2930	14.6/8.4	4.8	Δ265/Y460 Δ230/Y400	IE3/UL/CSA –	3520 3490	14.3/8.25 15.4/8.85	42689201603000GV	G023764
7		3~			–			4.8	YY230/Y460 208	IE3/UL/CSA –				
8		3~	4.0	Δ200/Y350	IE3	2930	16.6/9.6	4.8	Δ220/Y380-400 Δ200/Y350	IE3	3520 3490	16.6/9.6-9.45 17.7/10.1	42689285603000GV	G025267

1) DIN EN ISO 3744 (KpA = 3 dB(A)) interval of 1m, at medium load, both connection sides piped
DIN EN ISO 3744 (KpA = 3 dB(A)) Abstand von 1m, bei mittlerer Belastung, beide Seiten abgeleitet
DIN EN ISO 3744 (KpA = 3 dB(A)) intervalle de 1m, à régime moyen, avec dérivation des deux côtés
DIN EN ISO 3744 (KpA = 3 dB(A)) intervallo di 1m, a medio regime, entrambi i lati derivati
DIN EN ISO 3744 (KpA = 3 dB(A)) intervalo de 1m, en media carga, derivados de ambos lados

* Device dimensions without pedestal under the silencer, with rubber buffers on the enclosure cover
Geräteabmaße ohne Standfuß unter den Schalldämpfern, mit Gummipuffern am Gehäusedeckel
Dimension d'appareil sans pied sous les silencieux, avec tampons en caoutchouc sur le couvercle
Dimensioni del dispositivo senza piedistallo sotto gli insonorizzatori, con respingenti in gomma sul coperchio dell'alloggiamento
Dimensiones del aparato sin pie bajo los silenciadores, con topes de goma en la tapa de la carcasa

▪ Dimensions in mm
Maßangaben in mm
Mesures en mm
Misure in mm
Dimensiones en mm

BECKER
WWW.BECKER-INTERNATIONAL.COM

20.01.2017

Blast air rate • Blasluftmenge • Débit d'air soufflé • Volume d'aria soffiata • Volumen de aire soplado

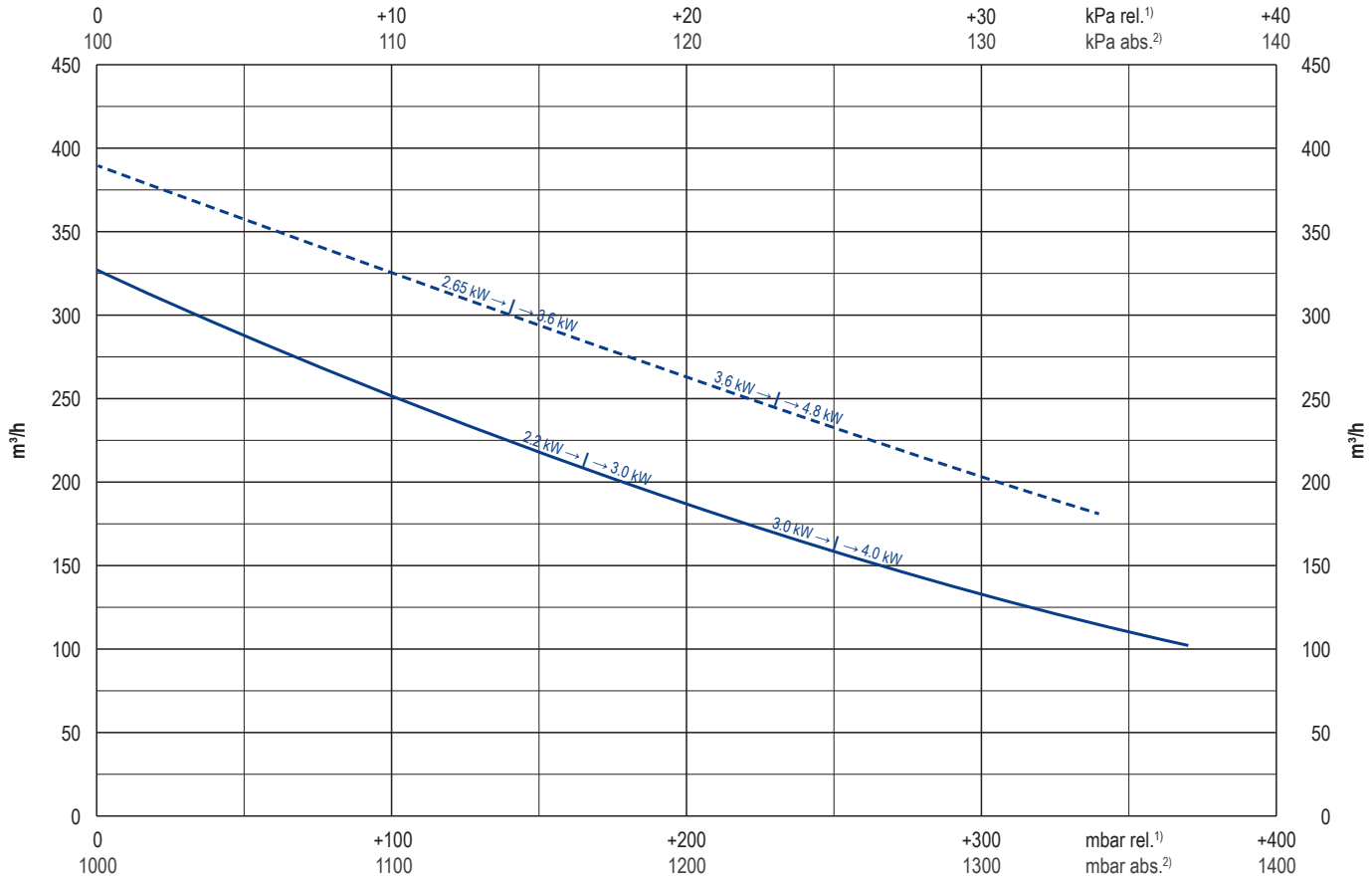

Exhaust air temperature • Ablufttemperatur • Température d'air à l'échappement
Temperatura dell'aria scarica • Temperatura del aire de escape

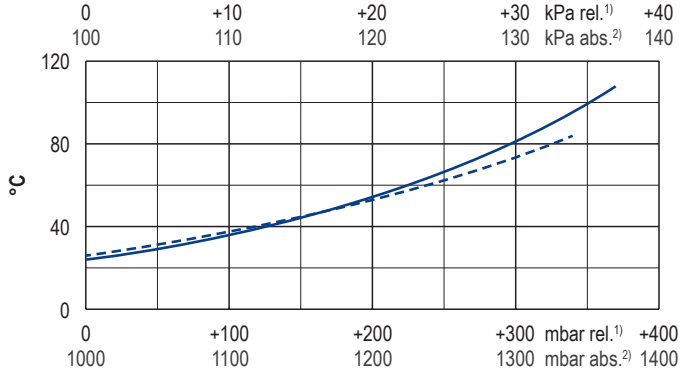

Motor shaft power • Wellenleistung • Puissance du moteur axe
Potenza del motore albero • Capacidad de eje del motor

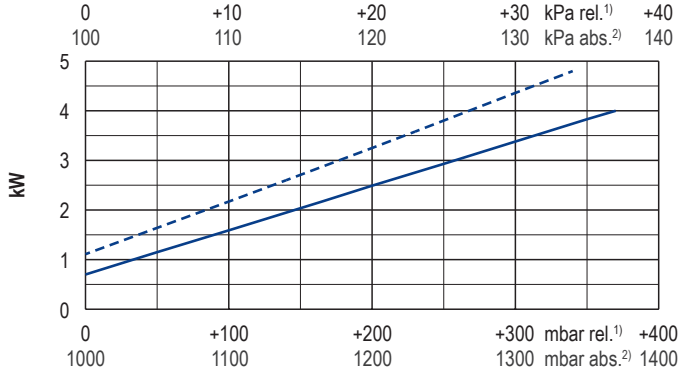

—— 50 Hz
- - - 60 Hz

1) relative relativ relatif relativo relativa
2) absolute absolut absolu assoluto absoluta

▪ Reference data (atmosphere) Bezugsdaten (Atmosphäre) Référence (atmosphère) Rifermento (atmosfera) Referencia (atmosférica) 1000 mbar, 20°C
▪ Tolerance Toleranz Tolérance Tolleranza Tolerancia ±10 %

Variants/Accessories	Varianten/Zubehör	Variantes/Accessoires	Varianti/Accessori	Variantes/Accesorios
- with internal safety valve	- mit internem Sicherheitsventil	- avec soupape de sécurité interne	- con valvola di sicurezza interno	- con válvula de seguridad interna
- with internal or external suction filter	- mit internem oder externem Ansaugfilter	- avec filtre d'aspration interne ou externe	- con filtro di aspirazione interno o esterno	- con filtro de aspiración interna o externo
- in sound proof box SH 18	- in Schallhaube SH 18	- dans caisse d'insonorisation SH 18	- in casse insonorizzanti SH 18	- en caja a prueba de sonido SH 18
- with increased corrosion protection	- mit erhöhtem Korrosionsschutz	- avec protection accrue contre la corrosion	- con una maggiore protezione anti-corrosione	- con el aumento de protección contra la corrosión
- without pedestal under the silencers, with rubber buffers on the enclosure cover	- ohne Standfuß unter den Schalldämpfern, mit Gummipuffern am Gehäusedeckel	- sans pieds sous les silencieux, avec tampons en caoutchouc sur le couvercle	- senza piedistallo sotto gli insonorizzatori, con respingenti in gomma sul coperchio dell'alloggiamento	- sin pie bajo los silenciadores, con topes de goma en la tapa de la carcasa
- without motor, prepared for flange motor	- ohne Motor, vorbereitet für Flanschmotor	- sans moteur, préparé pour moteur à bride	- senza motore, preparato per il motore a flangia	- sin motor, preparado para el motor de brida
- ATEX	- ATEX	- ATEX	- ATEX	- ATEX

VARIAIR UNIT

with frequency inverter	mit Frequenzumformer	avec convertisseur de fréquence	con convertitore di frequenza	con variador de frecuencia
Performance data / dimensions can differ Combinations on request	Leistungsdaten / Abmessungen können abweichen Kombinationen auf Anfrage	Données de performance / mesures peuvent différer Combinaisons sur demande	Dati di performance / misure possono differire Combinazioni su richiesta	Datos de rendimiento / dimensiones pueden diferir Combinaciones a petición

20.01.2017

BELL
Flow Systems

BGFT Gas Turbine Flow Meter

Technical Data Sheet

SPECIFICATIONS

Performance:

Repeatability:	±0.2%
Accuracy:	Standard: ±1.5% of reading; Optional: ±1.5% of reading or ±0.75% of reading

Wetted Components:

Housing:	Standard - Tungsten Carbide; Optional - 304, 316 Stainless Steel
Bearings and Shaft:	ABS (Corrosion Resist) or Aluminium-Alloy
Rotor:	ABS (Corrosion Resist) or Aluminium-Alloy
Retaining Rings:	304 Stainless Steel

Output Signal: (where applicable)

Sensor:	Pulse signal (Low Level: ≤0.8V; High Level: ≥8V)
Transmitter:	4 to 20 mA DC current signal

Signal Transmission Distance: ≤1,000 m

Electrical Connections:

Basic Type:	Hausman Connector or three-core cable
Explosion Proof Type:	ISO M20×1.5 Female

Explosion Proof Level:

Standard:	None
Optional:	ExdIIBT6

Protection Level: IP65

OPERATION CONDITIONS

Ambient:

Temperature: -10℃ to +55℃
Pressure: 86 to 106 KPa
Relative Humidity: 5% to 90%

Power Supply:

Sensor: +12V DC (Optional: +24V DC)
Transmitter: +24V DC
Field Display Type B: Integral 3.2V Lithium Battery
Field Display Type C: +24V DC

Fluid Temperature and Pressure:

Temperature: -30℃ to +80℃
Pressure: Fluid pressure should be limited according to flange rating.

Measurable Flow Rate Range and Pressure Level:

Table 1. Measurable Flow Rage Range and Pressure Rating

Nominal Diameter		Standard Flow Range (SFR)		Extended Flow Range (EFR)		Standard Pressure Rating
(mm)	(in.)	Mark	(m^3/h)	Mark	(m^3/h)	(MPa)
25	1	S1	3 to 30	W1	1.5 to 30	4.0
		S2	4 to 40	W2	2 to 40	4.0
				W3	0.5 to 4	4.0
				W4	0.7 to 7	4.0
				W5	1.5 to 30	4.0
40	1.5	S1	5 to 50	W1	2.5 to 50	4.0
		S2	8 to 80	W2	4 to 80	4.0
50	2	S1	10 to 100	W1	5 to 100	4.0
		S2	15 to 150	W2	8 to 150	4.0
65	2.5	S	15 to 200	W	10 to 200	1.6
80	3	S1	15 to 300	W1	10 to 300	1.6
		S2		W2	15 to 350	1.6
100	4	S	20 to 400	W1	15 to 400	1.6
				W2	20 to 500	1.6
125	5	S	20 to 800	W1	18 to 800	1.6
				W2	20 to 900	1.6
150	6	S	50 to 1000	W1	25 to 1000	1.6
				W2	50 to 1200	1.6
200	8	S	150 to 2000	W	80 to 2500	1.6
250	10	S	200 to 3000	W	150 to 3500	1.6
300	12	S	250 to 4000	W	200 to 4000	1.6

Model

Turbine Flow Sensor/Transmitter

GFT-N Type Sensor: 12 to 24V DC Power Supply; Pulse Output
GFT-A Type Transmitter: 24V DC Power Supply; 2-wire 4 to 20 mA Output

Basic Type (Without Explosion Proof) and Explosion Proof Type are optional for GFT-N and GFT-A.

Basic Type

Intelligent Integrated Turbine Flow Meter

- 4 digital instantaneous flow display
- 8 digital totalizator flow display (Resettable)
- With Explosion Proof (Level: ExdIIBT6)
- 3-Point Correction and Non-linearity Compensation on K-Factor

Note: The K-Factor represents the number of output pulses transmitted per cubic meter (Optional: Liter and Gallons) of fluid passing through the turbine meter. Each turbine has a unique K-Factor. However, turbine meters are not functionally consistent throughout the full flow range of the meter. Therefore, correction and non-linearity compensation on K-Factor can enhance accuracy.

GFT-B Type: powered with 3.2V10AH lithium battery (Battery life > 4 years); no output
GFT-C Type: 24V DC Power Supply; 2-wire 4 to 20 mA Output (Optional: RS485 or HART)

GFT-D Type (With temperature and pressure compensation): 24V DC Power Supply

MODEL AND SELECTION

Table 2. Model Selection Guidance

Model Suffix Code							Description (SFR: Standard Flow Range)
GFT-							
Type	N						Basic Type: +12V to +12V DC Power Supply; Pulse Output
	A						4 to 20 mA current output
	B						Battery Power Supply with filed Display
	C						Field Display and 4 to 20 mA current output
	D						Field Display and output; Temperature and Pressure Compensation
Nominal Diameter (mm)		25					DN25
		40					DN40
		50					DN50
		65					DN65
		80					DN80
		100					DN100
		125					DN125
		150					DN150
		200					DN200
		250					DN250
		300					DN300
Range Selection			W(X)				Extended Flow Range: Refer to table 1
			S(X)				Standard Flow Range: Refer to table 1
Housing Material				S			304 Stainless Steel
				L			Aluminium-Alloy
Core Material (Rotar, Bearing)					S		Corrosion Resistance ABS
					L		Aluminium-Alloy
Structure						N	Standard Structure
						A	For Oxygen Only (O_2 Only)
						B	Compressed-Air Only

METER CONSTRUCTION

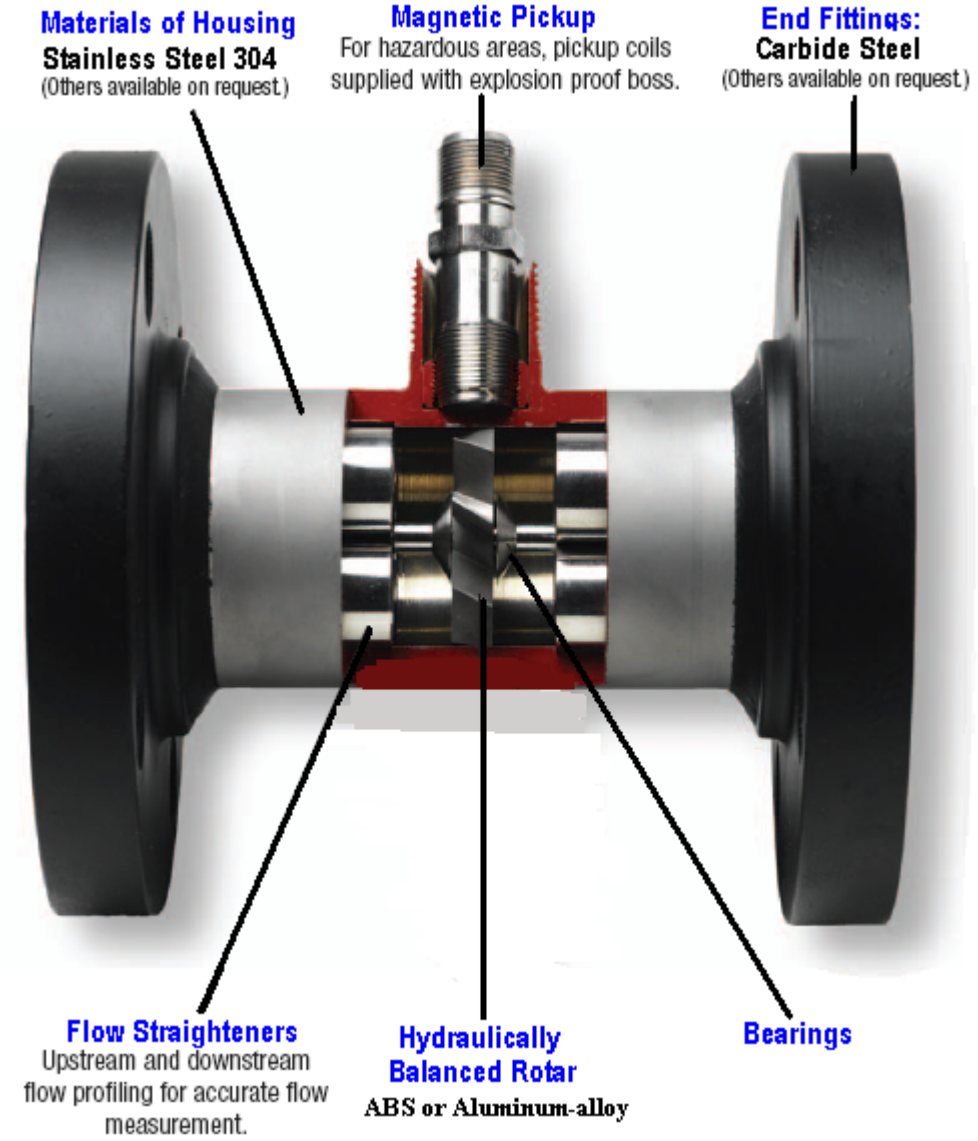

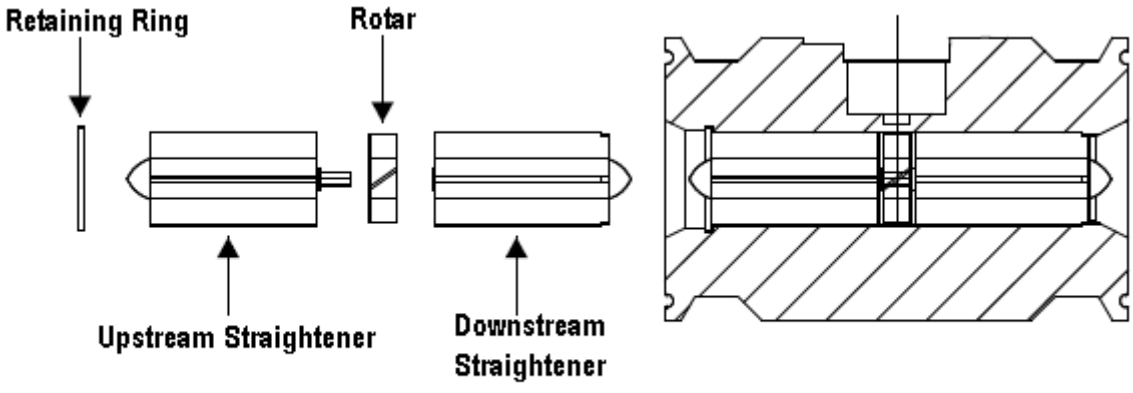

Exploded View of Internals

Assembled Internals

Bell Flow Systems
7 Swan Business Centre
Osier Way, Buckingham
Buckinghamshire
MK18 1TB

T: + 44 (0) 1280 817304
F: + 44 (0) 1280 817185
E: mail@bellflowsystems.co.uk

www.bellflowsystems.co.uk

Two LE 10000 HT air heaters and an ASO blower in combination with a shrinking tunnel.

High temperature air heater

LE 10 000 HT (up to 900 °C)

Technical data
High temperature LE 10000 HT

No integrated power electronics		•
Heating element tube with protective tube		•
Max. air outlet temperature	°C	900
Min. air flow	l/min	1200
Max. air inlet temperature	°C	100
Max. ambient temperature	°C	100
Weight	kg	4.0
Mark of conformity		CE
Protection classe I		⏚

Installation dimensions in mm

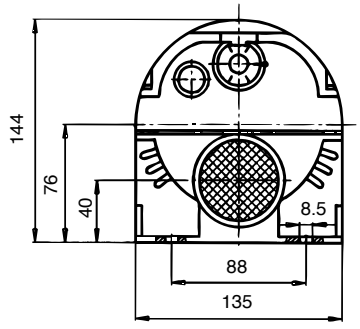

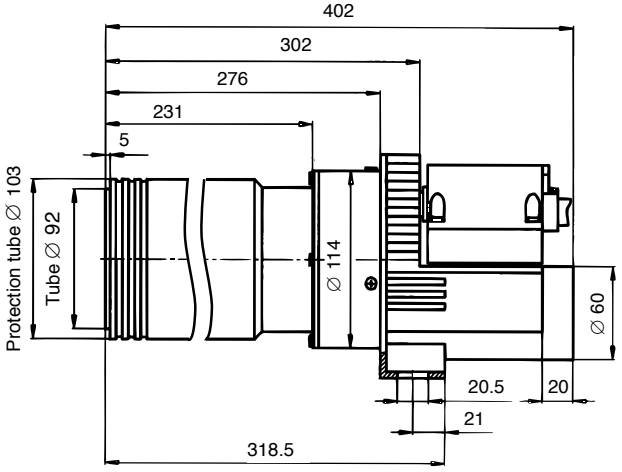

Optional power controller
DSE three-phase controller (page 51)

Optional temperature regulation
DSE three-phase controller (page 51) and KSR DIGITAL temperature regulator (page 50)

Voltage V ~	3 × 400	3 × 480
Power consumption kW	15	15
Order no.	**110.568**	**113.349**

Combination possibilities

- Leister air heater at maximum heat power and without nozzle with Leister blower at 50 Hz, 1.5 m hose length and unimpeded air outflow.
- Hot air temperature 3 mm after air outlet, measured at the hottest point.
- Air flow at 20 °C, 101.3 kPa compliant with ISO 6358.

Power Type	Number LE × Power consumption kW	Air flow l/min	Temperature °C
ROBUST	1 × 15	1 × 1100	850
ASO	1 × 15	1 × 2200	690
ASO	2 × 15	2 × 2100	700
AIRPACK	1 × 15	1 × 3400	340
AIRPACK	2 × 15	2 × 1650	620

Air flow and temperature values may deviate from those above based on the design of the entire hot air system (including nozzles, air hoses, environmental conditions).

➡ Accessories page 45

Shrinking a PE sleeve on cans with temperature regulated hot air produces precise quality.

Accessories LHS 61L / LE 10000 / LE 10000 HT (Ø 92 mm)

125.318	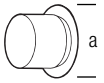	Flange connector, push-fit a = 120 mm
107.244	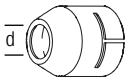	Round nozzle, push-fit d = 50 mm
107.273	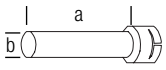	Extension nozzle, push-fit (a × b) 500 × 60 mm
107.269	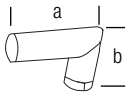	Angled nozzle, push-fit (a × b) Schenkellänge 175 × 175 mm
106.031 **106.035** **107.268** **106.036** **106.033** **106.038**	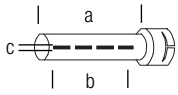	Tubular nozzle, push-fit (a × b × c) 1000 × 800 × 2 mm 1185 × 900 × 1.6 mm 1288 × 1000 × 1.5 mm 1535 × 1250 × 1.2 mm 1550 × 1350 × 1.1 mm 2225 × 2000 × 0.8 mm
107.274 **106.028** **107.272** **106.018** **106.024** **107.267** **106.023** **106.026**	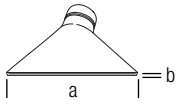	Wide slot nozzle, push-fit (a × b) 130 × 17 mm 220 × 12 mm 300 × 12 mm 400 × 10 mm 500 × 7 mm 500 × 15 mm 600 × 4 mm 600 × 9 mm
107.341	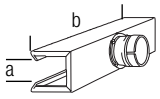	Shell reflector, push-fit (a × b) 160 × 370 mm
107.276	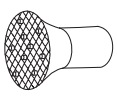	Sieve reflector, push-fit Ø 260 mm
133.517		Thermocouple holder
144.039		Compressed air connection **> LHS 61**

144.030 **144.028** **144.026**		System Interface cable 1 m 3 m 5 m one end single wires, one end RJ45

Acknowledgements

This project has been possible thanks to the help of great professionals. All of them have offered me their time and their attentive dedication.

First of all, I would like to express my special appreciation and thanks to my supervisor Kurt Engelbrecht for have given to me this unique opportunity to participate in such an interesting project and for his guidance during the development of my thesis. I would like to thank Maria Puig, Jesper Ahrenfeldt and Lasse R. Claussen for their collaboration in this work, and special thanks to Fabrizio Marongiu and Fabrizio Mayta for their fundamental role in this work as project mates.

I would like to express my very profound gratitude to my parents, Artur and Esther, and to my brother, Arnau, for providing me with unfailing support and continuous encouragement throughout my years of study and through the process of researching and writing this thesis. As well as my grandparents and all my family. This accomplishment would not have been possible without them.

I would like to thank my office mates Caterina Sanna and Fabrizio Mayta for their friendship and to all my friends at DTU Risø Campus.

Finally, I would like to thank all the people who formed part of this path and supported me in one way or another during all my university period.